TU Delft & Marin

The Propeller and Engine Performance of the 'Castillo de Tebra' subject to Waves

A thesis presented for the degree of Master of Science in Marine Technology

Josef Ferschtman, 4372735
January 7th, 2022

Thesis for the degree of MSc in Marine Technology in the specialization of Marine Engineering

The Propeller and Engine Performance of the 'Castillo de Tebra' subject to Waves

by

Josef Ferschtman

Performed at

TU Delft & MARIN

January 7th, 2022

Company Supervisors
Responsible Supervisor:
Dr. Joost Moulijn, MARIN
E-mail: J.C.Moulijn@marin.nl

Thesis Exam Committee
Chair/Responsible Supervisors:
Ir. K. Visser
Dr.Ir. P. de Vos
Staff Members:
Dr. C. Sui
Prof.dr.ir. T.J.C. van Terwisga

Author Details
Studynumber: 4372735
Author contact e-mail: josefferschtman@gmail.com

Abstract

In the modern world, environmental concerns arise due to an increase in the green house gas (GHG) emissions of the shipping industry; in 2015, 2,5% of global GHG emissions came from the shipping industry alone. Measures must be set in place to reduce the future emissions. One way to reduce emissions is by imposing the Energy Efficiency Design Index (EEDI). This is a measure to define the ratio between the CO_2-production and the cargo capacity and speed of a ship. In other words, this ratio defines the environmental cost over societal benefit of a ship. The International Maritime Organisation wants to have a set requirement on the EEDI of new ships and preferably reduce this for existing ships. One way to reduce the EEDI is by reducing the installed engine power of the ship. One risk is that the ship might then become underpowered when it sails in adverse weather. The underpowering of ships could lead to safety hazards for the passengers and crew. For that matter, this thesis will investigate whether the ocean-going chemical tanker 'Castillo de Tebra' is underpowered when sailing in large waves. Specifically, the effect of the waves on the inflow velocity of the propeller will be looked at and how this affects the propulsive performance of the vessel.

An extensive literature review was carried out in order to find out what the state-of-the-art is within the determination of ship propulsion in waves. This has been divided into three separate subjects, namely wave excitation, propeller and engine operating in waves and finally manoeuvring and seakeeping. When determining the forces that occur on a ship when it advances in waves, most methods use potential flow as the results are reliable and have low time effort. Determining propeller performance when the full wake distribution is known can also be done using potential flow methods. Basic open-water characteristics are a valid alternative as well. CFD can be used for both wave excitation and propeller performance calculations, but this is time consuming and computationally complex. When simulating manoeuvring and seakeeping behaviour of ships, two-time scale methods or unified methods are mainly used.

For the research part of this thesis, numerical simulations were performed to determine the change of inflow velocity at the propeller plane for a large range of wave frequencies and wave directions, for a vessel having a forward speed. This velocity change was used to determine what the thrust and torque generation of the propeller is in waves. The engine operating envelope and ship thrust envelope were used to check whether the engine has enough power to provide the torque that the propeller generates and whether the ship has enough thrust availability. Frequency-domain results were transformed into time records for irregular waves using the JONSWAP wave spectrum and a cosine function. It was concluded that the ship was underpowered in adverse weather conditions, when an instant control system was assumed that inject enough fuel instantly to keep the engine at the rated speed when it needs to deliver more power. It was also assumed that the ship speed was kept at the design speed. In reality, voluntary and involuntary speed loss will occur when a ship sails

in bad weather. Voluntary in the form of manual speed decrease by the captain and involuntary in the form of added resistance causing the ship to reduce in speed. A number of solutions are finally presented in this thesis to omit engine overloading in adverse weather.

Preface

Before you lies my thesis for the Masters degree in Marine Technology at the Technical University in Delft, The Netherlands. Commissioned by the TU Delft and with the help of MARIN (Maritime Research Institute Netherlands) this final project was fulfilled. After 7 years, with a year in between learning the ins and outs of Aerospace Engineering, my student career in Marine Technology comes to an end. Many ups and downs led to me getting to know myself and my working ability best. Besides that, a lot has been learned about the engineering world, specifically the maritime world. Doing this thesis during uncertain times like the Coronavirus pandemic, that started in February 2020, was at times hard, especially when living all by yourself in a studio and not having the opportunity to see other students and have a vibrant working space like the university library. However, by keeping my head straight and taking my time off when needed, it worked out in the end and this thesis is proof of that.

I would like to thank my supervisors at the TU Delft and MARIN for their excellent guidance, expertise and assistance during my graduation process. One by one, thanks to Peter de Vos for overseeing my graduation process and helping me in creating new ideas and modify thought processes as well as guiding me through the organizational phases of the graduation. Thanks to Congbiao Sui, for helping me on the marine engineering side of the project, helping me with the propulsion model and the theory that was involved with that. Thanks to Joost Moulijn, for helping me with acquiring the internship at MARIN and guiding me along the way. Besides that, his expertise on the hydrodynamic side of my thesis was also very useful and insightful. Thanks to Tom van Terwisga, helping me in the early stages of my graduation by guiding me to the right methodologies and ideas to fulfill my research. Thanks to MARIN and also Stephane Rapuc from MARIN in giving me the opportunity to use their available software packages for my research and giving me advice and pointers on how to use these software to acquire better results.

Finally, I would like to thank all students that I shared my time with at the TU Delft. They made my time at the university a pleasant one. They helped me when I did not understand some theory and vice versa, which was incredibly helpful. Also thanks to Lindert van Tongeren, who is doing his thesis on the same topic. Through brain-storm sessions, I gathered a lot of useful information and ideas on how to further do my research. I hope he did as well!

Josef Ferschtman
Amsterdam, January 2022

Contents

Nomenclature

Symbol	Description	Unit
B	Breadth	m
C_b	Block coefficient	$-$
C_E	Specific resistance coefficient	$-$
C_m	Midship coefficient	$-$
C_p	Prismatic coefficient	$-$
C_Q	Torque index	$-$
C_T	Thrust index	$-$
C_{wl}	Waterline coefficient	$-$
D_p	Propeller diameter	m
F_s	Safety factor	$-$
g	Gravitational constant	$\frac{m}{s^2}$
G	Green's function	$-$
h	Height of the sea bottom	m
$\frac{h_i}{h1}$	Normalized grid refinement ratio	$-$
$H(t)$	Position of the ship's hull	m
$H_{1/3}$	Significant wave height	m
J	Advance coefficient	$-$
k	Wave number	$\frac{1}{m}$
K_Q	Torque coefficient	$-$
K_T	Thrust coefficient	$-$
k_{xx}	Roll radius of gyration	m
k_{yy}	Pitch radius of gyration	m
k_{zz}	Yaw radius of gyration	m
L_{pp}	Length between perpendiculars	m
L_{wl}	Length on load waterline	m
lcb	Centre of buoyancy	m
M_p	Shaft torque	Nm
$\vec{n}$	Normal vector	$-$
n_e	Engine speed	rps
n_g	Number of grids	$-$
n_p	Propeller speed	rps
NP_1	Number of panels of the most fine grid	$-$
NP_i	Numer of panels of the i^{th} grid	$-$
p	Pressure	$\frac{N}{m^2}$
p	Grid convergence	$-$
P/D	Pitch-diameter ratio	$-$
p_0	Atmospheric pressure	$\frac{N}{m^2}$
P_B	Brake power	W
P_E	Effective towing power	W
Q	Propeller torque	Nm
R	Ship resistance	N

Symbol	Description	Unit
r	Distance between two points	m
S	Free surface function	$-$
S_ζ	Spectral density	$\frac{m^2}{s}$
T	Propeller thrust	N
t	Time	s
T	Design draft	m
t	Thrust deduction factor	$-$
T	Transfer term	$-$
T_P	Peak wave period	s
$\vec{u}$	Velocity vector of a fluid particle	$\frac{m}{s}$
U	Forward speed	$\frac{m}{s}$
U_ϕ	Uncertainty	$-$
v_a	Advance velocity	$\frac{m}{s}$
$v_i(t)$	Inflow velocity change	$\frac{m}{s}$
v_s	Ship speed	$\frac{m}{s}$ or kn
V_w	Mean wind speed	$\frac{m}{s}$
w	Calm water wake fraction	$-$
w_i	Term-weights	$-$
z	Height	m
α	Displacement	m^3
α	Constant	$-$
β_P	Hydrodynamic pitch angle	$\circ$
γ	Peakedness factor	$-$
ϵ_ϕ	Discretization error	$-$
$\delta\Omega$	Boundary	$-$
δ_{RE}	Error estimate	$-$
Δ	Ship mass	kg
ζ_a	Incoming wave amplitude	m
η_r	Relative rotative efficiency	$-$
μ	Wave direction	^{o}
ξ	Horizontal wave displacement	m
ρ	Water density	$\frac{kg}{m^3}$
σ	Source strength	$-$
σ	Step function of ω	$-$
σ_{RE}	Standard deviation	$-$
ϕ	Phase difference	$\circ$
ϕ	Unsteady velocity potential	$-$
ϕ_s	Disturbance to the uniform flow	$-$
Φ	Velocity potential	$-$
Φ_s	Stationary velocity potential	$-$
ω	Wave frequency	$\frac{rad}{s}$
ω_e	Encounter frequency	$\frac{rad}{s}$
Ω	Fluid domain	$-$
∇	Displacement	m^3

List of Figures

List of Tables

1 Introduction

1.1 Challenges in Shipping Industry

As global concerns regarding the environmental impact of shipping rise, the quest for more energy efficient propulsion methods becomes not only more necessary, but also more lucrative and interesting. It has been found that about 2.5% of the global greenhouse gas emissions comes from the shipping industry (IMO (2015)). To reduce the environmental impact of shipping, the International Maritime Organisation (IMO) introduced the Energy Efficiency Design Index (EEDI) (MEPC (2011)). This index defines the ratio between the CO_2-production of a ship and the cargo capacity and speed of the ship (Hon and Wang (2011)). In other words, this can be seen as the ratio between the environmental cost and societal benefit of the ship. This index is defined for the design condition of the ship. One way to reduce the EEDI is to reduce the installed engine power of the ship. This can however lead to severe safety issues. When sailing in heavy winds and waves, disturbances to the propeller and engine may occur which can overload the engine or even lead to complete thrust loss of the propeller. These problems show that there is a need in researching what the effect of wind and waves are on the propeller and engine of a ship, in order for shipbuilders to install the correct engine power on their ships and still try to meet the EEDI requirements set by the IMO. These concerns also were the foundation of a new EU funded research project, named SHOPERA, the acronym for Energy Efficient Safe Ship Operations. This project aimed at developing methods, tools and guidelines to effectively address these concerns (Papanikolaou et al. (2015)). One of the objectives was to develop criteria and corresponding environmental conditions to assess sufficiency of propulsion and steering systems of ships for manoeuvrability in adverse weather.

1.2 Knowledge Gap

The propulsive performance of ships is well-known theory. Shipbuilders can accurately calculate what the engine load and the fuel consumption is for specific ship speeds and routes for instance. For the behaviour of ship propulsion in certain sea states, many research has been done specifically in the seakeeping and manoeuvrability performance. Research in the field of dynamic propeller and engine behaviour in adverse sea conditions is however limited. As ship safety goes hand in hand with engine behaviour, it is very important to determine this behaviour in realistic sailing conditions and not only in calm water conditions.

1.3 Problem Definition

1.3.1 Research Goal

This thesis will focus on the disturbances of waves on the hydrodynamic performance of a chemical tanker. This research follows the work of PhD student Congbiao Sui,

who has been working on a 3 degrees of freedom manoeuvring simulation model of the chemical tanker 'Castillo de Tebra'. This model, developed in Matlab/Simulink, predicts the forces and moments on the hull during certain manoeuvring operations in calm water and therefore predicts the travelled distance, velocity, turning circles and other performance characteristics. Accurate engine modelling was included as well.
The goal of the present work however, is to expand this model and predict what these performance characteristics will be when the tanker is sailing in waves coming in at different angles. The disturbances of waves can be categorised into two separate topics, namely the disturbances of waves on the hull and the disturbances of waves on the propeller. On one hand, the waves excite forces on the hull in multiple degrees of freedom, depending on the wave direction, which influence the motion responses of the hull and the ship speed. This specific topic will be researched by Lindert van Tongeren in his thesis. On the other hand, the topic concerning the disturbances of the waves on the propeller will be researched in this thesis. Due to incoming waves, pressure and wake fluctuations will occur around the propeller. This will cause transient changes in the thrust, torque and rotational speed of the propeller and consequently the engine. Not only the waves will have an influence on these characteristics; oblique propeller inflow due to manoeuvring operations will also cause changes in the propeller performance. Ultimately, manoeuvring in waves will have a combination of these effects. By accurately predicting the performance of a vessel in waves, the correct engine power can be installed to ensure safe operations during adverse sea conditions, while still meeting the EEDI requirements for less environmental impact.

1.3.2 Research Questions

It became clear that in order to assure safe ship operations it is necessary to investigate the effects of adverse weather conditions, in this case waves, on the hydrodynamic performance of ships. Therefore, the following main research question is set up:

> **What is the influence of waves on the ship operational safety of the ocean-going chemical tanker 'Castillo de Tebra', sailing forward at its design speed?**

For this research question, a number of sub-questions need to be addressed to make the scope of the research more clear. These are stated below:

> **1. How is ship operational safety defined and how can it be quantified?**
> **2. What methods can be used to determine the influence of waves on the ship operational safety?**

In the present work, the ship operational safety is indicated by the ship thrust availability, especially when operating in adverse sea conditions. Some factors that influence the thrust availability (or unavailability for that matter) are insufficient driving power, thrust decrease due to propeller wake fluctuations, ventilation and

propeller emergence or even complete loss of thrust due to engine failure (Sui (2021)). Quantifying the ship operational safety will be a large part of the present work.

A number of additional research questions that can help bring a good structure to this research are set up as follows:

- What sea states are relevant for the assessment of the propulsive performance of the chemical tanker?
- Using the provided geometrical coefficients and parameters of the vessel, how can a 3D model of the ship hull be made for further use? And how does this hull shape compare to other similar tankers?

1.4 Research Approach

The work done by Congbiao Sui (Sui (2021)) includes an empirical wave and wind model that simulates the effect of certain sea states on the steady wave and wind forces on the hull and propeller wake variation. This model, as said, is based on empirical formulae from literature. Numerical results in the present work are going to expand this model in order to capture more realistic simulations. Wake variation in the propeller plane will specifically be looked at. This requires the use of flow solvers that solve the flow around a floating body, in this case a chemical tanker. The present work will therefore use a potential flow solver to determine the inflow velocity variation at the propeller plane when sailing in waves. This way, the advance velocity variation is determined, which can be used to determine the propulsive performance of the propeller when the open-water characteristics are known. With the known propeller performance, the required engine power can be calculated. Ultimately, the ship operational safety will be assessed on whether the engine reaches its limits in adverse weather.

1.5 Research Boundaries

The present work encompasses a wide variety of research fields, going from manoeuvring behaviour to propeller characteristics and from hydrodynamics to marine engineering. To do the work in an efficient and effective manner, it asks for a closing down the scope of the research. The research boundaries that are set are listed below:

- As this thesis investigates the influence of adverse weather conditions, which consist usually of a combination of hard wind and large waves, only the influence of waves will be considered. The work done by Congbiao Sui (Sui (2021)) included an empirical wind model that predicts the forces the ship experiences due to wind. The present work, as said, only takes into account the influence of the waves on the propulsive performance of the propeller and engine.

- While this thesis focuses on the influence of waves on the propeller and engine performance, one boundary that is set is that propeller ventilation and emergence is not taken into account. This means that the assumption is made that the propeller does not reach above or near the free surface.

- One limit to this thesis is that the 3D hull of the chemical tanker is not readily available, which means that a 3D hull must be made that has similar parameters and shape. With this approach, the results will not 100% represent the the results for the 'Castillo de Tebra'.

- This thesis investigates the ship operational safety. Hereby, engine operational safety is not considered, which is indicated by engine thermal loading, mechanical loading and engine over-speeding (Sui (2021)). Besides that, safety issues such as marine accidents which can be caused by either ship thrust unavailability will not be considered. Environmental impact and consequences on human lives as a result of such accidents will therefore not be taken into account

- When a ship is sailing in waves, the waves excite forces on the hull that add to the total resistance experienced by the ship. These forces are also able to make the ship deviate from it's path if the waves are oblique. Ship speed reduction is also a consequence of added resistance due to waves. This thesis does not consider these forces, as the only interest is about how the waves affect the propulsive performance in terms of thrust and torque generation. Literature is presented on wave excitation, but only for a broader understanding of wave effects.

- This research will consist of calculations done on the propulsive performance based on the design ship speed and design engine speed. This indicates that propulsion control systems are assumed to react instantaneously on feedback differences. Besides that, as mentioned before, ship speed reduction will not be taken into account.

1.6 Original Contribution

One of the main contribution of this thesis is that a quantitative investigation and evaluation is presented of the ship operational safety, specifically the thrust availability of an ocean-going cargo ship with a small EEDI under the influence of waves. Limited research has been done in this field, which makes the present work a valuable asset to the field of ship propulsion in adverse weather. What usually is done in the design phase of a ship is adding a sea margin to the maximum engine power, to account for additional power requirements in adverse weather. The present work will figure out whether this is enough, or that additional measures must be set in place for the benchmark chemical tanker.

Results are presented on a specific operating condition in terms of ship speed and engine speed. However, recommendations will be given on where improvements can

be made on the calculations. On the other hand, alternatives will be introduced to omit engine overloading.

In relation to the work done by Congbiao Sui (Sui (2021)), the contribution of this thesis is that the empirical wave disturbance model is expanded with verified numerical results. These results are obtained using a 3D hull shape geometry that is similar to the hull shape of the benchmark chemical tanker.

1.7 Ethical Principles

When conducting research for a university or a company, ethical principles need to be taken into account. These consist of for instance honesty, objectivity, carefulness, respect for intellectual property and many more (Shamoo and Resnik (2009)). With honesty comes honestly reporting data, results, methods and procedures. Data will not be fabricated, falsified or misrepresented. With objectivity comes presenting the data and results without any biases. With carefulness comes avoiding careless errors and negligence in data analysis. With respecting intellectual property comes not using unpublished data, methods or results without permission from the company. These ethical principles will be maintained throughout the entire research process.

Besides the ethical research principles, it is also important to think about how the present work touches on ethics in engineering. To begin, reducing green house gas emissions is a topic that all engineers should be focused on doing within their respective field of work. This is necessary to combat negative climate change. Diving into the present work, passenger and crew safety is also an ethical topic that is brought up. The research will investigate whether the ship is underpowered in adverse weather or not. Underpowered ships mean that the engine must deliver more power than it has available. This could result in engine overloading or even complete shutdowns. A consequence hereof could be that the safety of all people on board could be in jeopardy. Loss of life is something that engineers must avoid at all cost. Therefore, the present work will result in a conclusion on whether crew safety is maintained in adverse weather or not.

1.8 Thesis Layout

In this section, a depiction will be given on how the present work will be divided into separate chapters.

Chapter 2: Literature Review

Chapter 2 of this thesis will present the literature review. Three main topics will be discussed here, which are wave excitation, propeller (and engine) theory and manoeuvring & seakeeping behaviour. State-of-the-art research will be reviewed and conclusions will be drawn thereof.

Chapter 3: Methodology

Chapter 3 discusses the methodology of this thesis. The findings of the literature review will help in figuring out a way of doing the research effectively and efficiently, which results a concise description of the methodology.

Chapter 4: Flow Solver & Seakeeping Tool 'SEACAL'

Chapter 4 will introduce the seakeeping tool SEACAL, which will be used to determine the inflow velocity of the propeller when a ship sails forward in different wave directions. The mathematical and numerical theory behind the software will be briefly elaborated, followed by the required inputs. Results will be shown, followed by the processing of these results to acquire time records of the inflow velocity changes in a range of wave directions. Finally, the solutions will be verified using a grid convergence study.

Chapter 5: Ship Propulsion in Adverse Weather

Chapter 5 uses the acquired results to determine the propulsion capability of the ship in adverse weather. Propeller thrust and torque will be determined and used to investigate whether the engine has enough power to deliver the required torque to the propeller. A discussion will follow on what assumptions have been used and what would be more realistic results if these assumptions were not taken into account. Finally, conclusions are drawn on the effects of waves on the available engine power. Here, the research question will be answered to finalize the thesis.

Chapter 6: Conclusions & Recommendations

The final chapter of this work includes the conclusions that are drawn from the research that has been done. Besides that, a number of recommendations will be given on how this work can be improved and where opportunities lie in the field of ship propulsion in adverse weather conditions.

2 Literature Review

The following section will comprise of a review of research that has been done in the multiple fields that encompass this thesis. As the goal is to determine the propulsive performance of the chemical tanker, while sailing in waves, it is required to gather research in the following three fields: Wave excitation, propeller performance and seakeeping & manoeuvring behaviour. Besides that, a brief review is done on the dynamic engine-propeller interaction when a ship operates in waves.

2.1 Wave Excitation

There are multiple reasons to investigate the effects of wave excitation in relation to this thesis; waves cause added resistance to ships, increased fuel consumption and speed reduction. Besides that, waves cause motions responses that can impair safety by means of wave slamming or water on deck (Journée and Massie (2015)). In this section, a summary is given on numerous research that has been done in the field of wave effects on ships. This includes multiple methods to determine certain wave effects such as added resistance.

2.1.1 Computational Methods

Research in determining the wave drift forces dates way back to 1976, where Pinkster and Hooft (1976) introduced a computation method that is based on direct pressure integration over the wetted hull. By integrating the pressure of the water over the wetted hull, the total force on the hull can be calculated. Faltinsen and Loken (1978) used a similar approach on a two-dimensional cylinder in beam waves. Their research resulted in a complete solution that includes the mean wave drift force and low-frequency oscillating wave drift force in regular wave groups. It has been found that methods based on potential theory give good results for ships when compared to model tests.

Most computational methods that approach the problem of a ship advancing in waves rely heavily on the assumption that it can be represented by a linear system, in which the motion response amplitudes are linearly related to the incoming wave amplitude. Strip theory is a method that has been widely adopted early which uses aforementioned assumption. Strip theory is a potential flow method that divides the ship hull into a series of two dimensional cross-sectional strips, on which the hydrodynamic forces are computed separately. This method was first applied by Korvin-Kroukovsky and Jacobs (1957). They calculated the heave and pitch motions of a ship in regular waves. A disadvantage of this method is that it has shortcomings when it comes to asymmetrical motions such as roll, sway and yaw motions. This is mainly due to the three-dimensional flow that has large longitudinal interactions between the steady and unsteady flow. However, for a wide range of seakeeping applications it is still used as it is computationally cheap and gives reasonable estimates

of the motion behaviour of ships in waves.

Another method that approaches the problem of ships advancing in waves is the Rankine source method, which is also a potential flow method, based on the work of Dawson (1977). Here, Rankine sources are distributed over the free surface and the body surface satisfies a quasi-linearised free surface conditions. Bertram (1990) and Van't Veer (1998) developed and applied the method based on Dawson's method to ships having a forward speed.

The following will cover research that has been done in the field of mainly added resistance, as this causes a significant change in the propulsion performance of a vessel. This also contributes substantially to the operating cost of a ship, as more resistance means more power required for propulsion, thus needing more fuel. Söding and Shigunov (2015) have presented results of three different methods, namely potential second-order methods, that calculate the stationary (drift) forces and moments in regular waves. The three methods that have been presented are the Rankine source method, the Strip method and the Lee method. Conclusions from their research were that the Rankine source method and the Lee method appear to be suitable in predicting useful estimates of the added resistance. Where the Strip method fell short in wave lengths larger than 0.8 times the length of the ship and even gave unacceptable results for shorter wave lengths, the Rankine method and Lee method can actually be used with accurate results to optimise main dimension and block coefficients of ships, taking into account the effects of the seaway.

Continuing on the subject of added resistance, Crepier et al. (2019) have conducted research on the determination of added resistance in waves using Computational Fluid Dynamics (CFD). Where the Rankine source method and the Strip method use potential flow theory, in which the flow around a body is assumed to be inviscid and irrotational, CFD captures most flow characteristics, depending on the settings that are used. The use of CFD requires a lot of time and computational power. Therefore, usually it is not used when determining the operational performance of the vessel. Potential flow methods are still widely used as these are fairly reliable and quick. However, the assessment of the added resistance using CFD can still be relevant. The work done by Crepier at al. has demonstrated that the traditionally assumed quadratic relationship between the wave amplitude and the added resistance only is partly valid. The study presented results of performance calculations by the CFD solver ReFRESCO. Experiments were also carried out as well as calculations using the Rankine source potential flow solver FATIMA. All results were compared with each other and showed good agreement. This indicated that potential flow methods were sufficiently reliable in determining the added resistance of a ship in waves.

2.1.2 Conclusions

It can be concluded that determining the forces that occur when a ship advances in a seaway can be done rather reliably and fast using potential flow methods. In

particular, the Rankine source method stands out. The computational effort and time that is lost when using other methods such as CFD, are won in terms of accuracy. For the present work, excitation forces of waves will not be considered. However, it is useful to understand the principles of wave excitation forces as this takes a big part in manoeuvring operations and seakeeping in general.

2.2 Propeller & Engine Operating in Waves

This section will comprise a summary of research that has been done in the field of propeller and engine performance. Specifically, how propellers react to adverse sea conditions, and how the propeller performance can be determined numerically. Some research in the field of the dynamic engine-propeller responses will also be presented.

2.2.1 State-of-the-Art

Propellers are traditionally designed and optimized in calm water conditions. However, these are not realistic conditions. Ships regularly sail in waves, both short and long waves. These waves have a considerable effect on the propulsive performance of the propeller. Nakamura and Naito (1979) have shown by means of experiments that self-propulsion factors such as the wake fraction and thrust deduction vary with wave length in regular head waves. Besides that they have shown that propeller open-water efficiency decreases with increasing wave height in irregular waves. This would mean that for different wave heights, more power is needed to achieve the same ship speed as in calm water. Some other conclusions of their work is that the propeller load fluctuations in irregular waves can be predicted using open-water propeller characteristics. These fluctuations are mainly caused by the fluctuation of axial inflow velocity into the propeller disk.

Continuing on the research of Nakamura and Naito, Faltinsen (1980) proposed a procedure for calculating added resistance, transverse drift and mean yaw moment on a ship in regular waves of any wave direction. They touch upon the influence of wave induced motions on the propeller wake, open water characteristics and thrust deduction. The results of Nakamura and Naito's research in terms of the change of the propeller wake is elaborated by calculating the boundary layer and then using that to determine the change of the wake distribution and comparing it to the results of Nakamura and Naito. Similar results were obtained.

Taskar et al. (2015) have performed calculations on power increase and fuel efficiency decrease for one case vessel in waves. It was shown that even when the added resistance of the waves is neglected, fuel consumption is still increased by considerable amount when the ship travels in waves. This was mainly due to a change in the wake distribution behind the ship and propeller and surge motions of the ship. Engine-propeller interaction, specifically the engine dynamic response, was also taken into account. Some other conclusions from this paper are that changes in torque are mainly driven by average wake. Changes in the wake distribution mainly contribute to

pressure pulses and cavitation, and not so much on the average torque. As mentioned, their work neglects the effects of added resistance. Their reasoning for excluding this effect was to observe the effect of surge, wake change, out of water effect and engine dynamic response primarily. They state that the added resistance naturally is an important factor in increasing fuel consumption and decreasing efficiency. However, also due to length restrictions, they chose to leave it out of their scope of research.

2.2.2 Computational Methods

For the performance calculations of the propeller, the boundary element method (BEM) can be used. This method, that solves the incompressible potential flow is the PROCAL code, developed by Maritime Research Institue Netherlands (MARIN) within the Cooperative Research Ships (CRS). It is developed for the unsteady analysis of cavitating propellers operating in a prescribed ship wake (Bosschers et al. (2015)). Validation has been done for open water characteristics, shaft forces and moments, sheet cavitation extents and propeller induced hull–pressure fluctuations. The PROCAL code is a low order boundary element method that uses the Marino formulation (Bosschers (2009)) that solves for the velocity disturbance potential. Details on the mathematical and numerical model can be found in Vaz and Bosschers (2006) as well as in Bosschers (2009).

Rijpkema et al. (2013) have studied the propeller-hull interaction, using a combination of a steady viscous CFD method (RANS) for the ship flow and an unsteady potential-flow method (BEM) for the propeller loading. A propeller operating behind a ship causes interaction effects to occur which affect the resistance of the ship as well as the loading of the propeller. The research done here focuses on determining the effective wake field of the propeller. The RANS-BEM coupling they introduce provides an alternative way of obtaining the effective wake field. The BEM induced velocities are subtracted from the RANS computed total wake. This allows the determination of the effective wake directly at full scale Reynolds numbers, without the need of simulating both the ship and propeller using a viscous CFD approach which would requires large and complex grids and therefore large computation times. The following options to obtain the effective wake were given:

- Determine the effective inflow in a straight plane upstream of the propeller.
- Evaluate the effective inflow as close to the propeller as possible.
- Extrapolate the effective wake from two or more planes upstream of the propeller towards the propeller plane.

It became clear that extrapolation of the effective wake in downstream direction towards the propeller plane resulted in axial velocity increase which in turn resulted in an increase of 2 to 3% in rotation rate, when compared to a plane upstream of the

propeller. It must be noted that the effective inflow of the propeller was first determined using a RANS simulation, where the total wake field was subtracted with the induced velocities of the propeller that were computed using BEM, which provided the time-averaged body forces for different blade positions. The initial BEM calculations use the nominal wake field, which is a good initial condition since the nominal wake field has similarities to the effective wake field and also acts as a reference to the effective wake field. One shortcoming of the work discussed here in relation to the present work is that it was done in calm water conditions (steady flow). The present work ultimately aims at determining the propeller loads in a seaway.

Continuing on the effective wake field of a propeller, Ueno et al. (2013) have found a way to estimate and predict the effective wake field of a propeller in waves. The authors, by means of free running tests with a container ship model, used the open-water characteristics of a propeller to determine the effective inflow velocity by keeping the relation of the thrust and torque to the inflow velocity. They also applied theoretical estimates using a strip method to compare it with experimental data. The end product was a prediction model that determines the inflow velocity of a propeller in waves.

2.2.3 Engine-Propeller Coupling

Taskar et al. (2016) have shown that engine-propeller response such as power fluctuations, propeller speed fluctuations and torque fluctuations can be obtained through simulating the coupling between engine and propeller models. The presence of waves has a significant effect on the propulsion performance, compared to steady state operations. The direction of the waves also has a strong influence on the performance drop. Head sea conditions and bow quartering waves affect the performance the most. This work clearly shows that there is a need in accurately simulating the coupling between the engine and propeller when a ship is subject to waves.

Saettone et al. (2020) touch also upon the dynamics between the propeller and the engine when waves are considered. The purpose of their work was to determine the importance of time-varying wake field, ship motions, propeller emergence and engine response on the performance of a marine propulsion system in waves. Their propulsion system was modeled at three different complexity levels. The first is the steady-propeller engine model, which is the traditional way to estimate propeller performance in waves. The wave effects herein are only considered in the form of added resistance and change of propulsion point. Ship motions, propeller emergence and time-varying wake fields are neglected. The second model is the unsteady propeller-engine model with fixed engine speed. Herein, the engine speed is assumed to be time-invariant. However, ship motions, propeller emergence and time-varying wake are taken into account. The third model is the unsteady propeller-engine model with PID, in which all above mentioned conditions are taken into account, in addition to a PID controller that regulates the engine speed, which inherently means that the engine torque and speed are time-variant. Results of this work illustrate that there is

a considerable difference in engine torque and propeller efficiency between the steady and unsteady models, even when the propeller is far from the water surface. This concludes to the indication that neglecting time-varying wake field, ship motions and propeller emergence would lead to inaccurate prediction of the propulsion system performance in the presence of waves.

2.2.4 Conclusions

Again it becomes clear that potential flow theory can be used in determining the performance of a propeller with low time and computational effort. Especially the use of PROCAL seems interesting as this used the ship wake field as input, which can be determined from the potential flow theory that will be used on the ship when determining the forces and flow that occur due to the waves. Besides potential flow theory, the propeller performance can also be determined using the open-water characteristics of the propeller. This will be based on the average inflow velocity that the propeller experiences, which can also be determined from the flow solver on the ship hull. Both methods can also be done simultaneously and compared with each other.

What needs to be considered in the present work, is whether the research that comprises of the different types of propeller wake fields is useful. It gives a clear insight into how waves can affect the performance, but as said multiple times before, the usage of CFD takes up a lot of computational effort and time. For the present work it has been decided that CFD will not be used, which indicates that the determination of the complete wake distribution of the propeller will be left out. The corresponding literature has been added to the present work to give a more complete picture of what actually happens when a propeller operates in waves.

Finally, it became clear that the engine-propeller coupling needs to be simulated to accurately predict the propulsion performance of a vessel. Whether time-varying wake fluctuation for instance is taken into account or not can heavily affect the outcome of the simulation.

2.3 Manoeuvring and Seakeeping

Two main theories traditionally cover the study of ship dynamics: manoeuvring and seakeeping (Fossen (2011)). Where manoeuvring theory studies the motion of a ship in absence of wave excitation, seakeeping theory studies the motion of a ship while on constant heading and speed when there is wave excitation. For the present work, the influence of the waves on the propeller and engine performance will ultimately be tested on how it affects straight forward sailing of the chemical tanker. For further research, manoeuvring operations should also be looked into. Therefore, literature will be presented that encompasses manoeuvring and seakeeping.

2.3.1 Seakeeping

The seakeeping of ships is a topic that tries to investigate a number of issues. These go from determining the maximum speed in a seaway, figuring out if the structural design of a ship is capable to withhold certain seaway loads, investigating the habitation comfort and safety of people on board and operational limits for ships (Bertram (2012)). Seakeeping behaviour can be determined with many tools, but mainly relies on representing the natural seaway as a superposition of many regular (harmonic) waves, followed by calculating the reactions of ships in these waves and adding all separate reactions to a total reaction. Tools that predict seakeeping range from model tests, to full-scale measurements on ships at sea. Computations can also be done in either the frequency domain or time domain. Most seakeeping methods are linearized, which indicates that the ship reactions are proportional to the wave height. This drastically reduces the computation time. For extreme motions, such as capsizing investigations, non-linear computations need to be done.

2.3.2 Manoeuvring

The theory of ship manoeuvring mainly focuses on course keeping, course changing, track keeping and speed changing (Bertram (2012)). The manoeuvrability of a ship can be described by a couple of characteristics, being: initial turning ability, sustained turning ability, yaw checking, stopping ability, and yaw stability. As with the seakeeping of ships, manoeuvring concerns the time-dependent motions of a ship. In both fields, the main difficulty lies in determining the fluid forces on the hull due to the ship motions and waves. one thing that differs both dynamics is that manoeuvring is often investigated in shallow and usually calm water. Secondly, seakeeping dynamics can be approximated with linear relations between velocities and forces. In manoeuvring, this can only be applied for small rudder angles. Due to this difference, seakeeping is mostly investigated in the frequency domain and manoeuvring in the time domain. Finally, the motion equation in seakeeping are written in an inertial coordinate system, whereas a ship-fixed coordinate system is used in the manoeuvring
.

2.3.3 Computational Methods

Numerous research has been done in the field of predicting the manoeuvring and seakeeping behaviour of ships in waves. For instance, Skejic and Faltinsen (2008) have presented a theoretical study of combined seakeeping and manoeuvring of a ship in regular incident waves. A real-time simulation program was developed that is based on theoretical methods. As there are many sub-problems in a manoeuvring model, such as resistance, propulsion and calm water manoeuvring, a balance had to be made of how theoretically accurate each sub-problem should be. The authors in this research pursued a certain level of simplicity in their model, in order to satisfy the requirement of real-time execution of the ship manoeuvring simulation. This simplicity led to them not taking into account the change of propulsive coefficients such as wake fraction and thrust deduction due to sailing in waves. These changes however

will have significant impact on the propulsive performance of a ship in waves and will be looked into in the present work.

Quadvlieg et al. (2019) have presented a validation against model tests in which two tools are introduced that are able to simulate course and/or track keeping simulations in waves and wind. The first tool, called ManWav, is developed by the Cooperative Research Ships (CRS) and is a time domain simulation tool able to accurately predict the sustained ship speed, track and drift angle in wind and waves conditions. The second tool, called FREDYN, is developed by the Cooperative Research Navies (CRN) and is a fully coupled seakeeping and manoeuvring time domain tool. Where ManWav is classed as a "two-time scale method", which solves the equations of motion separately from each other, FREDYN is a "unified method", which acknowledges the fact that there is a coupling between the manoeuvring motions and the seakeeping motions. A technique is used of translating the frequency response in time domain using convolution integrals or impulse response functions. The equations of motions are solved as a system of ordinary differential equation, which take into account all forces and moments.
A number of advantages and disadvantages of both methods have also been presented. ManWav has an advantage that it computes the ship motions in a low frequency manner, which allows for an easier understanding of the results. A disadvantage is that the motions and waves remain in the linear range. This means that first-order phenomena cannot be included in the equations of motion. The advantage of FREDYN is that in extreme waves and under extreme angles, a complete force is modeled. However, due to the complex modeling, this leads to difficulties when trying to understand the results. Another disadvantage is that such strong coupling between the manoeuvring and seakeeping forces together with the non-linear forces result in incomplete second order wave drift forces. This is due to the fact that the wave elevation and the orbital velocities around the hull are limited to the sum of the undisturbed incoming wave and first order ship motions. FREDYN does not take into account the diffracted and radiated waves in order to calculate the relative wave elevation. The results of the validation in this research have shown that the predictions using ManWav are better than the results using FREDYN. ManWav provides a better estimate of the sustained ship speed and drifting velocity. FREDYN however shows that it performs better in higher sea states, which the tool was actually developed for.

The two-time scale method separates the seakeeping problem and manoeuvring problem and solves them along side each other. The separation is due to the assumption that the time scale of the waves varies rapidly (wave-frequency part), whereas the manoeuvring motion time scale varies slowly (low-frequency part). The full analysis is conducted similar to the analysis of manoeuvring in calm water, where the only addition being the consideration of wave effects as external sources of forces and moments (Tello Ruiz (2018)). Other work that has been done using the two-time scale method can be found in Seo and Kim (2011) and Zhang et al. (2017).

The main purpose of the unified method is to integrate the hydrodynamic phe-

nomena which correspond with body reaction forces and moments, also known as the radiation problem. Fossen (2005) developed a unified model for manoeuvring in a seaway by using the approach of using linear convolution integrals. These convolution integrals are a result of the frequency-dependent potential and viscous damping terms. Other work on unified methods include Sutulo and Soares (2006) and Subramanian and Beck (2015).

Bunnik et al. (2010) have compared a wide range of seakeeping methods and tools. They concluded that the best motion predictions are obtained by the so called double body (DB) method from Delft University of Technology and the non-linear steady (NLS) method from MARIN. Both methods make use of linear potential flow codes, where the DB method applied it in the frequency domain and the NLS method in the time domain. Both solutions are computed using Rankine sources on the free surface and the ship hull. The frequency-domain approach, which is a linear model is the fastest, as the time-dependence can be removed by assuming that the solution is harmonic in time. This however limits the simulations to only one frequency at a time. The time-domain approach is used when no assumption is made on the time behaviour of the solution. This is useful when random seas are simulated, as irregular frequencies might appear at which the solution becomes unbounded.

Computational Fluid Dynamics ultimately is the way forward, as the level of detail that can be captured with it is better than with the potential flow approaches. In recent years, CFD has been enhanced significantly with multiple studies presenting steady problems such as resistance and stationary manoeuvres. Due to the complexity of the fluid problem, CFD is demanding more time and recourses for full solutions, especially for unsteady problems such as manoeuvring in waves. Work done in this field can be found in Carrica et al. (2013) and Wang and Wan (2018).

Finally, a brief discussion will be done on experimental approaches of manoeuvring in waves. Scale model experiments still remain one of the most suitable methods of investigating the effect of wave forces on the manoeuvring performance of a ship. Experimental studies on ship manoeuvrability in waves date back to 1980, where Hirano et al. (1980) carried out turning circle tests of self-propelled RoRo model ships in regular waves. Ueno (2003) used a typical VLCC model ship to perform manoeuvring tests in regular waves. Yasukawa and Faizul (2006) also carried out turning tests, zig-zag manoeuvres and stopping tests with a SR108 container vessel in waves. More recently, Guo and Steen (2010) published data on experiments that were conducted on the KLVCC2 standard tanker in regular head waves at different speeds.

2.4 Summary and Discussion of Literature

In table 1, different methods are summarized for the three different topics. It must be noted that the mentioned methods do not encompass all the methods that exist for the specific topics. Rather, these are the methods that are most widely used and

matter the most when choosing the right method for this research.

Table 1: Summary of methods per research topic

Propeller & Engine Dynamics	Wave Excitation	Manoeuvring & Seakeeping
Experimental approach	Experimental approach	Experimental approach
Analytical approach	Analytical approach	Two-time scale method
RANS-BEM coupling	Rankine source method	Unified method
Coupled Simulation	Strip method	CFD
	CFD	

It becomes clear that for every topic, there exist experimental and analytical approaches. Experiments are carried out to validate the mathematical or numerical models that are developed or to capture unknown phenomena. Numerical simulations are carried out to verify the mathematics and physics involved in the theoretical models. The summary and comparison of the methods needs to provide a platform to determine what methods are going to be used in this research. The following conclusions can be made based on the literature review that has been done:

- The most used methods for the determination of the added resistance of ships are potential flow methods. The Rankine source method seem to be most suitable (Söding and Shigunov (2015), Bertram (1990), Van't Veer (1998)). CFD can also be used to determine the wave forces with more accuracy, however this comes with a lot more computational effort and time (Crepier et al. (2019)).
- The topic that covers the propeller performance introduced a number of methods that have been used to determine the effects of waves on propeller wake and performance (Taskar et al. (2015); Nakamura and Naito (1979); Rijpkema et al. (2013)). These methods consisted of experimental approaches, analytical approaches and the boundary element method.
- For predicting manoeuvring and seakeeping behaviour, most methods consist of two-time scale methods (Skejic and Faltinsen (2008)) and unified methods (Fossen (2005)).

From the work by Söding and Shigunov (2015), it can be concluded that the Rankine source method is best suited for determining added resistance of ships in waves, as the range of wave lengths in which it works accurately is not limited, as is with the Lee method.

Interesting literature on the propeller and engine dynamics has shown that propeller load fluctuations can be determined using propeller open-water characteristics, as these fluctuations are caused by axial inflow velocity fluctuations at the propeller disc. Besides that, torque fluctuations are mainly caused by average wake change and not so much on the actual wake distribution at the propeller disc. These conclusions will be taken into account in the present work.

From the elaboration in the previous chapter on the two-time scale method and unified method, it can be said and seen that they are based on the general assumption that the fluid effects can be separated into two main components, namely a seakeeping contribution and a calm water manoeuvring contribution. These are dominated by potential flow and viscous flow, respectively. The two-time scale method has the characteristics that the 6DOF problem is simplified in a 4DOF problem, where the first order wave contributions are neglected. Second order wave forces and moments are only accounted for. The unified method however tries to aim at a 6DOF manoeuvring problem. The wave forces are considered to be linear and by means of a correction for the Froude-Krilov forces and moments can be seen as somewhat nonlinear.

2.5 Gap Analysis

It is important to distinguish what research already has been done and what can be used for the present work. Most of the research that has been found, was research that investigated the effects of waves on specific part of the hydrodynamic performance of a ship. For instance, research was carried out specifically on the wake distribution of the propeller, where other research only investigated the added resistance and drift forces of waves on the hull. However, research has also shown that manoeuvring simulation in waves are something that has been looked at for a long time already. What became clear in for instance Skejic and Faltinsen (2008) is that models are developed that simulate the manoeuvring of ships in waves, but a touch of simplicity is added to make a balance in the sense that not every sub-problem in this simulation is approached with the utmost of accuracy.

Something that also became clear from the literature review, is that most research that tries to find the effects of waves on either the propeller performance or the manoeuvring behaviour of ships, only takes into account regular head waves. This is again a touch of simplicity that is added to most research. The present work however will include irregular waves in the process as well, considering multiple wave directions.

When talking about the propeller performance, most research takes into account uniform inflow when calculating the characteristics of the propeller (Skejic and Faltinsen (2008), Ueno et al. (2013)). Taskar et al. (2015) touch well upon the actual wake distribution in waves and state that wake data in waves is rarely available. Model scale wake was made available, but had to be contracted to obtain the ship scale wake. The work done by Taskar et al. will be a good reference point for the present work as it encompasses the same goal of the present work; finding the effects of waves on engine-propeller dynamics and propulsion performance of ships.

When manoeuvring operations are taken into account in the present work, Quadvlieg et al. (2019) present useful methods for the determination of the manoeuvring behaviour of ships in waves as a reference. Combining the propeller performance

determination as well as the manoeuvring behaviour insights, a better prediction of hydrodynamics in adverse weather can be investigated.

2.6 Conclusions

The underpowering of ocean-going ships due to new regulations concerning the environmental footprint of ships calls for accurate predictions of ship propulsion performance in adverse weather conditions. Due to heavy winds and waves, loss of power can occur when performing certain manoeuvring operations. The present work will investigate the effects of waves on the propulsive performance of the chemical tanker 'Castillo de Tebra'. Specifically, the wake fluctuations at the propeller will be determined under the influence of waves. With this, the propeller performance will be determined and ultimately it will be investigated whether the ship is underpowered in adverse weather or not.

Numerous research has been found that deals with the three topics that the present work encompasses, namely wave effects, propeller performance and manoeuvring/seakeeping behaviour of ships in adverse weather conditions. The literature review that has been presented gave an insight into a range of methods that have been used in determining certain aspects of wave influences on the propeller and also on the manoeuvring behaviour. What became clear is that when dealing with wave excitation forces, potential flow methods do the trick fairly accurate and cheap, compared to more accurate but significantly more expensive CFD methods.

When speaking about the propulsive performance of a ship in waves, research has shown that self-propulsion factors, such as thrust deduction and wake fraction change when a ship sails in waves. This would indicate that more power is needed, when sailing in adverse weather conditions. Besides that, changes in the wake distribution of the propeller have been shown to only affect the pressure pulses and cavitation along the propeller blade, and not so much on the average torque. The dynamic engine-propeller behaviour has also been investigated, which led to the conclusion that modeling the engine-propeller response in a steady solution or an unsteady solution changes the propulsive performance significantly. The difference herein is time-varying wake fluctuations and engine torque.

Finally, research has shown two main methods are used when modeling and simulating manoeuvring operations of ships, namely the two-time scale method and the unified method. In the two-time scale method, the seakeeping and manoeuvring problems are separated from each other, but solved along side each other. This is due to the varying time scale of the waves and manoeuvring motions. In the unified method, both problems are integrated. Usually, the two-time scale method reduces the problem to a four degrees of freedom model, whereas the unified method aims for a six degrees of freedom model.

3 Methodology

This section will cover the final choices that have been made regarding the methodology of the present work. Findings from the literature review will be used to make a concise structure of what needs to be done to reach the goal of this thesis.

3.1 Method Choice

From the previous section, it became clear that potential flow methods can be used for both the propeller performance determination as well as the calculation of wave forces on the ship. Therefore, a potential flow method will be used to acquire the velocity profile at the propeller plane. This will be determined by firstly acquiring the flow solution over the hull using potential flow theory. MARIN has made the software program SEACAL available for use, which is a continuation of FATIMA (Bunnik (1999)). Herein, reference points can be added to determine the velocity variations at the propeller disk at a range of wave frequencies and directions. These fluctuations are given in the form of response amplitude operators (RAOs) and phase shifts, indicating a frequency domain solution. The fluctuation over time, therefore the time-domain solution, can be analytically determined by transforming the wave responses using a cosine function and wave spectra.

Adding a large range of reference points at the propeller disc will lead to obtaining the nominal wake field of the propeller, assuming a potential flow solution, which can be used to further determine the actual propeller performance by for instance running the PROCAL code and extracting the propeller forces. For the present work, the propeller performance will be determined analytically using known open-water characteristics of a chosen propeller. Hereby, the propeller wake will be averaged over the reference points to have a uniform inflow for the calculation of the forces of the propeller.

Now that the velocity fluctuation at the propeller plane is known for a large range of regular and irregular waves, the results are used to determine whether the ship has enough power to propel the ship at the given conditions. The velocity fluctuations namely cause thrust and torque variations over time, which result in time-varying engine loads. By means of the engine operating envelope, it can be investigated whether the propeller load exceeds the engine limits. Looking at all wave directions, an assessment can be made on what wave directions cause the largest engine load fluctuations. A final conclusion will be drawn on the effect of waves on the hydrodynamic performance of the 'Castillo de Tebra'.

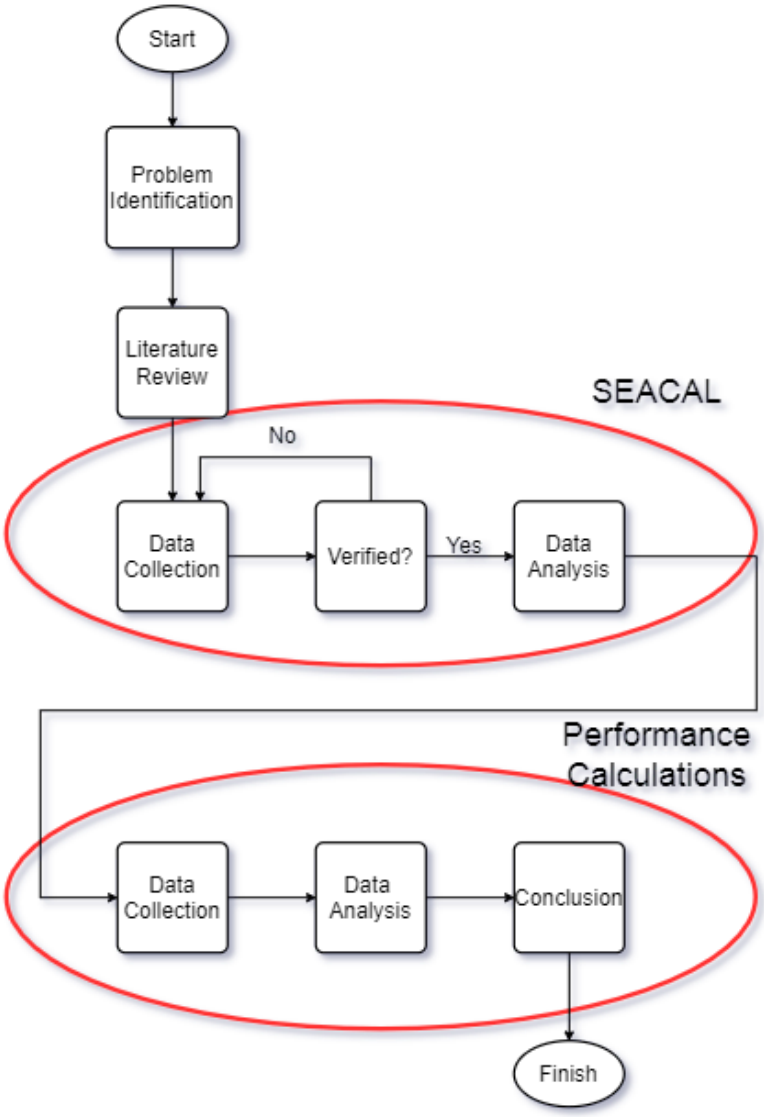

Figure 1: Research Methodology

In figure 1 a flowchart is visualized on how this thesis is decomposed in different processes. As can be seen, it is firstly separated in a part where SEACAL is used and results are analyzed and verified and secondly in the determination of the propulsive performance of the vessel in adverse weather. For both parts, data collection and data analysis are the core processes. The SEACAL part also comprises of data verification in the form of a grid convergence study.

3.2 Adressing the Research Questions

The methodology presented in this section has the aim to reach the goal of this thesis, which is to answer the research questions. The main research question is:

> **What is the influence of waves on the ship operational safety of the ocean-going chemical tanker 'Castillo de Tebra', sailing forward at its design speed?**

With the sub-questions being:

> **1. How is ship operational safety defined and how can it be quantified?**
> **2. What methods can be used to determine the influence of waves on the ship operational safety?**

The second sub-question is now answered by means of the presented methodology, namely using potential flow for the velocity variations at the propeller plane and afterwards analytically determining the propeller performance in terms of thrust and torque. These results will ultimately be used to determine what the ship operational safety be, by looking at the available thrust at the design speed and investigating whether the produces more than the available thrust or not. Conclusions for the main research question will now be drawn in the next sections after the research has been completed.

4 Flow Solver and Seakeeping Tool 'SEACAL'

This section will provide the mathematical and numerical theory that defines the seakeeping tool SEACAL that will be used in this research. Additionally, the input parameters as well as the acquired results will be discussed here. SEACAL is a software program that calculates ship behavior in waves. At an arbitrary speed and heading, the response to waves can be calculated. The program consists of 3 main programs, namely HYDMES, HYDCAL and RESCAL. HYDMES generates the hull surface description with 3D panels, HYDCAL calculates the hydrodynamic coefficients by solving the linearized boundary value problem. This means that small oscillatory ship motions and waves are assumed. RESCAL calculates the response of the ship in waves by solving the equations of motion. The theory manual of SEACAL (Van Daalen and Bunnik (2021)) is used as a reference. Also, Bunnik (1999) is used for additional theory.

4.1 Mathematical Theory

There are numerous ways to model the flow of water around a ship. The Navier-Stokes equations give the most exact description of the flow, which take into account the viscosity. Viscosity becomes important in areas where the flow is turbulent, such as near the propulsor, rudder and sharp edges of the hull. These viscous areas however do not contribute much to the large-scale interactions of ocean waves and ship motions. Besides that, taking viscosity into account would lead to complex and time-consuming problems. For that reason, viscosity has been neglected in the present work and use if made of potential theory to describe the flow of water.

A complex combination is formed when the fluid and ship are studied together, as they have typical characteristics but also interactions with each other. Due to the moving fluid, unsteady forces and moments are generated around the ship because of pressure changes in the fluid. The following mathematical descriptions will incorporate the behaviours of the fluid and the ship, as well as some conditions that describe the interaction between the two.

As said, viscosity is neglected. If the flow is assumed to be irrotational and incompressible as well, a velocity potential Φ exists, of which the gradient is the velocity of a fluid particle:

$$\vec{u} = \vec{\nabla}\Phi \tag{4.1}$$

From the conservation of mass, the Laplace equation follows which is satisfied inside the fluid domain:

$$\Delta\Phi = 0 \tag{4.2}$$

The solution of the Laplace equation is unique if a linear combination of the potential and its normal derivative is given on the boundaries of the fluid domain and if

in at least one point the potential is given. The solution is determinate. However, it is a constant if the value of the potential is nowhere specified. This constant disappears after differentiating, which indicates that it has no influence on the velocity field. By this reasoning, there must be conditions on the boundaries of the fluid domain, that relate the potential and its normal derivative. These boundaries are the free surface, the bottom of the water and the hull of the ship.

4.1.1 Sign Convection

The right-handed Cartesian coordinate system is used to formulate the mathematical model. Hereby, two coordinate systems are distinguished which are formulated as follows:

- Ship-fixed: Here, the origin it at the intersection of aft perpendicular, centerline and keel line of the ship. The x-axis points towards the bow, the y-axis points towards port side and the z-axis points upward.
- Global: Here the origin is in the calm water surface with the x-axis being parallel to the x-axis of the ship.

4.1.2 Boundary Conditions

First the free-surface boundary condition will be discussed. Here, two physical conditions hold, namely the dynamic and the kinematic condition. The dynamic condition states that the pressure on the free surface should be equal to the atmospheric pressure. The pressure follows from the Bernoulli equation:

$$-\frac{p-p_0}{\rho} = \frac{\partial \Phi}{\partial t} + \frac{1}{2}\vec{\nabla}\Phi \cdot \vec{\nabla}\Phi + gz - \frac{1}{2}U^2 \tag{4.3}$$

When the atmospheric pressure is imposed on the unknown free surface $z = \zeta$, the dynamic free-surface condition is given by:

$$\zeta = \frac{-1}{g}\left(\frac{\partial \Phi}{\partial t} + \frac{1}{2}\vec{\nabla}\Phi \cdot \vec{\nabla}\Phi - \frac{1}{2}U^2\right) \quad \text{on } z = \zeta \tag{4.4}$$

The kinematic boundary condition states that a fluid particle cannot leave the free surface. This is described by:

$$\frac{\partial \Phi}{\partial x}\frac{\partial \zeta}{\partial x} + \frac{\partial \Phi}{\partial y}\frac{\partial \zeta}{\partial y} + \frac{\partial \zeta}{\partial t} - \frac{\partial \Phi}{\partial z} = 0 \quad \text{on } z = \zeta \tag{4.5}$$

The bottom of the water is a fixed boundary, where no fluid particles can cross it. The implies that the normal velocity of a fluid particle at the bottom should be zero and that only a tangential component is allowed. This is expressed as follows:

$$\frac{\partial \Phi}{\partial n} = 0 \quad \text{at } z = -h \tag{4.6}$$

The hull of the ship has a similar condition as the bottom of the water, namely that no fluid particle can cross it. The water should in this case have the same normal velocity as the ship's hull:

$$\frac{\partial \Phi}{\partial n} = \frac{\partial \alpha}{\partial t} \cdot \vec{n} \quad \text{on } H(t) \tag{4.7}$$

Here, α is the displacement and $H(t)$ is the exact position of the ship's hull in the ship-fixed coordinate system. All the formulated equations above are non-linear, which is very difficult and time consuming when trying to solve them, especially when the ship has a forward speed. SEACAL linearizes these equations and the effect of the forward speed on the free surface boundary condition is modelled in two ways: by including the encounter frequency effect in the zero-speed free surface conditions or by including the steady flow effect in the linearized free surface conditions. When the free-surface boundary condition is linearized, the velocity potential is divided into a steady and an unsteady part:

$$\Phi = \Phi_s(x, y, z) + \phi(x, y, z, t) \tag{4.8}$$

The steady part (Φ_s) indicates the stationary velocity potential which corresponds to the steady fluid flow due to the ship moving at a constant forward speed. The unsteady part gives the time-dependent velocity potential. SEACAL offers two possibilities for the steady flow, which are uniform steady flow or double-body steady flow. With uniform flow, the presence of the ship is not felt by the water, meaning that the steady flow is uniform in the whole fluid domain. Assuming this leads to the advantage that the free-surface condition can be solved relatively easily. However, this is only valid for slender ships and low speeds. The double-body flow is more realistic, which approximates the flow around the ship by the flow around the double body. This is the ship together with its reflection in the calm water plane $z = 0$ (see figure 2). By doing this, there no longer is a free surface, hence no waves are generated there, which grants that the no-flux condition (equation 4.7) is satisfied.

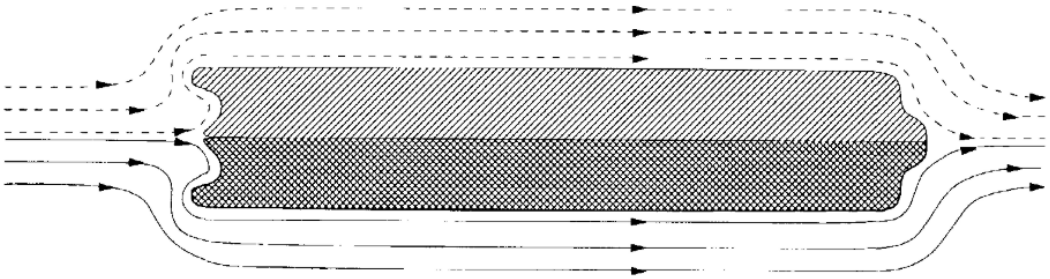

Figure 2: Side view of double-body flow approximation (from Bunnik (1999))

Uniform and double body steady flow are respectively formulated as follows:

$$\Phi_s = -Ux \tag{4.9}$$

$$\Phi_s = -Ux + \phi_s \tag{4.10}$$

With ϕ_s being the disturbance to the uniform flow due to the presence of the ship.

4.1.3 Solving the Laplace Equation

To solve the Laplace equation in the fluid domain, numerous methods have been developed, ranging from finite-element, finite-volume and finite-difference methods to boundary-integral methods. The latter is mostly used, and will be used in the present work as well. For the boundary-integral method, the grid generation is fairly easy as only the boundaries of the fluid domain have to be discretized. SEACAL specifically uses the Boundary Element Method (BEM), which is a term that denotes any method for the approximate numerical solution of the boundary integral equations (Costabel (1987)). The boundary-element method is based on Green's second identity, which is applied to the velocity potential ϕ in the fluid domain Ω with boundary $\delta\Omega$ and the following Green function:

$$G(\vec{x},\vec{\xi}) = -\frac{1}{4\pi r} - \frac{1}{4\pi r'}, \qquad r = |\vec{x}-\vec{\xi}|, \qquad r' = \left|\vec{x}-\vec{\xi}'\right| \tag{4.11}$$

Here, $\vec{\xi}'$ is the mirror image of $\vec{\xi}$ with respect to the bottom, B. The velocity potential in collocation point $\vec{x}$ is now represented by a Rankine source distribution, in which Rankine sources are placed on the boundary of the hull:

$$\phi(\vec{x}) = \iint_{\partial\Omega\backslash B} \sigma(\vec{\xi}) G(\vec{x},\vec{\xi}) dS_\xi \tag{4.12}$$

$$\vec{\nabla}\phi(\vec{x}) = (1-T)\sigma(\vec{x})\vec{n} + \iint_{\partial\Omega\backslash B} \sigma(\vec{\xi})\vec{\nabla}_{\vec{x}} G(\vec{x},\vec{\xi}) dS_\xi \tag{4.13}$$

Where

$$T = \begin{cases} 1 & \text{if } \vec{x} \in \Omega\backslash\partial\Omega \text{ or } \vec{x} \in B \\ \frac{1}{2} & \text{if } \vec{x} \in \partial\Omega\backslash B \\ 0 & \text{if } \vec{x} \notin \Omega \end{cases} \tag{4.14}$$

The concept of Rankine sources is explained as follows: if a a uniform flow is superimposed with a source at the origin of a boundary, a half body shape appears (White (2016)). Uniform stream flow and source & sinks at boundaries are two of the three basic principles of potential flow streams. The resulting body separates the source flow from the stream flow. This is visualized in figure 3. This half body is called a Rankine half-body. If uniform flow is superimposed with a sink, the rear half-body appears, also shown in figure 3. The concept of adding Rankine sources and sinks ultimately leads to a representation of a full Rankine body in potential flow.

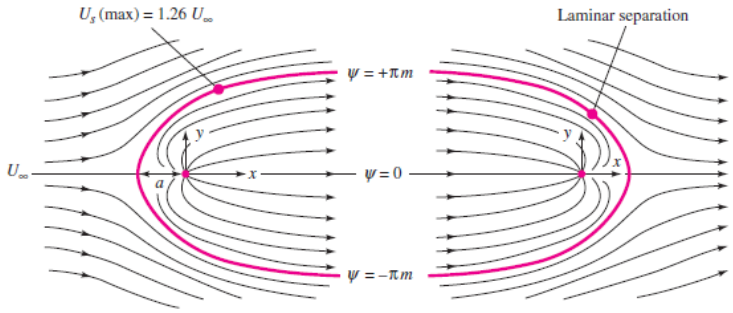

Figure 3: Superposition of a source (left) and sink (right) plus a uniform stream results in a Rankine half-body

If the source strengths are known in equation 4.13, then the velocities can be computed directly. Green's identity must be applied to a closed boundary. Therefore, the integral in equation 4.13 is not only over the free surface and the hull, but also over the boundary at infinity that connects the free surface and the bottom. The integral equation can then be solved by prescribing the potential, its normal derivative, or a linear combination of both in a finite number of collocation points on the boundary, which are predefined points in the domain. The boundary conditions in this case give the relation between the potential and its normal derivative. Doing this, a set of linear equations is found for the potential or its normal derivative. Standard numerical techniques can then be used to solve them. For more information on the theory behind the mathematical model of SEACAL, see Bunnik (1999) and Van Daalen and Bunnik (2021).

4.2 Numerical Theory

The mathematical theory that has been presented in the previous paragraph will be discretized here. This is necessary, because the analytical model cannot find a solution of the problem. The numerical model uses a first-order panel method, which means that the boundaries are divided into small quadrilateral panels with constant source strengths. The free-surface boundary condition contains tangential space and time derivatives. Where the space derivatives in the normal direction can be obtained directly from the integral equation, the tangential space derivatives need to be discretized using an upwind difference scheme. The time derivatives are obtained with backward differences schemes (Bunnik (1999)). The use of the frequency-domain is also possible, as opposed to the time-domain approach. Herein, the wave patterns are assumed to be harmonic in time at a certain frequency, which means that no time-stepping is required. A disadvantage of this approach is that waves with multiple frequencies cannot be simulated, which ignores the fact that waves with multiple frequencies cause slowly varying drift forces. The low-frequency part of these drift forces causes large ship motions, if this frequency is close to the resonance frequency of the ship. Another disadvantage of using a frequency-domain approach is that is cannot model non-linear effects.

4.2.1 Discretization of the Boundary Integral

The boundary integral will be discretized in 2 steps. Firstly, the steady free surface and the entire hull will be divided into panels. Secondly, a certain shape needs to be chosen for the source function σ. For the first part, we assume that each panel consists of two flat triangles, forming a quadrilateral. This allows the use of non-flat panels (see figure 4). With non-flat panels, curved parts of the boundary are easier discretized. As said, both the free surface and the hull are divided into panels. SEACAL divides the free surface automatically internally, whereas the hull is divided into panels manually. For the hull, a structured grid is used, which means that the hull is divided into segments along the x- and y-axis. The panel corners all coincide with panel corners of adjacent segments. The size of the panels must be small enough so that the smallest waves can be represented on them.

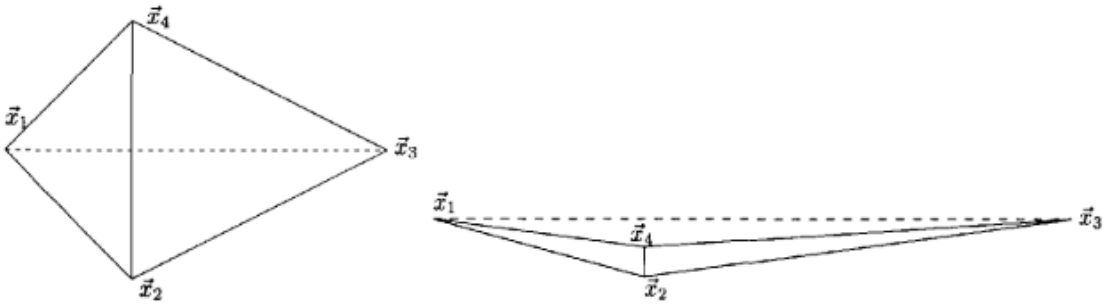

Figure 4: Top view (left) and side view (right) of a quadrilateral panel (from Bunnik (1999))

Following the panel distribution, the source function on the panels can be discretized. The boundary integral for the potential from equation 4.12 then turns into a sum over all panels, of source strength times an influence coefficient $G_{i,j}$. If we have N panels on the hull and free surface together, the potential in a collocation point $\vec{x}_i$ becomes:

$$\phi\left(\overrightarrow{x_i}\right) = \sum_{j=1}^{N} \sigma_j \iint_{\partial\Omega_j} G\left(\overrightarrow{x_i}, \vec{\xi}\right) dS_\xi = \sum_{j=1}^{N} \sigma_j G_{i,j} \tag{4.15}$$

The boundary integral for the velocity (equation 4.13) is discretized with the same procedure:

$$\vec{\nabla}\phi\left(\vec{x}_i\right) = (1-T)\sigma_i\vec{n} + \sum_{j=1}^{N} \sigma_j \iint_{\partial\Omega_i} \vec{\nabla}_x G\left(\overrightarrow{x_i}, \vec{\xi}\right) dS_\xi = (1-T)\sigma_i\vec{n} + \sum_{j=1}^{N} \sigma_j \overrightarrow{dG}_{i,j} \tag{4.16}$$

More details on the discretization of the mathematical model can be found in Bunnik (1999) and Van Daalen and Bunnik (2021).

4.2.2 Discretization of the Free-Surface Condition

When discretizing the free-surface boundary condition, numerical damping is required to suppress instabilities that occur when the free-surface condition is integrated over time (Bunnik (1999)). Here, upwind difference schemes are used to stabilize the numerical scheme. An upwind difference scheme uses so-called upwind variables to calculate the derivatives in a flow field. This means that data points are used which are upwind of the points that are being considered, with respect to the direction of the flow. Linear, time-dependent flow problems mostly are solved in the frequency domain, where the frequency describes the time dependence of the flow. Herein, non-linear effects are ignored. In a time-domain approach, the time derivatives that occur in the free-surface condition have to be discretized. Bunnik (1999) gives an extensive review of how that is done.

4.3 Calculating the Velocities, Forces & Moments

4.3.1 Velocity in Reference Points

What SEACAL is ultimately used for, is determining the water velocity change at the propeller plane. For this, reference points are added in the grid at different points in the propeller plane. The absolute longitudinal motion $x^{(R)}$ in a reference point is calculated as follows:

$$x^{(R)} = \sum_{i=1}^{N_{mode}} x_i \cdot \alpha_{x,i}^{(R)} \tag{4.17}$$

Where

N_{mode} is the number of system modes;
x_i is the system response amplitude of mode i;
$\alpha_{x,i}^{(R)}$ is the longitudinal modal displacement of mode i at R.

The system response amplitudes and the modal displacements of the reference points are calculated within SEACAL. The exact method of how these are determined can be found in Van Daalen and Bunnik (2021). For the present work, the relative longitudinal velocity is required. This is the velocity relative to the incoming waves, defined with the following equation:

$$v_{x,rel} = -i \cdot \omega_e \cdot x_{rel}^{(R)} \tag{4.18}$$

Here, ω_e is the encounter frequency.

4.3.2 Forces & Moments

Since SEACAL assumes the water to be inviscid, the forces and moments of the water on the hull are only dependent on the pressure. These forces and moments can be obtained by integrating the pressure over the hull:

$$\vec{F} = \iint_S p\vec{n}dS \qquad and \qquad \vec{M} = \iint_S p(\vec{x} - \vec{x_g}) \cdot \vec{n}dS \tag{4.19}$$

These forces and moments are divided into steady components, first-order and second-order components. The steady forces comprise of the wave resistance and the vertical pressure forces. The wave resistance is balanced by the propulsive force and the vertical pressure force is balanced by the gravitational force of the ship's mass. The steady moment is zero, since the ship is in equilibrium. The first order forces are dependent on the incoming wave height. Therefore, they are harmonic if the incoming waves are harmonic. The mean of the first-order forces is zero. The second order forces have products of first-order components and have non-zero mean values. This indicates, that there exist drift forces when taking into account second-order forces.

The forces and moments that the waves generate on the hull can be used to determine what resistance the ship needs to overcome in adverse weather conditions. This ultimately leads to additional power that the engine needs if it wants to keep the ship sailing at its design speed in adverse weather. However, for the present work, the forces and moments determined by SEACAL will not be used for further calculations.

4.4 Input Parameters

4.4.1 Main Parameters

To run SEACAL properly, the right input parameters need to be defined. These consist of the range of wave frequencies and ship speeds that need to be calculated, but also a panel distribution of the hull needs to be generated and assigned. Some additional hydrostatic parameters are added as well, consisting of the length, draft, mass, radii of gyration and centre of gravity. Besides that, the correct methods need to be specified, which in this case for the steady flow is the double-body (DB) flow method and for wave modelling it is the Rankine method. All above-mentioned parameters are shown in table 2.

The centre of gravity, not to be confused with the centre of buoyancy, has been assumed to be at 7m height, as this was not a given parameter. The three given radii of gyration are determined with the following equations (Söding et al. (2014)):

$$k_{xx} = 0.4 \cdot B_{wl} \tag{4.20}$$

$$k_{yy} = k_{zz} = 0.25 \cdot L_{pp} \tag{4.21}$$

The idea behind only taking into account wave directions up to 180° is that the ship is symmetic around the x-z plane. If the ship experience waves from 270 ° for instance, this would be seen as the same as waves from 90°, but with negative y-components.

Table 2: SEACAL input parameters

Parameter	Value
Ship speed (v_s)	13.3 kn
Wave frequency range (ω)	0.05 rad/s - 2.0 rad/s
Wave frequency interval	$\Delta\omega = 0.05$ rad/s
Wave direction range (μ)	0° - 180°
Wave direction interval	$\Delta\mu = 15°$
Length between perpendiculars (L_{pp})	113.8 m
Design draft (D)	8.5 m
Mass	17421.7 ton
Centre of Gravity (w.r.t. aft/centre/keel)	(58.6, 0.0, 7) m
Pitch radius of gyration (k_{xx})	8.8 m
Roll radius of gyration (k_{yy})	28.45
Yaw radius of gyration (k_{zz})	28.45

4.4.2 Ship Geometry and Meshes

SEACAL needs to know what meshes are used for the 3D model of the ship. The present work will use the chemical tanker 'Castillo de Tebra' for all its calculations. The ship parameters can be found in table 3. A picture of the ship is shown in figure 5.

Table 3: Ship parameters

Main parameter	Symbol	Unit	Value
Length between perpendiculars	L_{pp}	[m]	113.80
Length on load waterline	L_{wl}	[m]	116.60
Breadth	B	[m]	22.00
Draft	T	[m]	8.50
Displacement	∇	[m^3]	16988
Block coefficient	C_b	[-]	0.7791
Midship coefficient	C_w	[-]	0.991
Waterline coefficient	C_{wl}	[-]	0.897
Prismatic coefficient	Cp	[-]	0.7862
Centre of buoyancy, forward of $L_{pp}/2$	lcb	[m]	1.698

Flow solvers require the ship geometry in the form of a mesh or grid. This is a distribution of the ship in a number of nodes in 3 dimensions, which if connected form a panel distribution. For the present work, no geometry of the ship has been provided. Only geometrical parameters (shown in table 3) have been given. For that matter, a similar tanker has been found, namely the KVLCC2. This is the Kriso Very Large Crude Carrier 2, a modified version of the KVLCC, a non-existing tanker that has been conceived to provide data for CFD validation and flow physics explication around a modern tanker with a bulbous bow and stern (NMRI (2000)). This tanker has been modified to the parameters of the Castillo de Tebra with the use of the

Figure 5: Castillo de Tebra (retrieved from https://www.marinetraffic.com/en/ais/details/ships/shipid:4659057/mmsi:710031630/imo:9753636/vessel:CASTILLO_DE_TEBRA)

software package *MaxSurf*. Herein, an IGES-file can be imported and reshaped to fit the correct parameters. The new geometry can be seen in figures 6 and 7. Only the underwater ship has been defined, as this is what is required for SEACAL calculations. It needs to be noted that the representation of the 3D model in relation to the actual ship is not accurate, since the actual model is not available. The model that has been made is a modification of the already existing KVLCC2, using similar parameters and coefficients. What can be seen is that the stern of the ship is not realistic, as the part where the propeller needs to be placed is rather flat. This has been left this way to keep the coefficients similar to the ones that have been provided in table 3. More accurate results can be achieved when the model of the ship is made more realistic, however for the present work it is assumed that the generated model is satisfactory.

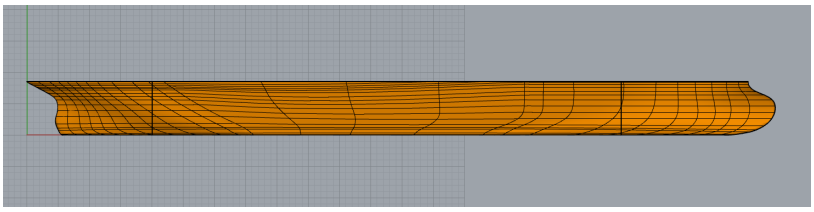

Figure 6: Side view of the modified KVLCC2

From the 3D model, using MARIN plug-ins for the software package *Rhinoceros*, multiple meshes can be made. These meshes need to define the ship hull forms well, there where they are most important. Thus, the bulb and stern are more concentrated with nodes and thus panels than midship for instance. This is mainly because the gradients of the fluid velocity are expected to be largest there, as opposed to the midship. A total of 5 different meshes have been made, ranging from a coarse grid

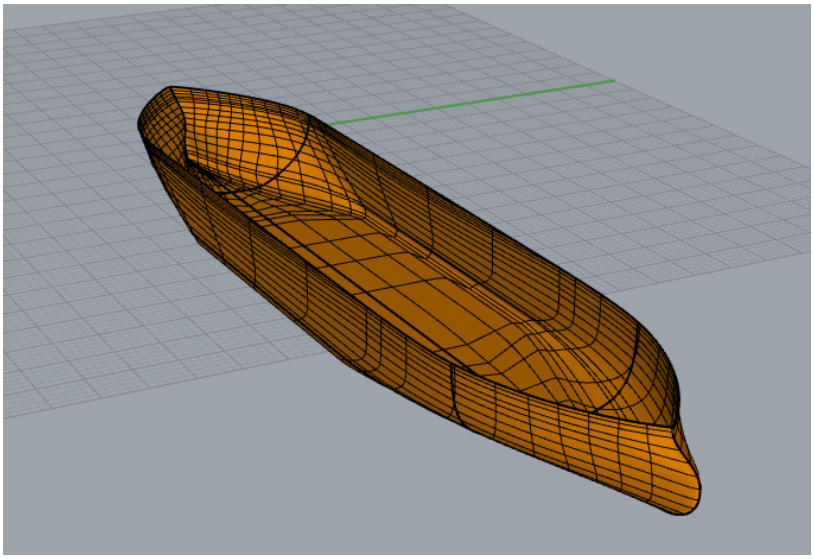

Figure 7: Perspective view of the modified KVLCC2

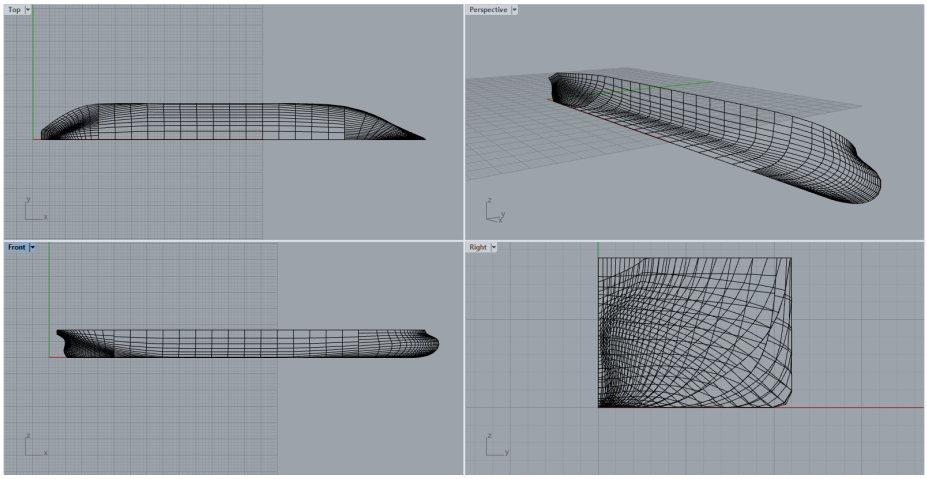

Figure 8: Coarse mesh, multiple views

with few panels to a very fine grid with a large amount of panels. All these meshes are only for half the hull, as this is enough for further calculations. The coarse mesh is shown in figure 8. The other meshes are shown in Appendix A.1.

4.4.3 Reference Points

Another input parameter that is required for this research, is a list of the reference points. These points have been chosen in 5 points in the propeller plane. These are the propeller hub, top side, starboard side, bottom side and port side of the propeller plane. A schematic overview is shown in figure 9. These points have been chosen on the 70% point of the propeller radius, where the total resultant force can be assumed to be applied (Klein Woud and Stapersma (2003)).

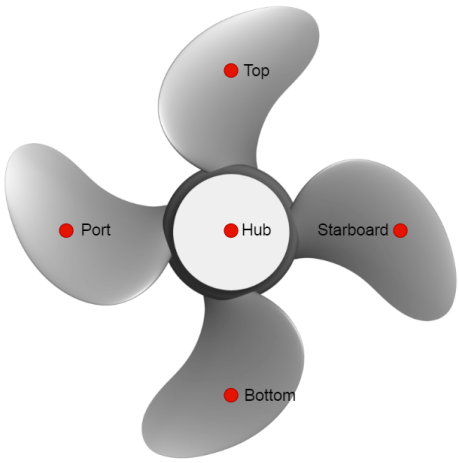

Figure 9: Schematic front view of reference points on the propeller plane

The coordinates of the 5 reference points are given in table 4. These coordinates are with respect to the aft, centre and keel of the ship. The reference points are visualised on the 3D hull in figure 10. Here it can be seen where the reference points lie with respect to the stern of the ship.

Table 4: SEACAL reference points

Reference point	x [m]	y [m]	z [m]
Hub	4	0	2.3
Top	4	0	3.8
Port	4	1.5	2.3
Bottom	4	0	0.8
Starboard	4	-1.5	2.3

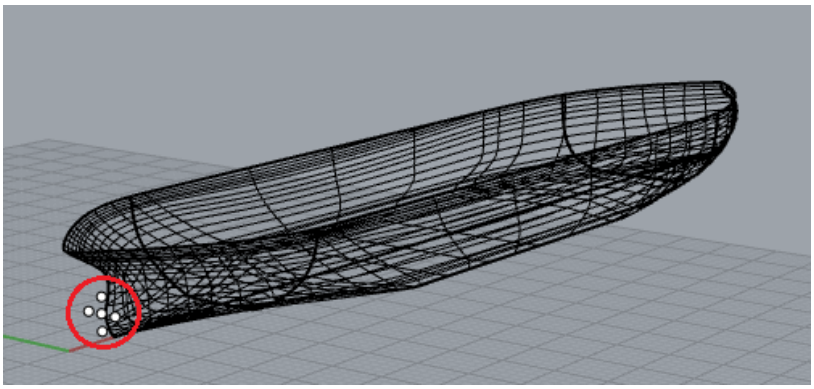

Figure 10: Reference points with respect to ship stern

4.5 Solution Verification

In this paragraph, a solution verification will be carried out on the acquired results from SEACAL. This is done by running multiple simulations with different mesh sizes and finding the numerical uncertainty within the grid convergence. This is also called a grid refinement study. The main purpose hereof is to show that the 'equations are solved right' (Eça and Hoekstra (2014)). Verification consists of two different activities, namely code verification and solution verification. The purpose of code verification is to verify, by error evaluation, that a given code solves the equations of the model correctly. Solution verification intends to estimate the uncertainty of a calculation when an exact solution is unknown. From the above definitions, it needs to be noted that there is a difference between errors and uncertainties. According to Roache (2009), an error requires the knowledge of the exact solution and has a sign (+ or -). The definition of uncertainty is an interval that should contain the exact solution within a certain confidence interval. In this paragraph, a solution verification is carried out. The code verification has been done already by MARIN. Solution verification will ultimately check whether grid refinement leads to less numerical uncertainty. Figure 11 shows the results of the inflow velocity RAOs for 5 different mesh sizes, for two wave directions. These two wave directions have been chosen as the results here vary the most, as opposed to the other wave directions where the results of all 5 meshes are almost equal. Solution verification will check whether the results from the different grids are mutually consistent or not.

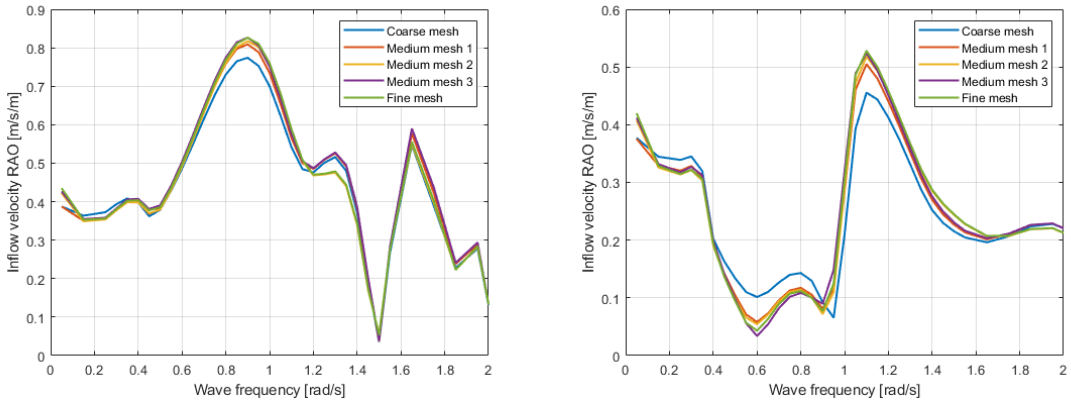

Figure 11: Results for different mesh sizes for 60° (left) and 90° (right) wave direction, top part propeller plane

The procedure proposed by Eça and Hoekstra (2014) is based on an error estimation which gives the numerical uncertainty if it is multiplied with a safety factor. For this, the grid convergence p needs to be calculated. The exact procedure is dependent on the value of the grid convergence; for $0.5 \leq p \leq 2$, the second-order method is valid. When p is higher than 2, the error would be underestimated. When p is lower than 0.5, the error estimation would be too conservative, due to the value going to infinity. If p is within 0.5 and 2, the error ϵ_ϕ is equal to δ_{RE}, which can be calculated

by solving equation 4.22. h_i/h_1 is the grid refinement ratio. The results that are looked at, referred as ϕ in all equations, is the fluctuating inflow velocity amplitude for a specific wave frequency, position and wave direction.

$$\delta_{RE} = \alpha h_i^p \tag{4.22}$$

The grid refinement ratios for the simulations that have been done earlier in this section are determined based on the amount of panels that the hull has been distributed in. The normalized grid refinement ratios are determined using the following equation:

$$\frac{h_i}{h_1} = \frac{NP_1}{NP_i} \tag{4.23}$$

Here, NP_1 is the number of panels of the most fine grid and NP_i is the number of panels of the ith grid. The grid refinement ratios are given in table 5. The results of the grids have also been added to the table. They correspond to results taken from the following points:

$\mu = 60°, \omega = 1.0 rad/s$ and $\mu = 90°, \omega = 1.1 rad/s$

Table 5: Grid refinement ratios and corresponding simulation results

Grid	NP	$\frac{h_i}{h_1}$	$v_{fluct,1}$	$v_{fluct,2}$
1	5725	1	0.7602	0.3865
2	5160	1.1095	0.7507	0.3767
3	4300	1.3314	0.7521	0.3830
4	2963	1.9322	0.7344	0.3450
5	1260	4.4380	0.6999	0.2740

Using a non-weighted and a weighted approach, this equation is solved using a least-squares power series expansion. There where the standard deviation is the lowest, will be used for further use in the uncertainty determination. The weight for each term in the non-weighted approach is equal to $w_i = 1/n_g$, where n_g is equal to 5, the number of grids that were used in the numerical computations. For the weighted approach, each weight is equal to:

$$w_i = \frac{1}{h_i} \left(\sum_{i=1}^{n_g} \frac{1}{h_i} \right)^{-1} \tag{4.24}$$

In both cases, the sum of the weights equals 1 ($\sum_{i=1}^{n_g} w_i = 1$). The following function needs to be minimised in the least-squares error estimation:

$$S_{RE}\left(\phi_0\right), \alpha, p) = \sqrt{\sum_{i=1}^{n_g} w_i \left(\phi_i - (\phi_0 + \alpha h_i^p)\right)^2} \tag{4.25}$$

This leads to the system of non-linear equations shown in 4.26. For both the non-weighted and weighted approach, this system is solved.

$$
\begin{aligned}
\phi_0 &= \sum_{i=1}^{n_g} w_i \phi_i - \alpha \sum_{i=1}^{n_g} w_i h_i^p \\
\alpha &= \frac{\sum_{i=1}^{n_g} w_i \phi_i h_i^p - \left(\sum_{i=1}^{n_g} w_i \phi_i\right)\left(\sum_{i=1}^{n_g} w_i h_i^p\right)}{\sum_{i=1}^{n_g} w_i h_i^{2p} - \left(\sum_{i=1}^{n_g} w_i h_i^p\right)\left(\sum_{i=1}^{n_g} w_i h_i^p\right)} \\
&\sum_{i=1}^{n_g} w_i \phi_i h_i^p \log(h_i) - \phi_0 \sum_{i=1}^{n_g} w_i h_i^p \log(h_i) - \alpha \sum_{i=1}^{n_g} w_i h_i^{2p} \log(h_i) = 0
\end{aligned}
\tag{4.26}
$$

The standard deviation is calculated using the following equation:

$$
\sigma_{RE} = \sqrt{\frac{\sum_{i=1}^{n_g} n_g w_i \left(\phi_i - (\phi_0 + \alpha h_i^p)\right)^2}{(n_g - 3)}} \tag{4.27}
$$

The results of all the operations mentioned above are given in table 6 for the two mentioned points in figure 11

Table 6: Standard deviations of non-weighted and weighted least-squares methods for the two data points

	Non-weighted	Weighted
ϕ_0	0.876	0.869
α	-0.117	-0.110
p	0.272	0.285
σ	$4.102 \cdot 10^{-3}$	$4.599 \cdot 10^{-3}$

	Non-weighted	Weighted
ϕ_0	0.463	0.446
α	$-7.533 \cdot 10^{-2}$	$-5.810 \cdot 10^{-2}$
p	0.617	0.727
σ	$8.903 \cdot 10^{-3}$	$9.291 \cdot 10^{-3}$

From these results it can be concluded that the results from the non-weighted approach will be used further, as the standard deviation is smaller. The results for the first data point shows that the grid refinement ratio p is less than 0.5, indicating that the error estimate would be too conservative (Eça and Hoekstra (2014)). The next step in the procedure is to determine the quality of the fit through the numerical data points, which is used to obtain the error estimate ϵ_ϕ. This is done by determining a data range parameter, calculated with equation 4.28. This parameter needs to be compared to the standard deviation to obtain the correct safety factor F_s. If the standard deviation is smaller than data range parameter, the data is reliable enough to use a safety factor of 1.25. Otherwise, the safety factor is set to 3.0. The value for Δ_ϕ is 0.0040, therefore the safety factor is 1.25, as this is larger than the standard deviation of the non-weighted approach.

$$\Delta_\phi = \frac{\phi_{max} - \phi_{min}}{n_g - 1} \tag{4.28}$$

For the uncertainty determination, a fit through the numerical data points is made. A second order polynomial is fitted using the MATLAB operator `fit`. The difference between each numerically obtained value for ϕ_i and the fitted curve is then used together with the safety factor and standard deviation to calculate the uncertainty for each numerical data point:

$$U_\phi(\phi_i) = F_s \epsilon_\phi + \sigma_{RE} + |\phi_i - \phi_{i,fit}| \tag{4.29}$$

The results are shown in figure 12. The fitted curve is also visualized, and plotted through the estimation of the exact solution. The uncertainty of the numerical data points are shown with error bars.

What can be concluded from these results, is that the numerical data points are mutually consistent. This is due to the error bars overlapping each other. What is also clear from figure 12 is that the numerical uncertainty converges with decreasing grid refinement ratio, which indicates that the estimation of the exact solution can be said with very small uncertainty. The actual numerical uncertainty of the data points is however rather large. One explanation is that the orthogonality of the grids was not satisfactory within the refinement, therefore generating different results for different grids. However, based on the procedure by Eça and Hoekstra (2014) it can be concluded that the solution is verified.

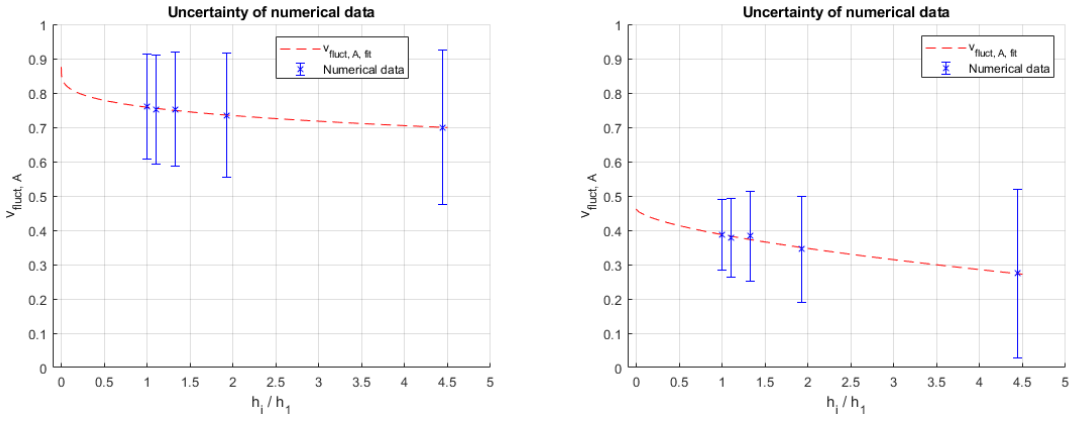

Figure 12: Numerical uncertainty results

4.6 Simulation Results

This paragraph will present the results that have been obtained from the seakeeping program SEACAL. These results comprise of inflow velocity changes (longitudinal, vertical and transverse) in the form of amplitudes and phase shifts in a wide range of wave direction and frequencies. Besides that, SEACAL also presents the ship motions in all six degrees of freedom for the same range of wave directions and frequencies. The ship motions will mainly be used to clarify some aspects of the inflow velocity results. Finally, SEACAL offers results of the wave forces in all six degrees of freedom. However, the variable that will be mostly looked into for the present work is the longitudinal inflow velocity. The reason for leaving out the transverse and vertical inflow velocity is that they do not ave a large effect on the propulsive performance of the propeller. This is explained with the fact that if the a propeller feels a transverse increase in the inflow velocity, with a right-handed propeller, the top part will generate more thrust whereas the bottom part will lose a bit of thrust. What is gained in the top part, is lost in the bottom part so it is assumed to cancel out. For the complete picture, the results are shown but they will not be used for further calculations.

4.6.1 Results in the Frequency Domain

The sign convention the following results will be that 0° waves are following waves and 180° waves are head waves. For wave directions 30° and 60°, the longitudinal inflow velocity amplitudes for a range of wave frequencies is shown in figure 13. These waves were chosen to visualize as they show some characteristics that can be clarified by the zero encounter frequency as well as the ship motions. All other wave directions are shown in Appendix A.2.

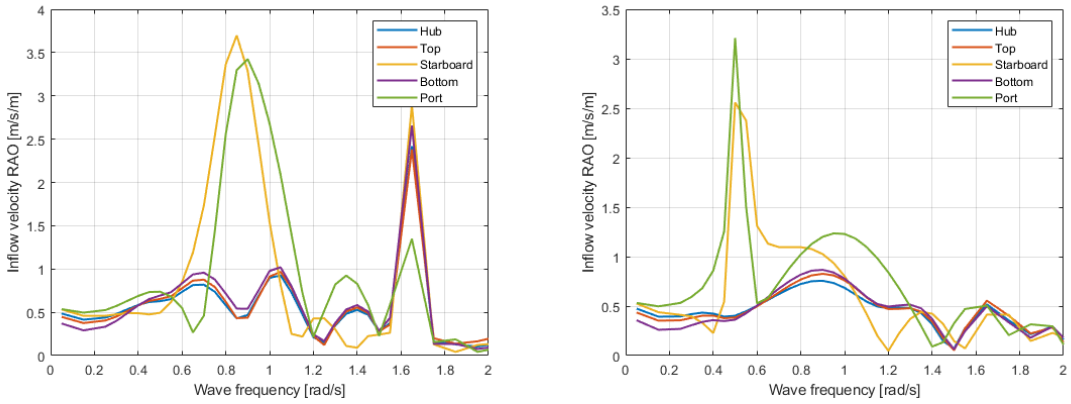

Figure 13: Longitudinal inflow velocity amplitude for 30° (left) and 60° (right) wave direction

What can clearly be seen from the graphs is that there is a significant change in inflow velocity for the different reference points. This indicates that at different parts of the propeller, a different inflow velocity is experienced at this specific wave

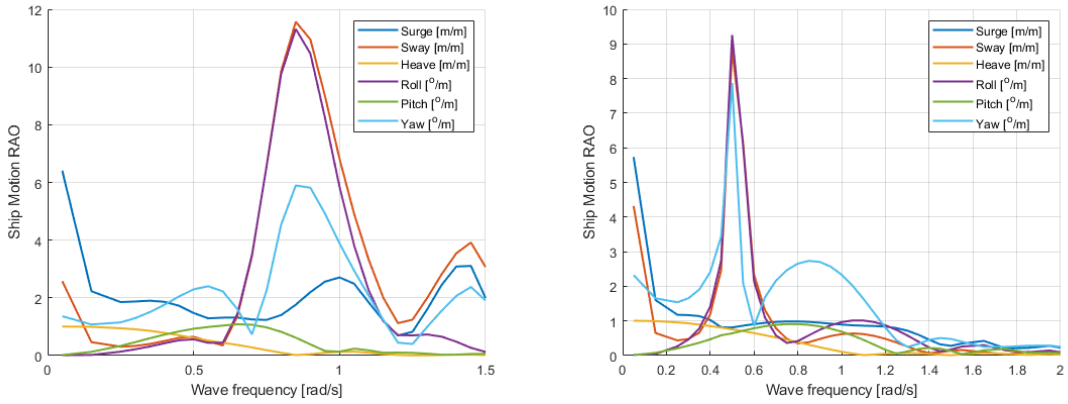

Figure 14: Ship motions at 30° (left) and 60° (right) wave direction

direction. This would change the effective angle of attack along the blade and therefore also the thrust generation. What is also made clear, is that the starboard and port side of the propeller have larger inflow velocity amplitudes at the lower wave frequencies than other parts of the propeller. This trend was found in all wave directions (see Appendix A.2), except for head waves and following waves. This means that the longitudinal velocity change at those parts of the propeller plane resonate largely with the corresponding waves. This will be further clarified by looking at the ship motions. The motions in the six degrees of freedom are shown in figure 14. Here, it can be seen that both peaks in the inflow velocity coincide with the peaks of the ship motions, specifically the sway, roll and yaw motions of the ship. The peak at larger frequencies at 30° waves in figure 13 is clarified by looking at the contour plot of the longitudinal inflow velocity RAOs, averaged over the 4 reference points (top, starboard, bottom and port) in the propeller plane, shown in figure 15. Herein, a line is drawn that shows for which wave frequencies and directions the encounter frequency equals zero. A zero encounter frequency indicates that the ship sails at the same speed as the longitudinal wave component, therefore not feeling any difference in wave heights. What can be seen along this line is that there are irregularities in the RAOs, mainly due to the encounter frequency being zero. When encounter frequency is close to zero, some interesting physical phenomena happen. For instance, when encountering following waves (9°), what happens then is that the ship basically starts 'surfing' on the waves. Due to these phenomena, peaks exist near an encounter frequency of 0. At 30° waves, at large wave frequencies, the encounter frequency nears zero. Therefore, a peak appears at this wave direction and frequency. What can also be seen from this figure is that at beam waves (90°), the RAOs are rather small. This indicates that beam waves do not have a large influence on the longitudinal inflow velocity change at the propeller plane.

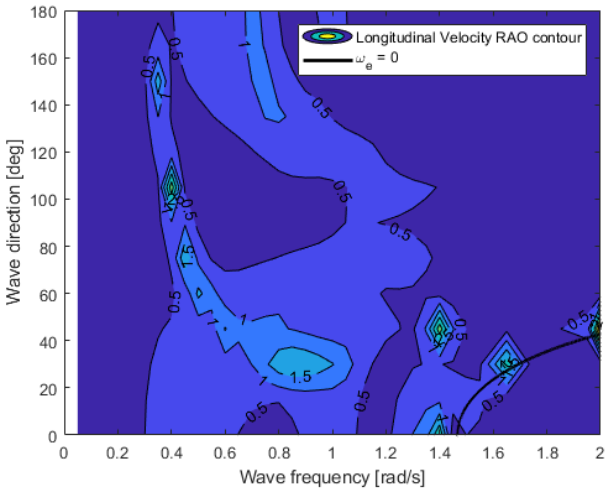

Figure 15: Contour plot of the longitudinal inflow velocity RAOs (averaged over propeller plane)

Results for wave directions 0° and 180° are shown in figure 16. What can be noticed here is that there is an overlap between the starboard side and port side of the propeller. The is because of both head and following waves having no sideways velocity components. With these waves, the flow is symmetrical over the port side and starboard side of the hull, which results in an equal longitudinal velocity at starboard and port side. There is however still a difference in the top side and bottom side of the propeller, which will still result in a thrust difference along the propeller blade. A different aspect in the graph for following waves is the peak at $\omega = 1.4$ rad/s. This peak is an irregularity due to the the fact that the encounter frequency at that wave frequency and wave direction equals zero. This can be seen in the contour plot as well in figure 15. The peak in the graph for 180° waves can be traced back to the ship motions, shown in figure 17. Here, peaks occur at the same frequencies for the heave and surge motion.

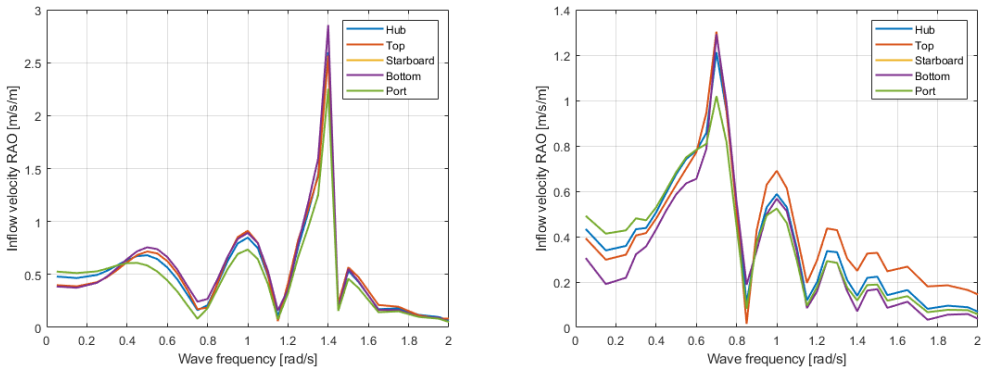

Figure 16: Longitudinal inflow velocity amplitude at 0° (left) and 180° (right) wave direction

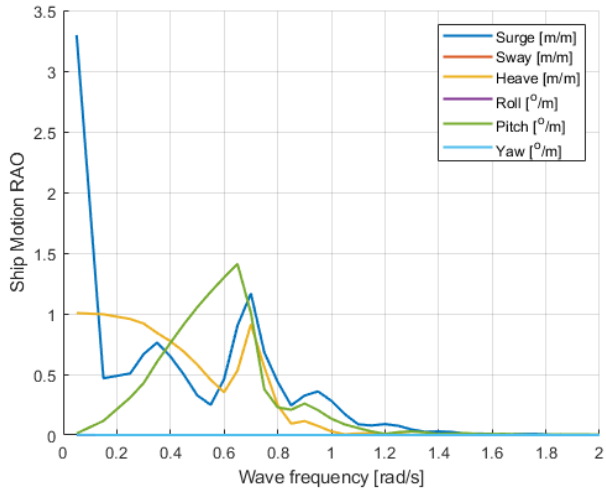

Figure 17: Ship motion RAOs at 180° waves

All previous results have only shown what the longitudinal velocity RAOs are per wave frequency and wave direction. It is also important to look at the transverse (y-direction) and vertical (z-direction) velocity RAOs to see how the waves affect the propeller wake in those directions. The contours for the transverse and vertical velocity RAOs are shown in figures 18 and 19 respectively.

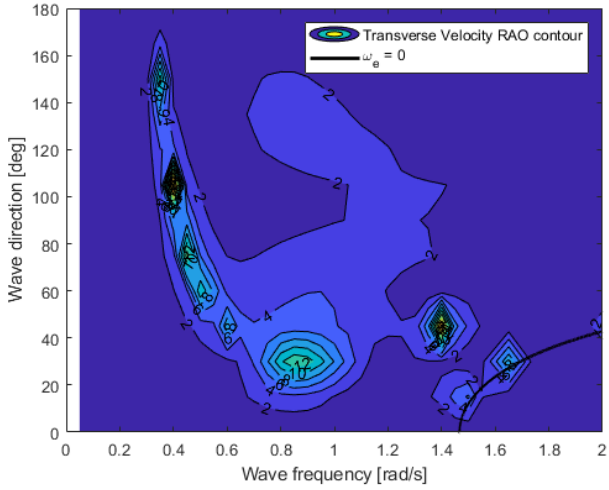

Figure 18: Contour plot of the transverse inflow velocity RAOs (averaged over propeller plane)

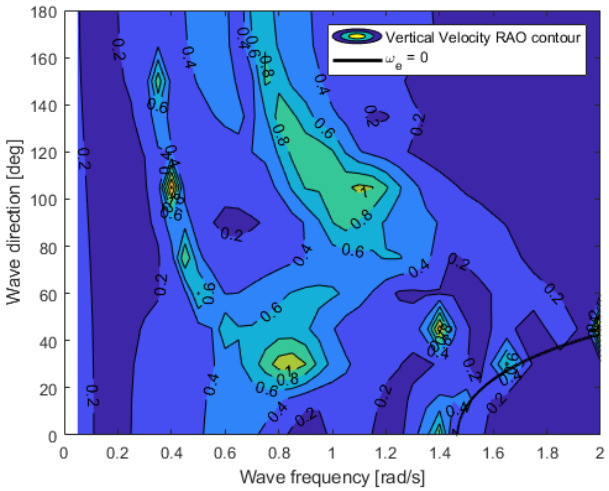

Figure 19: Contour plot of the vertical inflow velocity RAOs (averaged over propeller plane)

One thing that stands out notably is the fact that the transverse velocity RAOs are much larger than the longitudinal and vertical, which can be seen in the peak at ω = 0.9 rad/s, $\mu = 30°$ for instance. This is because the sway motions of the ship were calculated to be much larger, in all wave directions (see figure 14 and Appendix A.3). Due to larger sway motions in comparison to heave motions, the relative transverse water velocities also are larger than the vertical velocities.

4.6.2 Time Domain Transformation

From the gathered results, it is possible to transform the frequency domain into the time domain. This is done as follows: The results from SEACAL give frequency domain results, based on wave frequency. This indicates that for every wave frequency, there is an amplitude and a phase difference with respect to the incoming wave. However, for a ship that has a constant heading and speed, the frequency in which the ship 'feels' the waves changes for different wave directions and frequencies. Therefore, for the transformation into the time domain, firstly the wave frequency needs to be changed into the encounter frequency. This is defined with equation 4.30 (Journée and Massie (2015)).

$$\omega_e = \omega - k \cdot v_s \cdot cos(\mu) = \omega - \frac{\omega^2 \cdot v_s}{g} \cdot cos(\mu) \tag{4.30}$$

This equation uses the dispersion relation in deep water, defined as follows:

$$k = \frac{\omega^2}{g} \tag{4.31}$$

For regular waves, the transformation to a time domain is done using a cosine function.

$$v_i(t) = \zeta_A \cdot v_{i,A} \cdot cos(\omega_e t - \phi_i) \tag{4.32}$$

For all following time records, the average values within the propeller plane have been taken. This means that the average of the top, bottom, port and starboard side has been calculated for both the amplitude as well as the phase shift. The inflow velocity amplitudes ($v_{i,A}$) that are obtained from SEACAL are per meter wave amplitude. Therefore, to obtain the time domain, a multiplication is done with the wave amplitude (ζ_A). All the following figures for regular waves will use a wave amplitude of 1m. It needs to be noted that the results of the time domain do not show the actual inflow velocity of the propeller, but the change over time of the inflow velocity as a results of the incoming waves.

4.6.3 Results for Regular Waves

In figure 20, the inflow velocity change over time is shown for 2 different wave directions (30° and 120°) for a wave frequency of 0.3 rad/s, which corresponds to an encounter frequency of 0.247 rad/s and 0.331 rad/s for wave directions 30° and 120° respectively. These wave directions have purely been chosen to visualize the difference in encounter frequency in the time record. The difference in encounter frequency is clearly shown here. For different wave directions, waves are felt more frequent than others when a ship sails at a constant speed. The difference in amplitude comes from the height of the RAOs that has been determined within SEACAL.

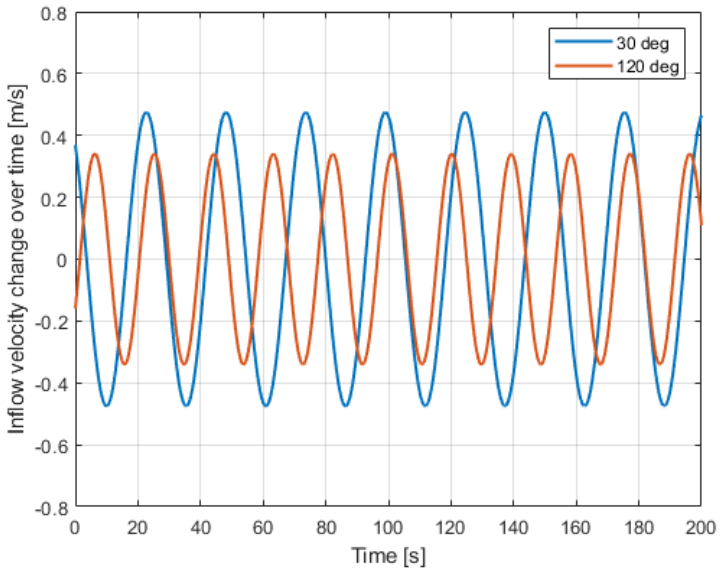

Figure 20: Inflow velocity change at top side propeller, at 30° and 120° wave direction

For the present work, irregular waves will be used to firstly determine what the adverse weather conditions are, and secondly use those conditions to determine what

the advance velocity of the propeller will be. Regular waves have been shown here to visualize what the change of inflow velocity is for different wave directions and encounter frequencies. Results for irregular waves will also show the difference in encounter frequency.

4.6.4 Procedure for Irregular Waves

For irregular waves, use of wave spectra is required (Journée and Massie (2015)). An irregular wave is seen as the superposition of a series of sinusoidal waves. A time record of the inflow velocity in irregular waves can be done by means of an inverse Fourier transform in the form of the following equation:

$$v_i(t) = \sum_{n=1}^{N} v_{i,A} \cdot \zeta_{a_n} \cdot cos(\omega_e t - \phi_n) \tag{4.33}$$

The wave amplitude $\zeta_{a,n}$ can be expressed in a wave spectrum, which is defined as follows:

$$S_\zeta(\omega_n) \cdot \Delta\omega = \sum_{\omega_n}^{\omega_n+\Delta\omega} \frac{1}{2}\zeta_{a_n}^2(\omega) \tag{4.34}$$

The wave amplitudes can be determined using the known wave spectra. With the knowledge that the area under the associated segment of the spectrum, $S_\zeta(\omega) \cdot \Delta\omega$, is equal to the variance of the wave component, equation 4.34 can be rewritten as follows:

$$\zeta_{a_n} = \sqrt{2 \cdot S_\zeta(\omega) \cdot \Delta\omega} \tag{4.35}$$

The two most important standard forms of wave spectra are the Bretschneider and JONSWAP wave spectra. These spectra indicate the energy density of irregular waves per frequency. They are unidirectional wave spectra, which means they are not dependent on the wave direction. They are based on the significant wave height ($H_{1/3}$) and the average wave periods ($\bar{T}$):

$$S_\zeta(\omega) = H_{1/3}^2 \cdot f(\omega, \bar{T}) \tag{4.36}$$

Bretschneider Spectrum

The Bretschneider is the oldest and most popular wave spectra and is well suited for open sea areas. The mathematical formulation is given as follows:

$$S_\zeta(\omega) = \frac{173 \cdot H_{1/3}^2}{T_1^4} \cdot \omega^{-5} \cdot \exp\left\{\frac{-692}{T_1^4} \cdot \omega^{-4}\right\} \tag{4.37}$$

The theoretical relationships between the characteristics periods T_1, T_2 and T_p are:

$$\begin{aligned} T_1 &= 1.086 \cdot T_2 = 0.772 \cdot T_p \\ 0.921 \cdot T_1 &= T_2 = 0.711 \cdot T_p \\ 1.296 \cdot T_1 &= 1.407 \cdot T_2 = T_p \end{aligned} \tag{4.38}$$

JONSWAP Wave Spectrum

The JONSWAP wave spectra stands for the Joint North Sea Wave Project, which was an extensive wave measurement program along a line extending over 100 miles into the North Sea. The wave spectra is defined by the following mathematical formulation:

$$S_\zeta(\omega) = \frac{320 \cdot {H_{1/3}}^2}{T_p^4} \cdot \omega^{-5} \cdot \exp\left\{\frac{-1950}{T_p^4} \cdot \omega^{-4}\right\} \cdot \gamma^A \tag{4.39}$$

With:

γ = 3.3 (peakedness factor)

$A = \exp\left\{-\left(\frac{\frac{\omega}{\omega_s}-1}{\sigma\sqrt{2}}\right)^2\right\}$

ω_ρ = $2\pi/T_p$ (circular frequency at spectral peak)

σ = a step function of ω :

$$\begin{aligned} if \quad \omega < \omega_p \quad then: \quad \sigma = 0.07 \\ if \quad \omega > \omega_p \quad then: \quad \sigma = 0.09 \end{aligned}$$

The JONSWAP wave spectra can be changed back to the Bretschneider wave spectra by taking $\gamma^A = 1.522$ with the peak period T_p. The relationship between the characteristic periods are:

$$\begin{aligned} T_1 &= 1.073 \cdot T_2 = 0.834 \cdot T_p \\ 0.932 \cdot T_1 &= T_2 = 0.777 \cdot T_p \\ 1.199 \cdot T_1 &= 1.287 \cdot T_2 = T_p \end{aligned} \tag{4.40}$$

Now, when the significant wave height and peak period of the sailing condition are known, the spectra can be determined, which will ultimately result in a time record of the wave height. Using the encounter frequency and the phase shifts of the waves over the whole frequency range, a time record of the inflow velocity of the propeller can be determined. Further results will be shown in the next chapter, where the propeller performance in terms of thrust and torque will be given, for the predefined adverse weather conditions.

4.7 Discussion & Shortcomings

The use of SEACAL and the processing of its results was done taking into account the fact that some physical phenomena were neglected. Some have already been mentioned, such as the viscosity of the water which is not considered with potential flow theory, while near the propulsor, this would have significant impact on the results. This paragraph will give a brief discussion on the shortcomings of the use of SEACAL and where improvements can be made in the future.

4.7.1 Water Viscosity

Leaving out the water viscosity in the determination of the inflow velocity is a rather drastic measure, since the propulsor mostly operates in flow in which viscosity has a large impact. CFD could be used to increase the accuracy of the results. This would however come at the expense of time effort and complexity. One of the phenomena that is left out when neglecting viscosity is oblique propeller inflow. Propellers experience this when sailing in waves at an angle or performing manoeuvres. Since SEACAL is a potential flow method, it does not take into account crucial boundary layer phenomena near the propeller, which ultimately lead to changes in the propeller wake field. When a propeller experiences inflow from different angles, this wake field also changes, which results in a change in propeller performance. Dubbioso et al. (2013) presented a CFD experiment in which they investigated the propeller performance in oblique flow. During off-design conditions, propeller loads can increase abruptly due to complex flow field phenomena and interactions between hull, propeller and rudder. Also, additional forces and moments are generated in the propeller plane, which can result in a change in the dynamic response of the ship. Results have shown that indeed, both thrust and torque increase with increasing drift angle. Additional side forces and moments are also generated due to different pressure distributions along the vertical and horizontal axis.

Leaving out the effects of water viscosity does not give a realistic picture of what the propeller performance would look like in adverse weather conditions, specifically if manoeuvres were taken into account. However, for the scope of the present work it has been left out as it would require a completely different methodology and therefore also would be more time consuming to consider it.

4.7.2 Multiple Ship Speeds

All the results that have been given are only done at the design ship speed. For the bigger picture it would be better to simulate multiple ship speeds to see how the inflow velocity changes when the ship sails at lower speeds. This would also be useful when determining the propeller and engine performance at lower ship speeds, because the ship speed changes due to second order wave drift forces. The effect of second order wave drift forces is however not taken into account in this research. Only simulating at the design speed would therefore not result in a realistic picture of the propeller performance in waves. Simulating more ship speeds would naturally

cost more simulation time, as at each ship speed, all wave directions and frequencies need to be simulated again.

4.7.3 Limited SEACAL Expertise

A limiting factor to the use of SEACAL is the lack of expertise involved in the software program. It has been found with consultation from Dr. J. Moulijn (MARIN) that some results, especially the ship motions, are inaccurate. Reasons for this could be traced back to the input parameters and the meshing of the 3D hull. For further research it could be useful to put more time and effort in investigating whether the acquired results are accurate and where they can be improved if found to be inaccurate.

5 Ship Propulsion in Adverse Weather

This section will cover the details of how the results from section 4.6 are used to determine how the ship propulsion system operates in adverse weather conditions. Mostly, those results will be implemented so that the propeller performance can be calculated and evaluated at different wave directions. Using these results, it can be determined whether the ship becomes underpowered or not. The present work will only look into straight forward sailing in different waves, as SEACAL only determined the results based on forward ship motion. Therefore, the manoeuvring operations of the ship will not be taken into account.

5.1 Adverse Weather Conditions

It is important to understand in what realistic conditions the vessel sails to determine the performance of the propeller and engine. For this, use is made of IMO (2013), which are the guidelines for determining the minimum propulsion power to maintain manoeuvrability of ships in adverse conditions. The purpose thereof is to verify whether ships comply with minimum propulsion power requirements. These guidelines have set up the following parameters to define adverse sea conditions corresponding with Beaufort number 7:

Significant wave height $H_{1/3}$ [m]	4.0
Peak wave period T_P [s]	7.0 - 15.0
Mean wind speed V_w [m/s]	15.7

Table 7: Adverse sea condition definition

The lower boundary of the peak wave period is slightly conservative, because the theoretical maximum storm steepness boundary in the relevant range of significant wave heights is crossed. The upper boundary is unnecessarily large, because such large wave periods are not critical for propulsion or steering ability (MEPC (2017)). In the introduction, the research project SHOPERA was mentioned, which has the aim to develop criteria and corresponding environmental conditions to assess sufficiency of propulsion and steering systems of ship for manoeuvrability in adverse weather. Here, the same definition for adverse weather condition was used. This definition is however only for ships having a deadweight larger than 20.000 DWT. The chemical tanker that is investigated in the present work has a deadweight of 13.000 DWT. It is assumed here that the same adverse weather condition holds for smaller vessels.

The SHOPERA project defined several criteria for the manoeuvrability of ships in adverse weather, namely being able to weather vane in heavy weather in the open sea and the ability to steer and propel in increasing coastal areas (MEPC (2017)). For this, environmental conditions are defined, as mentioned before. However, manoeuvrability performance depends largely on vessel characteristics and the operational experiences of the ship master. The weather conditions that have been defined are

not very severe, because in practice ship masters usually do not stay near the coast in increasing storm. They normally look for shelter or leave to the open sea where a position is sought that has enough room for drifting (Papanikolaou et al. (2015)). The recommended environmental conditions shown in table 7 were derived by benchmarking tankers, bulk carriers and container ships in the EEDI database against the two criteria mentioned above.

Now that the actual adverse sea conditions are known, the vessel needs to be tested on them. The defined parameters are based on the JONSWAP sea spectrum. Therefore, the propeller characteristics and performance limits will be tested on the given JONSWAP parameters in the following paragraphs. For the given parameters, the spectrum is shown in figure 21.

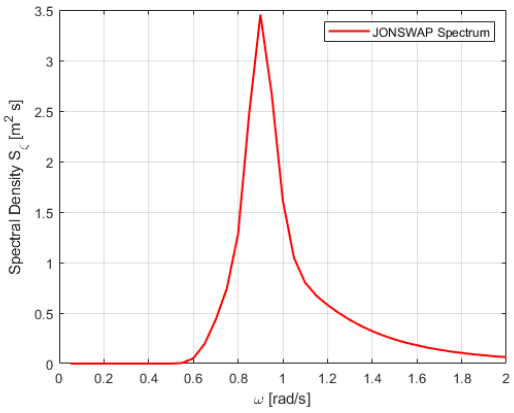

Figure 21: JONSWAP Spectrum for $H_S = 4m$ and $T_P = 7s$

5.2 Propeller Performance Characteristics

5.2.1 Propeller Thrust and Torque

This part will elaborate on how the propeller performance is defined and quantified. The performance will be mainly dictated by the thrust production and the corresponding torque generation of the propeller. In order to determine thrust and torque, the main parameter to determine is the advance velocity that the propeller experiences. The previous chapter has given the change in inflow velocity of the propeller under certain wave directions and frequencies. The advance velocity consists of the ship speed and the calm water wake fraction together with the fluctuating inflow velocity, defined in equation 5.1.

$$v_a = v_s \cdot (1 - w) + v_i(t) \tag{5.1}$$

Here, v_s is the ship speed and w is the calm water wake fraction. For the ship speed, the design ship speed of 13.3 knots is used, as all SEACAL results are based on the design ship speed. The thrust of the propeller is calculated using the non-dimensional thrust index C_T (ITTC (1999)):

$$T = C_T \cdot \frac{\pi}{8} \cdot \rho \cdot D_p^2 \cdot \left[v_a^2 + (0.7 \cdot \pi \cdot n_p \cdot D_p)^2\right] \tag{5.2}$$

$$T = K_T \cdot \rho \cdot n_p^2 \cdot D_p^4 \tag{5.3}$$

This form of the thrust, which normally is defined as shown in equation 5.3, is seen as more useful as the thrust characteristics can now be presented over a range of advance velocities, which is the changing variable in this research. This thrust index is a function of the hydrodynamic pitch angle β_P and the propeller pitch ratio P/D, shown in the following equation:

$$C_T = f\left(\beta_P, P/D\right) \tag{5.4}$$

Where the hydrodynamic pitch angle is defined as follows (ITTC (1999)):

$$\beta_P = \arctan\left(\frac{v_a}{0.7\pi \cdot n_p \cdot D_p}\right) \tag{5.5}$$

Using equations 5.2 and 5.5, the thrust production can be determined with the main variable being the time varying advance velocity v_a, keeping the propeller speed n constant as well as the pitch ratio. The torque demands can be determined similarly using equation 5.6, with equation 5.7 being the normally used way of determining the torque using the open-water diagram:

$$Q = C_Q \cdot \frac{\pi}{8} \cdot \rho \cdot D_p^3 \cdot \left[v_a^2 + (0.7 \cdot \pi \cdot n_p \cdot D_p)^2\right] \tag{5.6}$$

$$Q = K_Q \cdot \rho \cdot n_p^2 \cdot D_p^5 \tag{5.7}$$

Here, the non-dimensional torque coefficient C_Q is again a function of the propeller pitch ratio and hydrodynamic pitch angle:

$$C_Q = f\left(\beta_P, P/D\right) \tag{5.8}$$

5.2.2 Open-Water Diagram

This paragraph will briefly introduce the open-water diagram that is used further in this section. The open-water characteristics have been extracted from the original propulsion & manoeuvring model, worked on by Sui (2021). Here, the open-water test data of the original MAN Alpha propeller has been given, followed by a correction that has been executed to find the right open-water characteristics for the Wageningen C4-55 propeller that are similar to the original MAN Alpha propeller. A nominal pitch of P/D = 0.8 has been chosen for the C4-55, as its blade area ratio (0.55) and design pitch are similar to the ones of the MAN Alpha propeller installed in the benchmark ship, which has a blade ratio of 0.52 and design pitch of P/D = 0.7075. Details on the correction can be found in Sui (2021). The original and corrected open-water diagram is shown in figure 22.

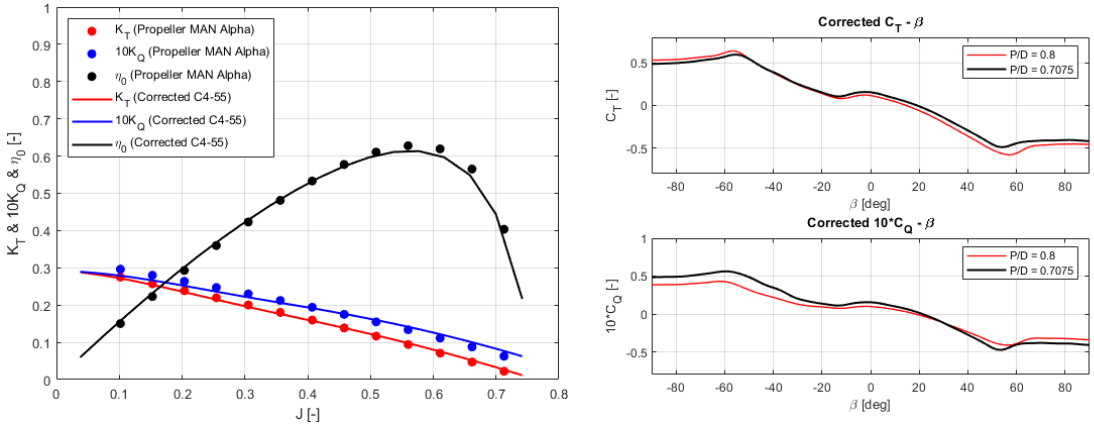

Figure 22: Original and corrected open-water diagram and thrust/torque index coefficients

Not only the thrust and torque coefficients are corrected, the thrust and torque index coefficients (equations 5.4 and 5.8) also need to be corrected for the Wageningen C4-55 propeller at design pitch P/D=0.8. Again, for further details, see Sui (2021). For the design pitch, the C_T and C_Q graphs are also plotted in figure 22.

5.3 Engine Performance Characteristics

This paragraph will cover how the engine responds to the changes in propeller performance due to adverse weather conditions.

5.3.1 Engine Layout & Parameters

The layout of the power plant installed on the benchmark chemical tanker is shown in figure 23. The propulsion system is a controllable pitch propeller (CPP) that is directly driven by a 2-stroke main diesel engine. The main engine parameters are given in table 8. The CPP adds better manoeuvrability to the ship and are better for adapting to different operating conditions (Klein Woud and Stapersma (2003)). For the present work, the CPP is assumed to be set at a constant pitch of P/D = 0.7075

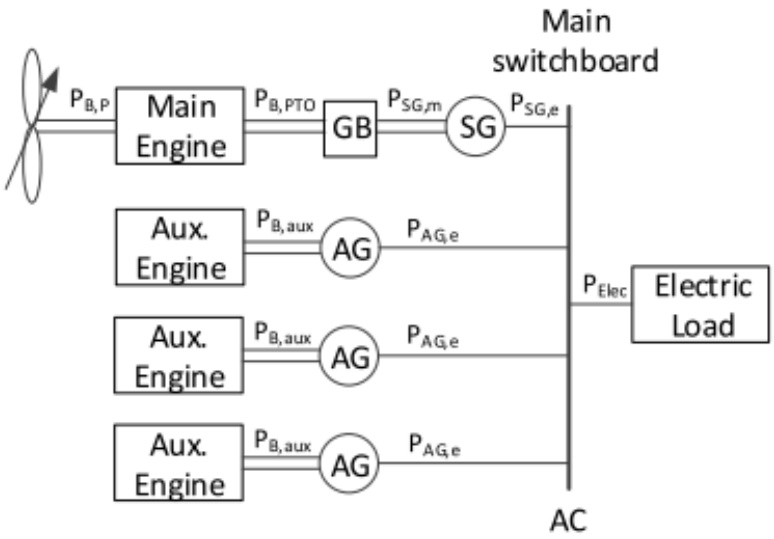

Figure 23: Power plant layout

Table 8: Engine parameters (Sui (2021))

Parameter	Main Engine
Engine Type	MAN 6S35ME-B9.3-TII (2-stroke)
Number of Engines [-]	1
Maximum Continuous Rating (MCR) [kW]	4170
Rated Speed [rpm]	167

The electric power generation system that is installed on board of the chemical tanker has a shaft generator (SG) and three auxiliary generators (AG). The shaft generator is powered by the main engine using a power take-off (PTO) gearbox. This means that part of the main engine is used for electric power generation. The auxiliary generators are driven by three auxiliary diesel engines.

5.3.2 Engine Operating Envelope

This paragraph will consist of details about the engine operating envelope, which is a diagram that shows what engine power limits are reached at what engine speeds. This diagram consists of five limits (Stapersma and Woud (2005)), namely minimum engine speed, maximum engine speed, maximum torque, turbocharger limit and a minimum torque limit. Operating the engine within these five limits is allowed, whereas operating below the minimum torque limit is allowed during manoeuvring only. The operating envelope of the engine is shown in figure 24. The layout figure has been inspired by the work done by Sui (2021). Here, the overload power limit is 110% of the MCR and the overload speed limit is 105% of the design engine speed (MAN (2014)).

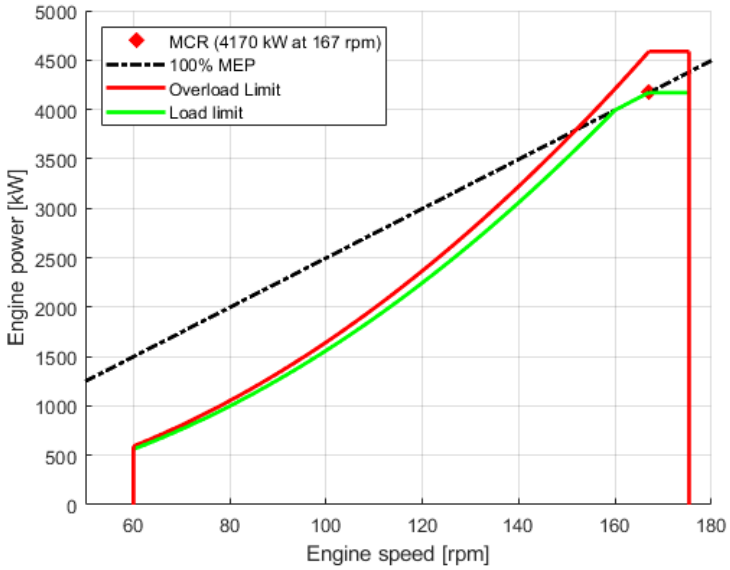

Figure 24: Engine operating envelope

To find the operating curve of the propeller in adverse weather, first the nominal propeller curve will be determined. For this, the resistance - ship speed (R/v_s) relation needs to be converted to a brake power - engine speed (P_B/n_e) relation. To find the ship resistance, the effective towing power of the ship needs to be determined. This is done using the following equation:

$$P_E = C_E \cdot \rho^{\frac{1}{3}} \cdot \Delta^{\frac{2}{3}} \cdot v_s^3 \tag{5.9}$$

Here it is shown that the effective towing power is dependent on the specific resistance coefficient (C_E), which is a function of ship speed, hull form, fouling, sea state and water depth. From the effective towing power, the resistance is given by:

$$R = \frac{P_E}{v_s} \tag{5.10}$$

Some main assumptions here are that a fixed-pitch propeller is used and that a quadratic resistance curve is assumed. From the quadratic relation, the following equation can be set up:

$$R = c_1 * v_s^2 \tag{5.11}$$

At a specific point on the resistance curve, c_1 can be determined. This can also be rewritten using the wake fraction and advance velocity:

$$v_a = (1 - w) \cdot v_s \tag{5.12}$$

$$R = c_1 \cdot \left(\frac{v_a}{1 - w} \right)^2 \tag{5.13}$$

With the thrust deduction, the thrust follows:

$$T = \frac{R}{1 - t} = \frac{c_1 \cdot v_a^2}{(1 - t) \cdot (1 - w)^2} = c_8 * v_a^2 \tag{5.14}$$

The required thrust coefficient for this ship at speed v_s is then:

$$K_{T,\text{ ship}} = \frac{c_8 \cdot v_a^2}{\rho \cdot n_p^2 \cdot D_p^4} = \frac{c_8}{\rho \cdot D_p 2} \cdot \frac{v_a^2}{n_p^2 \cdot D_p^2} = \frac{c_8}{\rho \cdot D_p^2} \cdot J^2 = c_7 \cdot J^2 \tag{5.15}$$

Plotting this graph in the open-water diagram of the fixed pitch propeller, the operating point of the propeller can be found. This is the intersection of the $K_{T,\text{ ship}}$ line and the $K_{T,\text{ prop}}$ line. From this, also the torque coefficient and open-water efficiency can be read. With the torque coefficient, the propeller load can be determined as follows:

$$K_Q = \frac{Q_p}{\rho \cdot n_p^2 \cdot D_p^5} = \frac{\eta_r \cdot \eta_s \cdot M_p}{\rho \cdot n_p^2 \cdot D^5} \quad \rightarrow \quad M_p = \frac{\rho \cdot D_p^5}{\eta_R} \cdot K_Q \cdot n_p^2 \tag{5.16}$$

Finally, the engine brake power is determined with the next equation:

$$P_B = 2 \cdot \pi \cdot M_p \cdot n_e \tag{5.17}$$

The actual design load line and design point of the vessel is determined based on the nominal torque coefficient K_Q, nominal advance ratio J and nominal ship speed v_s, given in Sui (2021), which are the shown in table 9.

$K_{Q,nom}$ [-]	J_{nom} [-]	$v_{s,nom}$ [knots]
0.01942	0.4072	13.3

Table 9: Nominal advance ratio and ship speed

Using the equation below, the nominal propeller speed can be calculated which is 167 rpm. The brake power at the corresponding engine speed is 3965 kW. This is visualized in figure 25.

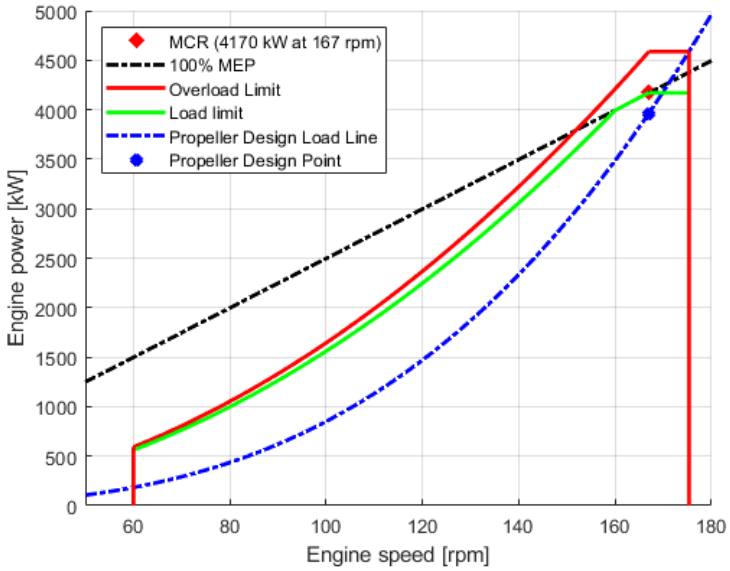

Figure 25: Engine operating envelope with propeller load at design condition

5.3.3 Ship Thrust Envelope

A different approach of looking at the operating limits of a ship is to look at the ship thrust envelope. Here, the load limits of the engine envelope are transformed from power-speed limits to thrust-speed limits, in terms of ship speed instead of engine rotating speed. For the load limits, the following procedure is done. Every point of the load and overload limit lines in the engine operating envelope has a value for the engine speed, corresponding to its power limit. To transform this line into the ship thrust envelope, first the K_Q values for those points need to be determined. This is done using the following set of equations:

$$M_{limit} = \frac{P_{limit}}{n_{limit} \cdot 2\pi} \tag{5.18}$$

$$Q_{P,limit} = M_{limit} \cdot \eta_s \cdot \eta_r \tag{5.19}$$

$$K_{Q,limit} = \frac{Q_{P,limit}}{\rho \cdot D_p^5 \cdot n_{limit}^5} \tag{5.20}$$

After determining the K_Q values, the corresponding J and K_T values can be determined using the open-water diagram. The ship thrust is finally determined using the following equation:

$$T_s = K_T \cdot \rho \cdot D_p^4 \cdot n_{limit}^2 \cdot (1 - t) \tag{5.21}$$

The full ship thrust envelope is pictured in figure 26. Again, inspiration has been drawn from Sui (2021) for the layout of this figure.

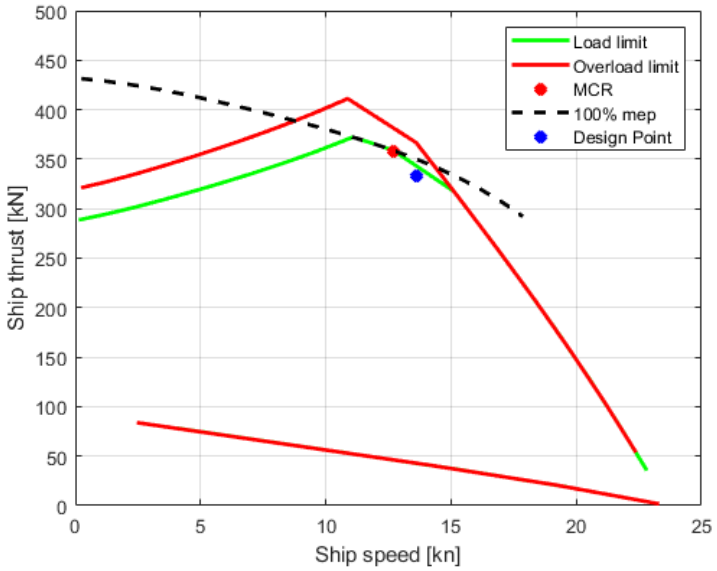

Figure 26: Ship thrust envelope

What is seen here, is that the design point and the MCR point are dispersed slightly on the x-axis and y-axis. This is explained by the fact that both points have a different value for K_Q, and thus a different value for J and K_T. With equal rotational speed, a different value for the ship thrust and advance velocity is achieved.

5.4 Testing the Engine Limit

This paragraph will verify whether the vessel has enough power to sail in the defined adverse sea conditions, depicted in table 7. The propeller performance during these adverse sea conditions will be plotted inside both the engine operating envelope as well as the ship thrust envelope, defined in paragraph 5.3.2.

With the given adverse weather conditions, the generated thrust and torque of the propeller can be determined over time. Based on the JONSWAP spectrum, given in figure 21, the fluctuating inflow velocity is determined and ultimately the thrust and torque of the propeller. The fluctuating inflow velocity for following and head waves is visualized in figure 27. From this figure, it can be clearly seen that the direction of waves has an influence on the amplitude of the inflow velocity, as well as on the frequency of change. The latter is explained with the encounter frequency, which is much larger with head waves than following waves when the ship has a forward velocity. The inflow velocity changes for all wave directions are shown in Appendix A.4.

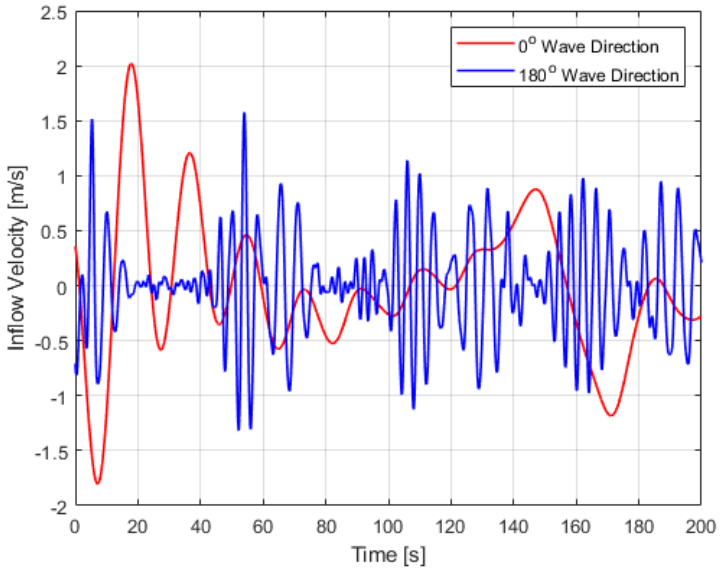

Figure 27: Fluctuating inflow velocity in irregular waves

5.4.1 Thrust and Torque in Adverse Weather

The thrust and torque of the propeller are, as mentioned before, dependent on the advance angle β_P, which is a function of the advance velocity and rotational speed of the propeller. The advance velocity is given with equation 5.1 and the resulting advance angle is given with equation 5.5. The advance angle, together with the pitch ratio, results in the thrust and torque index coefficients. With this reasoning of thinking, the thrust and torque fluctuate not only directly with the advance velocity, shown in equation 5.2 and 5.6, but also indirectly through their respective index coefficients C_T and C_Q. Therefore, the thrust and torque will not fluctuate in the same behaviour as the advance velocity. In figure 28, the thrust and torque index coefficients are plotted over time. Here it can be seen that the peaks and troughs are at different points in time that the ones for the inflow velocity.

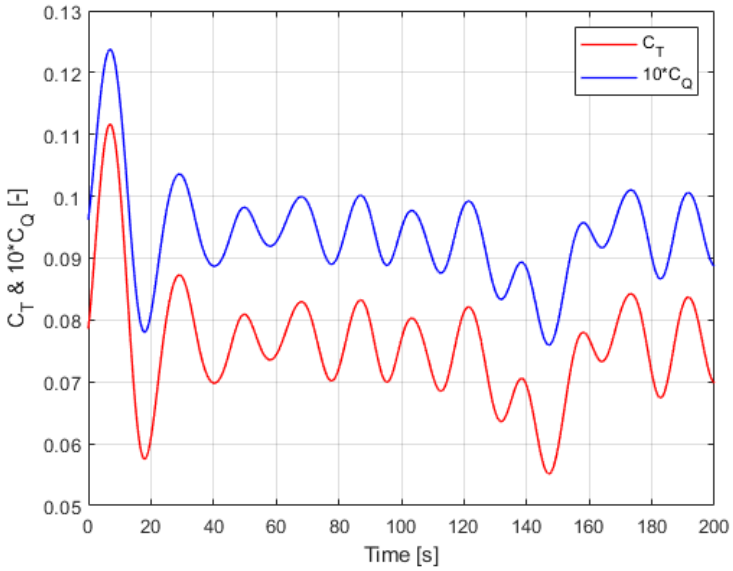

Figure 28: C_T and C_Q change over time (0° wave direction)

Finally, the thrust and torque are calculated for different wave directions and plotted in figure 29. The design propeller rotating speed of 167 is used.

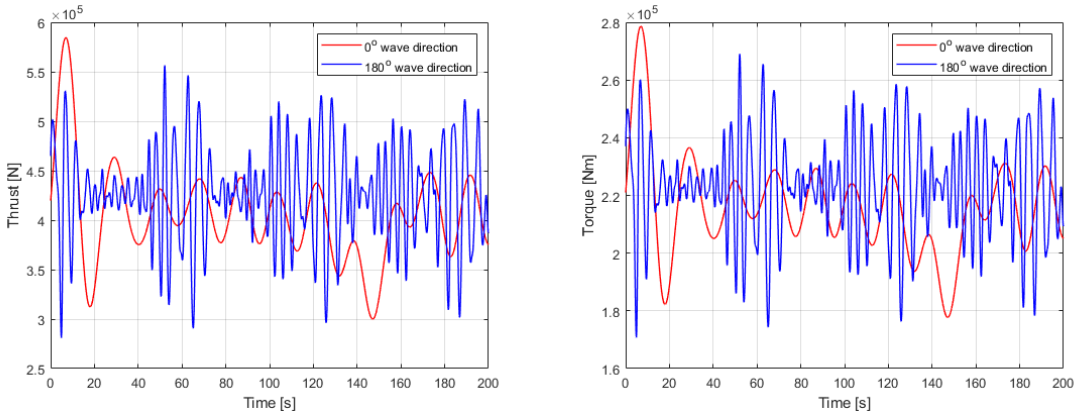

Figure 29: Thrust (left) and torque (right) over time for multiple wave directions

5.4.2 Propeller Load in Engine Envelope

The propeller load is plotted in the engine operating envelope as follows: The propeller torque that is generated due to the waves is transformed to the engine brake power using equation 5.17, assuming that the shaft efficiency (η_s) and relative rotative efficiency (η_r) are equal to 1. Due to the fluctuating advance velocity, a minimum and a maximum torque is experienced within the time record. These are however calculated for the design engine speed of 167 rpm. Therefore, in the engine operating envelope this will look like a vertical line. This is shown in figure 30 for following waves (0°) and head waves (180°). All other wave directions are shown in Appendix

A.5.

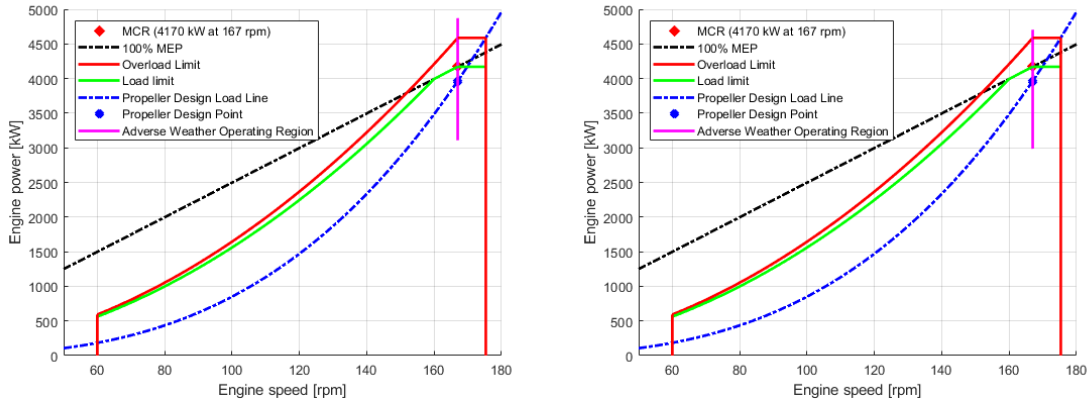

Figure 30: Engine operating envelope in adverse weather conditions (following (left) and head (right) waves)

Clearly it can be seen that the power in adverse weather conditions exceeds the engine limits at the nominal ship speed and engine speed and this trend is seen in all other wave directions as well. This is mainly because of the thrust and torque fluctuations that have been calculated at the nominal conditions in terms of ship speed and engine speed. The design point is already close to the engine limit, which would result in overloading if significant fluctuations are added to that design point. From all wave directions, it can be said that the head waves and following waves have the least amount of effect on the required power. This is due to the fact that the longitudinal velocity fluctuations are smallest here.

For the present work, the propeller torque has been purely determined based on the nominal engine speed, which is 167 rpm. From this, the conclusion can be made that the engine overloads in adverse weather conditions, when it sails at its design speed of 13.3 knots and has the engine rotating at 167 rpm. In other words, the ship is underpowered when it sails in adverse weather conditions at the specified speeds. However, the present work did not take into account that the ship experiences added resistance when it sails in waves. Due to this, the propeller load curve will move to the left as well, forcing the engine to run at a lower speed. The ship speed will therefore also decrease. Not only can the ship speed decrease due to added resistance; the captain can and will manually decrease the ship speed when it sails in large waves for safety reasons. For this reason, the results do not represent a realistic picture, as sailing at the design speed in adverse weather is not often done.

5.4.3 Propulsion Control System

Something that needs to be noted, is that when the engine feels a changing torque on the propeller, the propulsion control system will increase or decrease the fuel injection to generate less or more torque in the engine. For the present work, it is assumed

that the control system reacts instantly to the change in propeller torque, resulting in a vertical line in figure 30. Therefore, the rotational speed of the engine does not change. In reality, when the propeller generates more torque than what the engine delivers, the control system will decrease the speed, afterwards start injecting more fuel and then increasing the engine speed again to match the propeller torque and keep the ship speed constant. In figure 30 the adverse weather line would incline to the left.

5.4.4 Propeller Load in Ship Thrust Envelope

This paragraph will show where the propeller load in adverse weather conditions lies in the ship thrust envelope, which was introduced in paragraph 5.3.2. For head waves and following waves, the results are shown in figure 31. It must be noted here that the x-axis is not the ship speed in knots, but the advance velocity in m/s. The results for all other wave directions are shown in Appendix A.6.

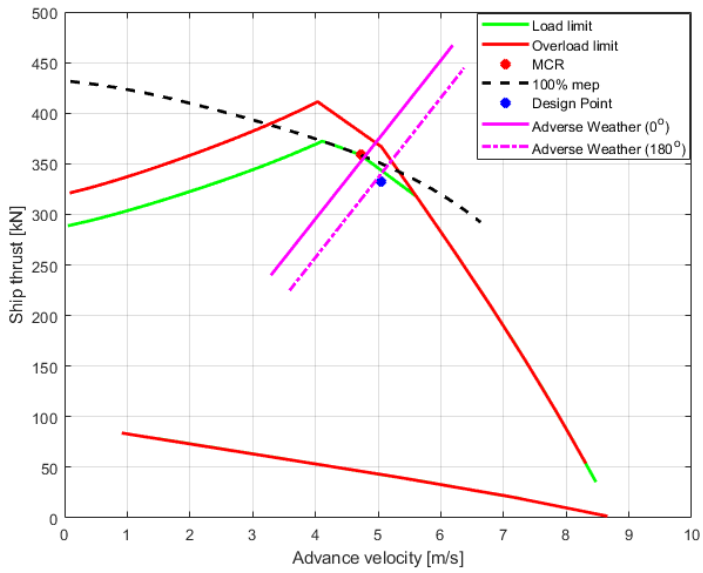

Figure 31: Ship thrust envelope in adverse weather (0° & 180°)

Here, it can also be clearly seen that the thrust that is produced exceeds the limits of the engine at certain advance velocities for both following as well as head waves. The ship thrust for head waves is smaller, because the advance velocity is larger on average, which leads to a decrease in the thrust index coefficient (figure 22). The decrease in thrust index coefficient is larger than the increase in advance velocity, which leads to a decrease in the total thrust generation. From this figure, it can be read at what advance velocity the limit is reached. In conclusion it can be said that the waves produce too much of a change in the advance velocity of the propeller, causing it to generate too much thrust. Again, the explanation of the ship thrust going over the

limits has to do with the fact that the calculations have been made based on nominal ship speed and engine speed. As this is close to the MCR of the engine already, the additional fluctuations due to the waves push the thrust and torque over the limits. Therefore, the conclusion can be drawn that the ship is underpowered when it sails at its design speed of 13.3 knots and has its engine running at 167 rpm.

5.5 Comparison to Previous Research

As the present work is a continuation of the work done by Sui (2021), it is useful to compare his results to the results acquired here. Here, the difference can be discovered of the empirical wave model and numerical results. These will be compared in terms of advance velocity fluctuations in two sailing conditions, namely in Beaufort 7 (BF7) and Beaufort 8 (BF8). Sui (2021) found that in BF7, the ship attains a velocity of 7 knots in regular head waves with a wave height of 4 m. In BF8, the ship attained a velocity of 2.6 knots in regular head waves with a wave height of 5.5 m. The results of Sui (2021) are shown in figure 32 on the left.

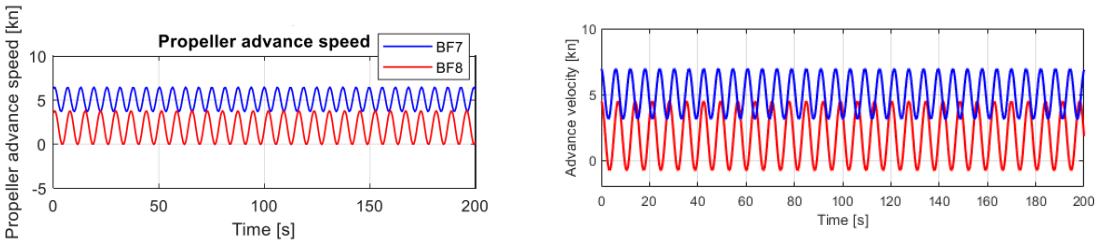

Figure 32: Advance velocities for BF7 (blue) and BF8 (red) from Sui (2021) (left) and the present work (right)

The advance velocities for the same conditions, determined in the present work are also shown in 32 on the right. It can be seen here that the fluctuation of the advance velocities is fairly comparable. The fluctuation is larger due to the fact that the inflow velocity RAOs are determined with having a ship speed of 13.3 knots, and them therefore being larger than the RAOs for lower velocities. The reason that only the advance velocity is compared, is the fact that the work done by Sui (2021) incorporated a propulsion control system that determines the engine rotating speed fluctuation, whereas the present work does not make use of that. The advance velocity does however give a good indication of what the propeller performance might be. If they are comparable, then it means that the numerical results are comparable to the empirical equations for wake fluctuation.

5.6 Conclusions

The conclusions that have been drawn in this section are supposed to answer the main research question of this work, which was the following:

What is the influence of waves on the ship operational safety of the ocean-going chemical tanker 'Castillo de Tebra', sailing forward at its design speed?

The definition of ship operational safety is whether or not the ship has enough thrust availability when operating in adverse weather conditions. As it has been concluded, the influence of waves on the ship operational safety is that for the design ship speed and engine speed of the ship, the engine would overload for all wave direction, when irregular waves are considered. The reason is that the thrust and torque that the propeller produces in adverse weather conditions would be too large for the engine to handle. This would mean that the ship is underpowered during adverse weather conditions. Also, the results have shown that the ship thrust availability is not satisfactory to overcome the thrust that the propeller produces in adverse weather. This research did not take into account what the ship speed change would be if it sailed in adverse weather condition, making the research limited to only one sailing condition. Adverse weather conditions are inherently *not* the design condition of the vessel, therefore the results of the present work do not paint a realistic picture of how the vessel would operate in adverse weather. However, taking into account the assumption that the results are representative, the conclusion of this research is that the predefined adverse weather conditions would result in the fact that the 'Castillo de Tebra' is underpowered. Therefore, lowering the EEDI of this ship would result in dangerous situations as the engine would overload in large waves.

5.7 Discussion & Shortcomings

This paragraph will provide some points of discussion that concern the present work in relation to the propeller and engine performances that have been determined. Some recommendations will be presented as well.

5.7.1 Conflict of EEDI and Minimum Propulsion Power in Adverse Weather

One of the reasons that this research has been proposed, is to find out whether the ship in question will be underpowered in adverse weather conditions. In response to the IMO, introducing the concept of the Energy Efficiency Design Index (EEDI), it seemed necessary to check whether just lowering the installed engine power would suffice when the ship sails in realistic conditions. MEPC (2019) proposes a concept that satisfied both problems; reducing engine power and thus ship speed for normal operating conditions and maintaining safe operation when sailing in adverse weather conditions. The proposed solution is limiting the available engine power in normal condition, whereas providing an additional reserve of engine power for manoeuvres in adverse weather for instance. This in practice would mean that the master of a ship can release an "emergency button" to use the power reserve and therefore using the full installed engine power. MEPC (2019) gives more details on the specifics of this concept, when to use it and other requirements.

5.7.2 Minimum Propulsion Power Guidelines

Since it has been shown that the benchmark ship is underpowered in adverse weather conditions, a look can be given into the minimum propulsion power guidelines. The guidelines given in MEPC (2019) have a level 1 and 2 assessment on what the minimum power should be of a ship. The first level only considers the minimum installed propulsion power. It therefore has no requirements on minimum ship thrust and minimum ship speed in adverse weather conditions. The ship operational safety is however dictated by the available propeller thrust and ship speed. These are limited by the available engine torque due to the torque-speed limit, rather than the installed MCR. The second level assessment does consider the available propeller thrust and minimum ship speed in adverse weather. The torque-speed limit is taken into account, but only the static engine load limit rather than the dynamic engine load limit. The engine could still be overloaded due to dynamic loads caused by waves. Sui (2021) proposes that an additional engine margin is considered in the assessment to take into account dynamic engine overloading.

5.7.3 Lower Ship Speeds and Propeller Revolutions

The calculations that have been carried out so far, have all used the assumption that the ship speed and propeller revolutions are constant. In reality, when a ship sails in waves, the speed constantly changes due to the added resistance that the ship experience from the waves. The present work has not taken into account the change in added resistance that occurs when sailing in waves. A ship not only experiences added resistance but also wave drift forces when it sails in waves. These are forces that vary with the low-frequency part of waves that have multiple frequencies. These forces also contribute to the added resistance that a ship feels, which would also have consequences on the propeller performance as there is more power needed to sail at the same ship speed.

For the present work, it was not possible to do any calculation on a lower ship speed. All SEACAL simulations were done on the design ship speed, additional simulations could not be done due to time limitations on the availability of SEACAL. Performing simulations on lower ship speeds could lead to investigating at what ship speeds the engine would not overload, when sailing forward at different wave directions. This could have been useful to present a clear image of what ship speeds are safe for the crew on board of the 'Castillo de Tebra'. Possible alternatives that could have been implemented to look into different ship speeds were either by multiplying all SEACAL RAOs by the ratio of the ship speed to the design ship speed. this would however not be realistic, as for instance with a zero ship speed there would be zero velocity changes due to waves. This is naturally not true, as waves cause circular water motions and thus velocities, even with zero ship speed.

A different way of changing the RAOs is by changing the ship speed in the equa-

tion for the encounter frequency (equations 4.30). This would however only lead to different RAOs at different encounter frequencies, but not specifically changing them based to the actual ship speed in SEACAL.

Nevertheless, this section will provide a brief evaluation of the thrust and torque generation and power requirements at lower ship speeds and propeller revolutions. This is realized by finding out what ship speeds are attained at which propeller revolutions in calm water. In other words, the $v_s - n_p$ graph needs to be found. From the propulsion and engine model used in Sui (2021) this graph could be extracted. This is shown in figure 33.

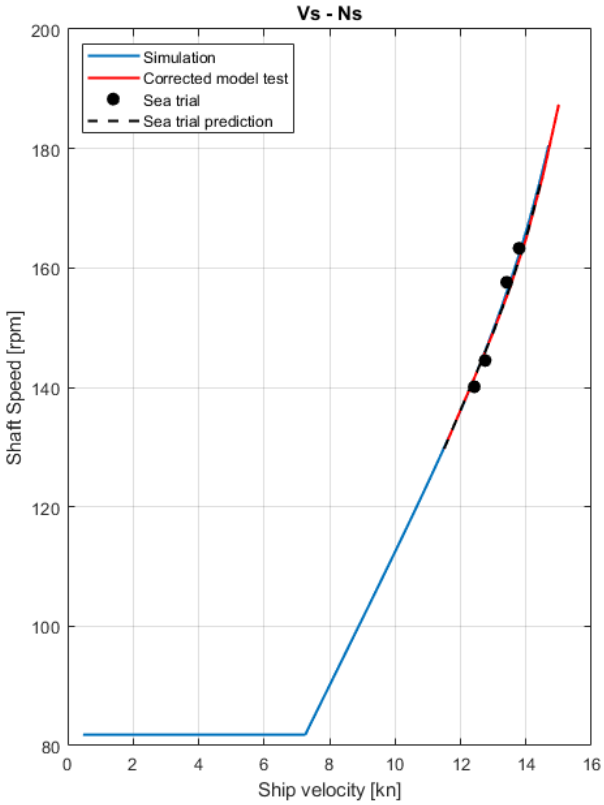

Figure 33: Ship speed - propeller revolutions graph

From this graph, three additional sailing points have been read, given in table 10.

n_p [rpm]	v_s [kn]
80	7.2
100	8.8
133	11.9

Table 10: Sailing points

Using these points, new calculations are made for the thrust and torque production of the propeller. Using the same procedure as the one discussed in paragraph 5.4.2, the brake power can again be depicted in the engine operating envelope and ship thrust envelope. These are given in figure 34 for following waves (0°).

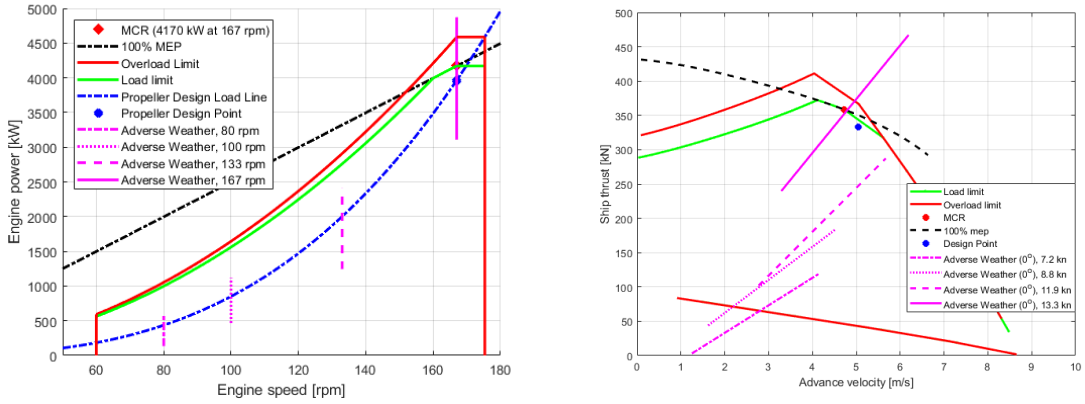

Figure 34: Engine operating envelope and ship thrust envelope for reduced ship and propeller speeds

In the engine operating envelope, it can be clearly seen that running on reduced ship and propeller speeds, the engine has enough power to account for the torque variations caused by the waves. However, when looking at the ship thrust envelope, only the reduction to 11.9 knots suffices, as the other reductions exceed the lower load limits. This indicates that more time and effort needs to be put into calculating engine loading in adverse weather at lower ship and propeller speeds. Taking into account added resistance is also vital here.

For lower engine loads and speeds, an auxiliary blower can be used. This is an electrically driven machine that assists in air supply to the engine below an engine load of about 30% (Yum et al. (2017)). Below this engine load, the turbocharger is not able to sufficient air for the scavenging process. Sui (2021) modeled the effect of an auxiliary blower on the engine process for different engine loads. Figure 35 shows the engine mass flow as well as the specific fuel consumption for the full range of engine load (0% - 100%).

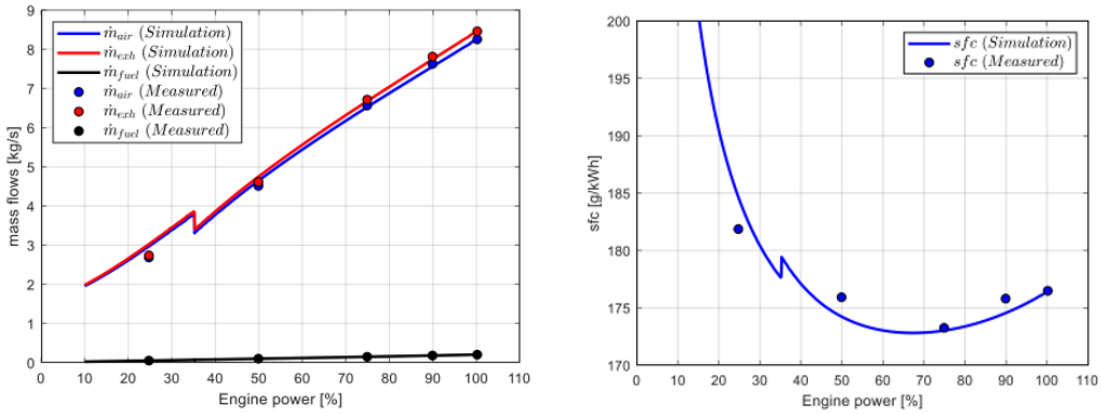

Figure 35: Mass flow (left) and specific fuel consumption (right) of the engine with auxiliary blower (Sui (2021))

Below en engine load of 35%, it can be seen that the auxiliary blower is used as the mass flow is higher there than if it were switched off. It also helps in decreasing the fuel consumption slightly, which leads to a decrease in emissions. When the engine load passes the 35% mark, the auxiliary blower is switched off again as the turbocharger can do its work well enough. This shows that at low engine loads, an auxiliary blower is helpful in increasing the mass flow and reducing fuel consumption.

5.7.4 Power Take Off & Power Take In

The benchmark chemical tanker uses the main engine for PTO mode, meaning that power is taken off from the main engine to generate electric power. The results from the present work did not take PTO mode into account. Actually, using PTO mode would only result in having less available power for propulsion, ultimately resulting in the ship becoming even more underpowered in adverse weather. However, if the shaft generator of the benchmark chemical tanker were to be updated to be able to have a power take-in (PTI) mode as well, then the engine would be able to provide more power. PTI mode means that the shaft generator provides additional power to boost the main engine. This would mean that both the engine operating envelope as well as the ship thrust envelope would widen. Additional research should investigate whether the engine with PTI mode would overload in adverse weather. Obviously it would overload in the present work in PTO mode as less propulsion power would be available.

Some drawbacks of using a shaft generator are that the efficiency of propeller and engine is reduced at low propulsion power. Besides that, no power generation is realised in port as the primary mover is in stop condition. Also, engine load increases slightly when the shaft generator is used due to the additional attachment of the shaft to the engine (MAN (2021)).

A quantitative evaluation of the benefits of PTI for the present work will be given

here. Two different PTI power modes will be used, namely 500 kW and 1000 kW. What basically changes, is that these amounts of power are added to the MCR of the engine. That would indicate that the new MCR of the engine would be 4670 kW and 5170 kW respectively. This naturally enlarges the engine operating envelope. The new operating envelopes for a PTI of 500 kW and 1000 kW are shown in figure 36 for following waves.

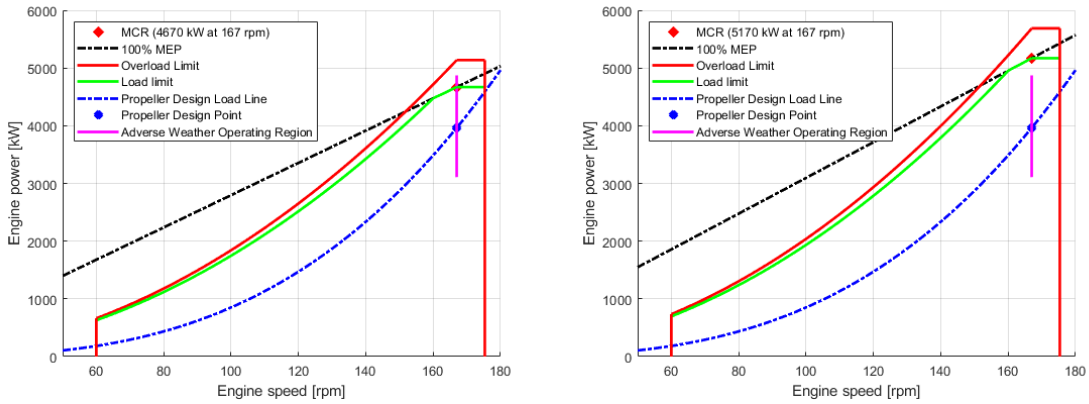

Figure 36: Engine operating envelopes for following waves with installed PTI of 500 kW (left) and 1000 kW (right)

Here it can be seen that the adverse weather load lines fall within the operating envelope of the engine, indicating that the ship could sail at the design speed with the engine running at its design speed in following waves. For a PTI of 500 kW, this conclusion was also drawn for waves coming from 15°, 90°, 105°, 165° and 180° wave directions. For a PTI of 1000 kW, more wave directions are viable for sailing at the design speeds, namely 75°, 135° and 150° waves are added to the prior list. Installing a PTI would therefore be a viable solution for the present work.

The ship thrust envelope also changes as a result of the use of a PTI. Figure 37 shows the ship thrust envelope for following waves with a PTI of 1000 kW. Here it can be clearly seen that only for the lower advance velocities, the ship thrust envelope limits increase in comparison to figure 31. The actual ship thrust that is generated by the propeller still goes over the limits for the same ship speed and propeller speed. Therefore, at lower advance velocities, there is more ship thrust availability when a PTI is installed. At higher advance velocities, the ship thrust availability remains equal.

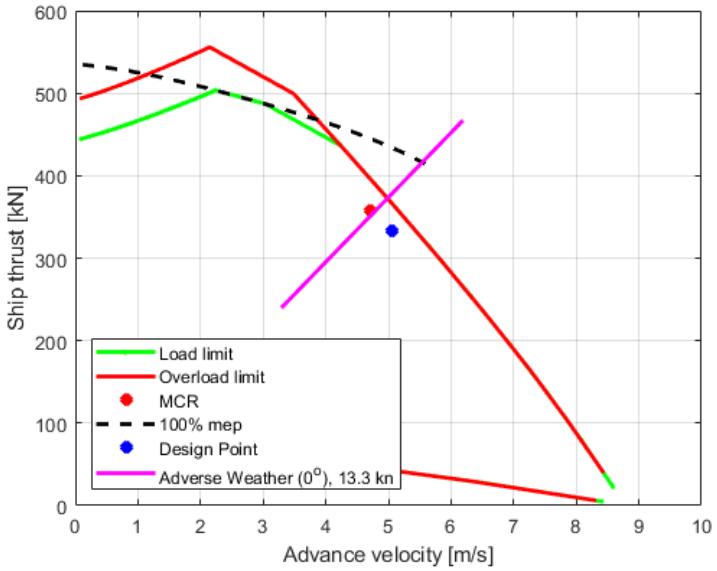

Figure 37: Ship thrust envelope with PTI

5.7.5 Controllable Pitch Propeller

The present work made all calculations based on having a fixed pitch propeller. The chemical tanker 'Castillo de Tebra' actually has a controllable pitch propeller, which can change its pitch when operating certain manoeuvres or encountering different weather conditions to provide the highest efficiency per operating condition. The calculations that have been performed so far only considered the design pitch of the CPP, thus making it a fixed pitch propeller. Different pitch settings however will influence the propeller load in the engine operating envelope. Also the limits in the ship thrust envelope will be affected, as these are dependent on the open-water characteristics, which change with different pitch settings. The pitch that has been used for all calculations was P/D = 0.7075. Figure 38 shows two engine operating envelopes with propeller load lines having a pitch of P/D = 0.6 and P/D = 0.8, respectively.

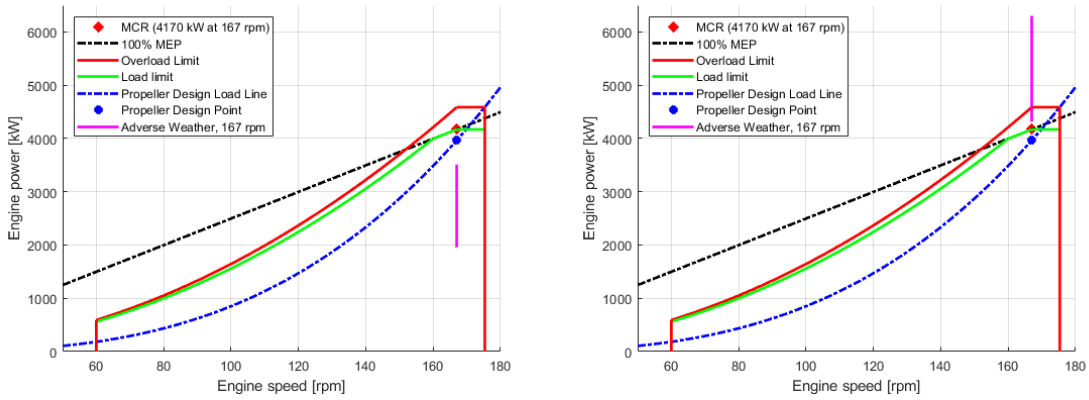

Figure 38: Effect of CPP on propeller load (left: PD=0.6, right: PD=0/8)

What is clear here, is that lowering the pitch setting of the propeller lowers the propeller load at the design ship speed and propeller speed. In other words, less torque is produced. A larger pitch shows that the load is increased, generating more torque.

The change of the propeller pitch also changes the ship thrust envelope. Figure 39 shows the thrust envelopes and the propeller loads for P/D = 0.6 and P/D = 0.8.

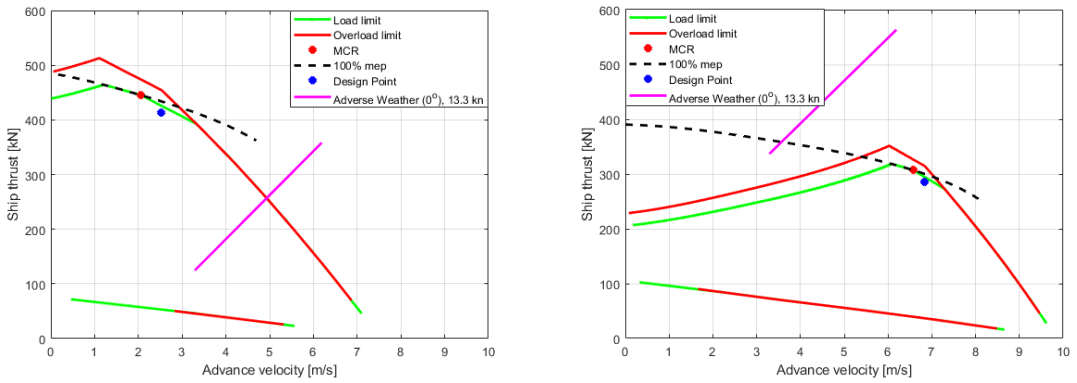

Figure 39: Ship thrust envelopes with P/D = 0.6 (left) and P/D = 0.8 (right)

Lowering the pitch ratio ensures more ship thrust availability in lower advance velocities whereas increasing the pitch ratio gives a bit more ship thrust availability in the larger advance velocity at the expense of lower advance velocities. In both cases, the propeller load does not fit inside the ship thrust envelope. Decreasing the ship speed and propeller speed again in adverse weather would probably make the propeller load fit inside the envelope. Further research must point that out. Another thing that needs to be noted is that lowering the pitch ratio decreases the ship thrust production and therefore will probably automatically decrease the ship speed, because the ship thrust does not cover the ship resistance.

5.7.6 Larger Engine

Another idea to omit engine overloading is installing a larger engine on the ship. Sui (2021) found that if an engine with an MCR of 5220 kW, 167 rpm was installed, then the larger engine has a larger reserved power for ship operation in heavy loading conditions. Besides that, in adverse weather conditions, the ship could attain larger ship speeds due to larger ship thrust availability. Thus, the ship's propulsion capability and the ship operational safety are improved when a larger engine is installed. At high ship speeds, the larger engine would not influence the emissions much. However, during manoeuvring and low loads, the engine would not run at its design condition and therefore would ensure a lower efficiency and higher emissions.

5.7.7 Manoeuvring Operations

The ship propulsion characteristics in adverse weather that have been calculated in this section used forward sailing at the design speed as its main sailing condition. This is already a step forward in the design process, as adverse weather conditions are rarely taken into account. However, operations such as crash-stop and zig-zag manoeuvres need to be investigated as well. These operations require large off-design engine loads, especially when the ship in an area with large waves. Leaving these out of the research means that there is still a conclusion to be drawn on whether the ship is underpowered when performing manoeuvres in adverse weather.

6 Conclusions & Recommendations

The need for ships to be designed taking into account how they behave in adverse weather conditions is gaining more attention, as it is important to find out whether a ship is underpowered or not when it sails in large waves. The present work aimed at determining whether the installed engine in the chemical tanker 'Castillo de Tebra' is capable of delivering enough power to propel the ship in large waves at its design ship speed and design engine speed, without overloading. The conclusions drawn from this research will be summarized here, adding to that a number of recommendations for further research.

6.1 Addressing the Research Questions

The main research question for the present work was:

> **What is the influence of waves on the ship operational safety of the ocean-going chemical tanker 'Castillo de Tebra', sailing forward at its design speed?**

With the following sub-questions:

> **1. How is ship operational safety defined and how can it be quantified?**
> **2. What methods can be used to determine the influence of waves on the ship operational safety?**

To answer these questions, firstly a literature review has been carried out on what the state-of-the art is in the field of ship propulsion in adverse weather conditions, specifically how the propeller and engine behave when a ship sails in waves. The ship operational safety is defined as the ship thrust availability when operating in adverse weather. This was quantified by determining the thrust and torque generation of the propeller when the ship sails forward in various wave directions and frequencies in the research part of this work. This part saw numerous simulations being done on a 3D hull of the chemical tanker. The variable that was sought after was the water velocity change at the propeller plane. This was then used to determine what the thrust and torque generation is of the propeller at a specific wave height and period, for a number of wave directions. It was concluded that when a ship sails at its design speed and has nominal engine speed, the engine overloads in all wave directions. Naturally, the engine will decrease its speed according to the fluctuations of the propeller torque to not overload. This will however be at the expense of ship speed. Added resistance was not taken into account in the present work. If this were considered, then the ship speed would also decrease, as the ship needs more (unavailable) power to sail at a constant speed.

There are a number of ways to make sure that the ship does not become underpowered in adverse weather. One of them is installing an engine with more available

propulsion power. An evaluation of the engine load in waves when sailing at lower ship speeds and engine speeds has also been done and showed that for following waves, the engine has enough power to sail at lower ship speeds. However, the lower ship thrust limit would be reached at ship speeds lower than 12 knots. When a Power Take-In of 1000 kW were to be installed, the engine would not be overloaded anymore for 0°, 15°, 75°, 90°, 105°, 135°, 150°, 165°, and 180° waves. Lowering the pitch of the propeller would also decrease the engine load for following waves such that the engine limits would not be reached and the ship would not become underpowered. However, lowering the pitch would also lead to a decrease in thrust production, which ultimately would lead to a decrease in ship speed. This has not been considered in the calculations.

A number of additional questions were also asked at the beginning of this thesis, being:

- What sea states are relevant for the assessment of the propulsive performance of the chemical tanker?
- What methods are used for determining the effects of waves on propeller performances in straight ahead sailing in waves, manoeuvring in calm water and manoeuvring in waves?
- Using the provided geometrical coefficients and parameters of the vessel, how can a 3D model of the ship hull be made for further use? And how does this hull shape compare to other similar tankers?

It was found that adverse weather conditions were defined by IMO (2013) with the following parameters:

Significant wave height $H_{1/3}$ [m]	4.0
Peak wave period T_P [s]	7.0
Mean wind speed V_w [m/s]	15.7

Table 11: Adverse sea condition definition

For the second additional question, it has been found that potential flow theory works well for determining the effects of the excited forces of waves on ship hulls. However, it would be better to take into account viscous effects when looking into effects of waves on propulsors. Computational fluid dynamics would be a good alternative to use instead of potential flow. This would however lead to longer and more complex simulations.

The third additional question was answered in section 4.4.2. Here it was shown that a simple KVLCC2-model was modified to have approximately the same geometrical coefficients as the hull of the Castillo de Tebra. A more detailed hull than the one used here would lead to more accurate results. However, it was assumed that the

used hull would suffice for the present work.

After answering all the research questions, it can be concluded that the present work was limited by looking at what the influence of waves would be on the ship, sailing at the design speed and the engine turning at its rated speed. A ship however would not sail at the design speed in adverse weather conditions, due to both voluntary as well as involuntary speed reduction. The voluntary speed reduction is caused by the captain, reducing the speed for safety reason. The involuntary speed reduction is caused by the added resistance of the waves on the ship, leading to the engine needing more power to sail at a constant speed and therefore the ship reducing its speed.

6.2 Recommendations for Further Research

One of the biggest shortcomings in the present work is that velocity changes near the propeller plane have been determined using a potential flow solver. The flow at the stern of a ship is largely viscous in nature, as the ship's hull form changes a lot at the stern, which would alter the boundary layers and make the flow turbulent and possibly even separate. Using a potential flow solver, these effects are neglected. A uniform flow is assumed along the hull, which is not realistic. A way to solve this problem in the future, is to use Computational Fluid Dynamics (CFD). With CFD, viscous effects are not neglected and will therefore give more accurate results. The downside of CFD is the time consumption it takes for a single simulation to complete. Besides that, it is even harder to simulate waves in a CFD simulation, together with a ship that has a forward speed. For the present work, the potential flow solver SEACAL made it very simple to simulate different wave directions combined with a forward ship speed. However, as mentioned, the results would be more accurate if CFD was used.

Neglecting the effects of oblique propeller inflow was a simplification that was made for the present work, which in reality would result in an incomplete representation of the amount of forces and moments that occur by the propeller as well as on the propeller. Taking into account the effects of oblique propeller inflow, either analytically or numerically, a better picture can be drawn of the forces the propeller generates as well as the side-forces and moments the propeller and ship experience.

Further research should investigate what the ship speed change and engine load is when performing certain manoeuvres in adverse weather. Only taking into consideration that the ship sails forward at its design speed does not paint the whole picture of whether a ship is underpowered when sailing or manoeuvring in large waves. During manoeuvres, velocity changes at the propeller plane will change differently then when it sails forward. Oblique propeller inflow will also occur, indicating that propeller performance will change and additional side-forces and moments will be generated on the hull.

The present work made use of a 3D hull that had similar geometrical coefficient as the chemical tanker 'Castillo de Tebra'. However, the exact hull form has not been achieved. Especially the stern of the used hull form was not very realistic, nor did it exactlty look like the one of the chemical tanker. The stern of the ship however, is the most important part for the present work, since the advance velocity is highly dependent on the form of the stern. By putting more time into creating the most accurate hull form, the results would be more accurate. This would require a lot of experience and time however which was not available for this moment.

A ship sailing in waves experiences added resistance, which was neglected in the present work. Added resistance ultimately leads to a decrease of ship speed when the engine operates at its maximum continuous rating, because the engine needs more power than it has available when it want to sail at the design speed. For the present work, the added resistance component has been left out, mainly due to lack of time. It is however important to take it into account to figure out how the engine operates in adverse weather conditions.

A Appendix

A.1 Ship Meshes

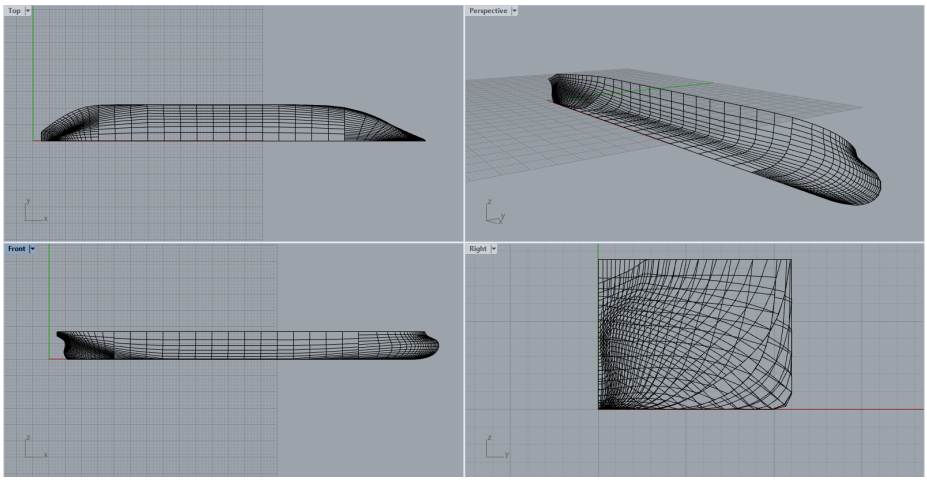

Figure 40: Coarse mesh

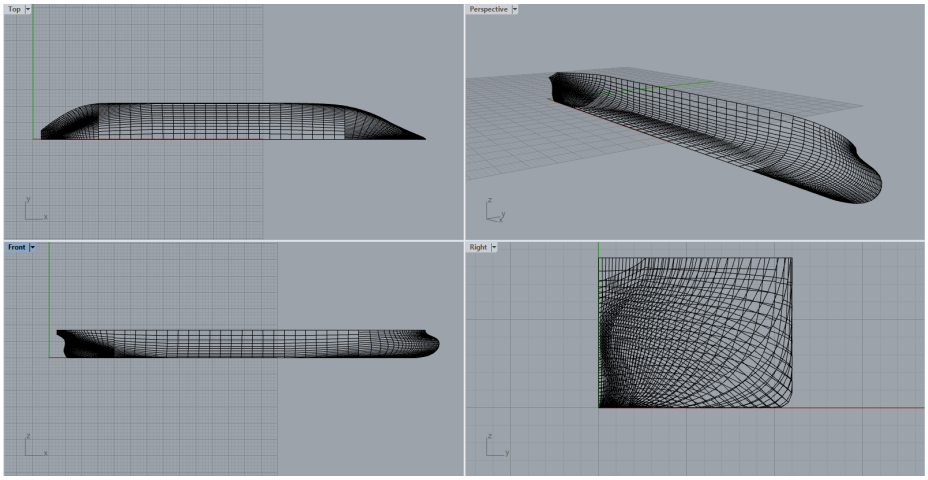

Figure 41: Medium mesh

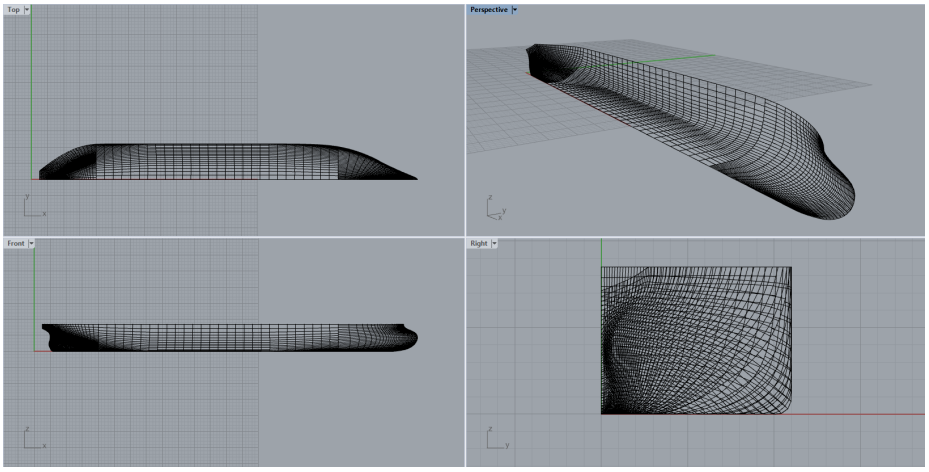

Figure 42: Medium mesh 2

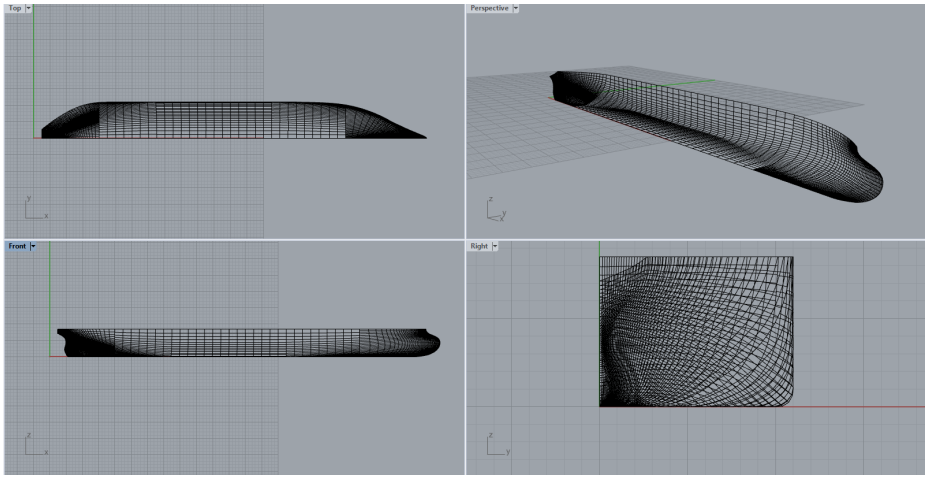

Figure 43: Fine mesh

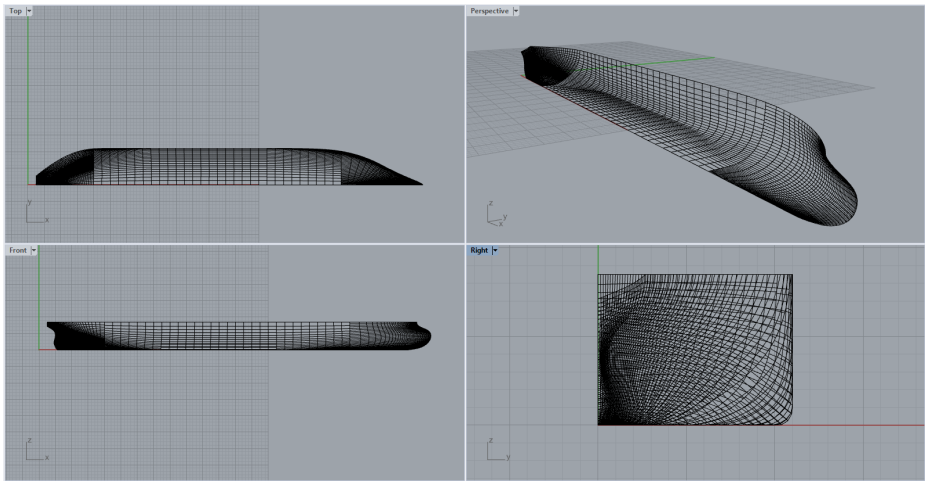

Figure 44: Very fine mesh

A.2 Longitudinal Velocity RAOs for All Wave Directions

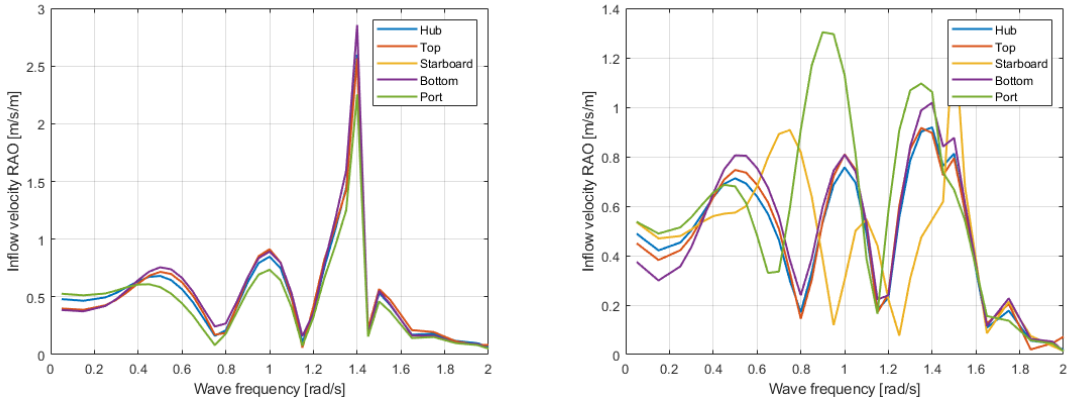

Figure 45: Longitudinal velocity RAOs at 5 reference points (0° and 15° waves)

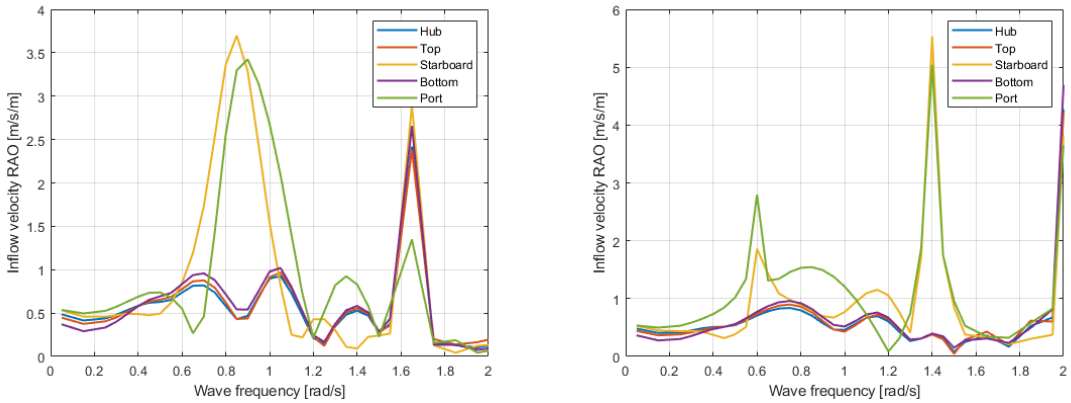

Figure 46: Longitudinal velocity RAOs at 5 reference points (30° and 45° waves)

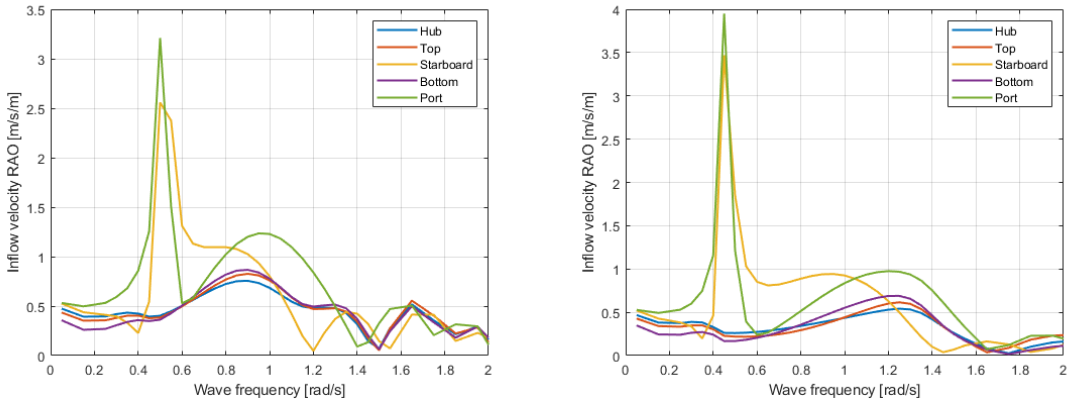

Figure 47: Longitudinal velocity RAOs at 5 reference points (60° and 75° waves)

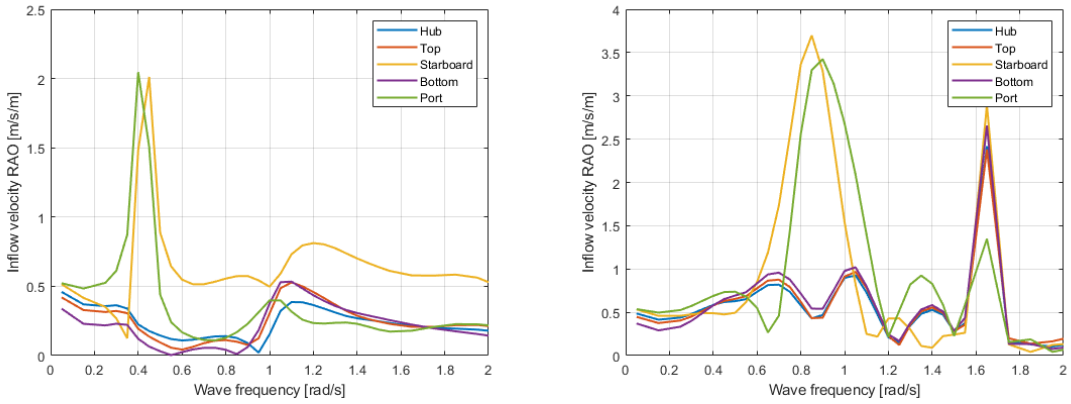

Figure 48: Longitudinal velocity RAOs at 5 reference points (90° and 105° waves)

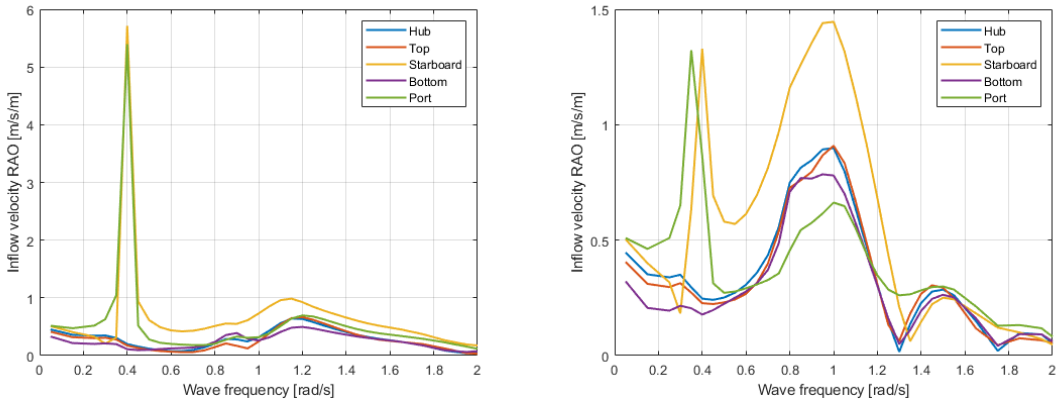

Figure 49: Longitudinal velocity RAOs at 5 reference points (120° and 135° waves)

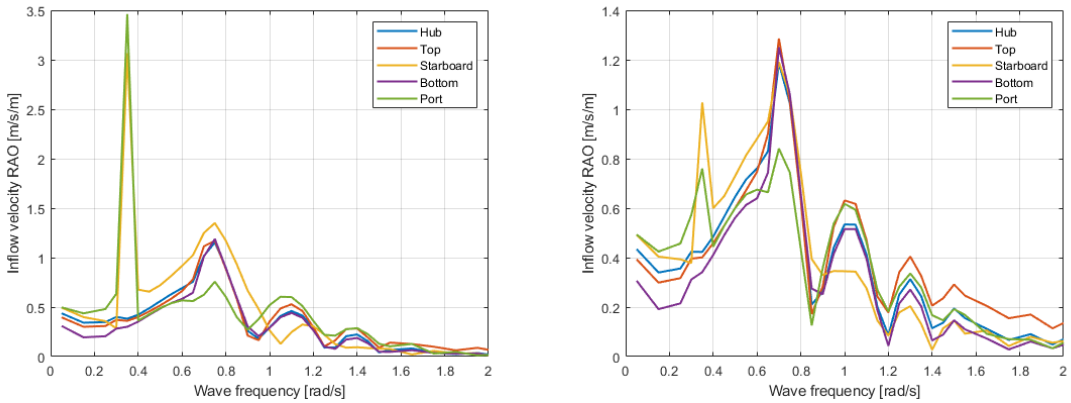

Figure 50: Longitudinal velocity RAOs at 5 reference points (150° and 165° waves)

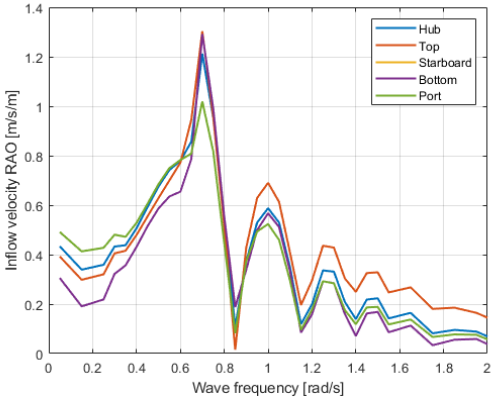

Figure 51: Longitudinal velocity RAOs at 5 reference points (180° waves)

A.3 Ship Motions in All Wave Directions

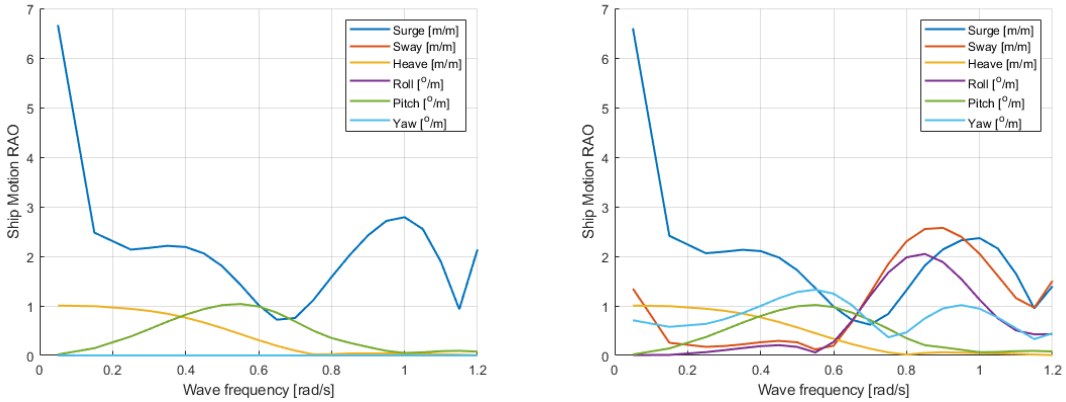

Figure 52: Ship motion RAOs at 0° and 15° waves

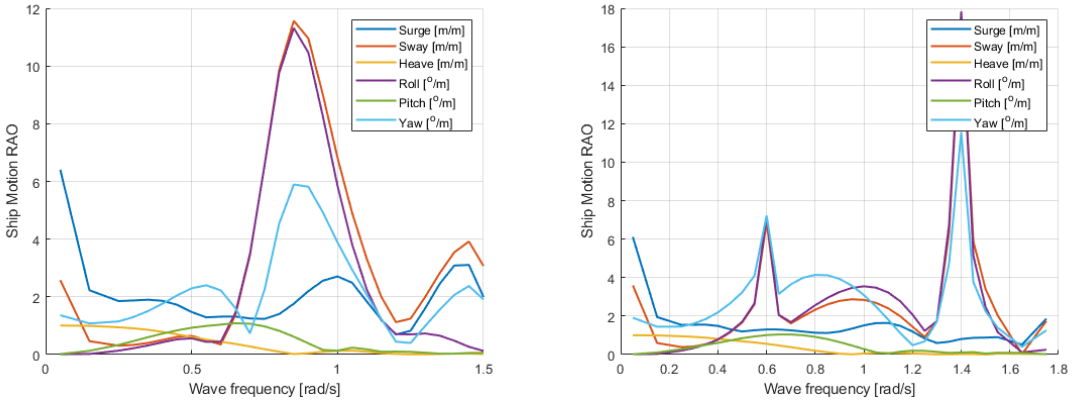

Figure 53: Ship motion RAOs at 30° and 45° waves

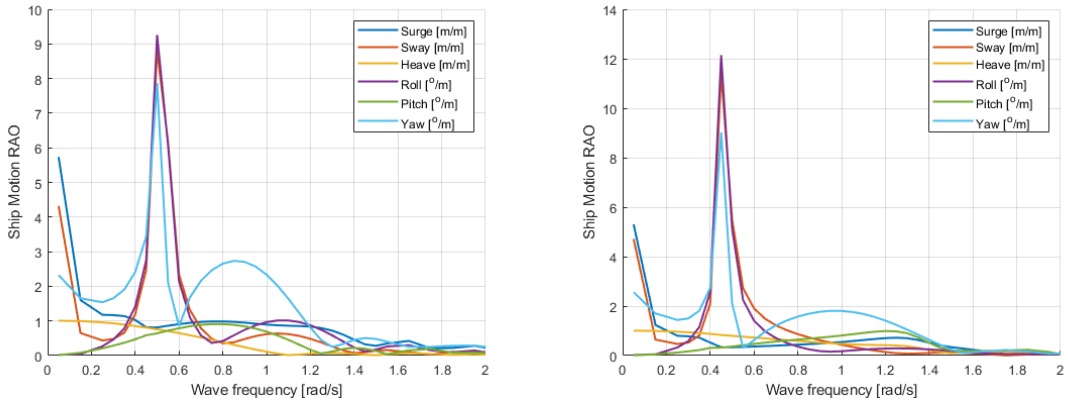

Figure 54: Ship motion RAOs at 60° and 75° waves

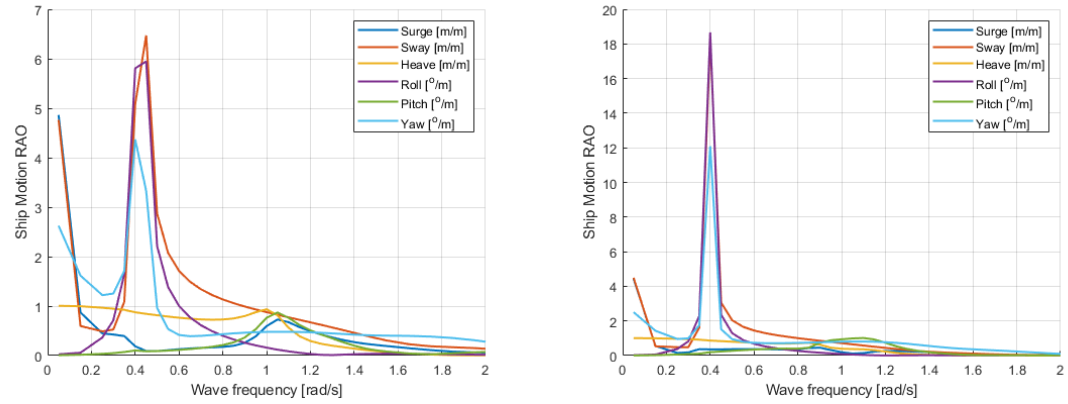

Figure 55: Ship motion RAOs at 90° and 105° waves

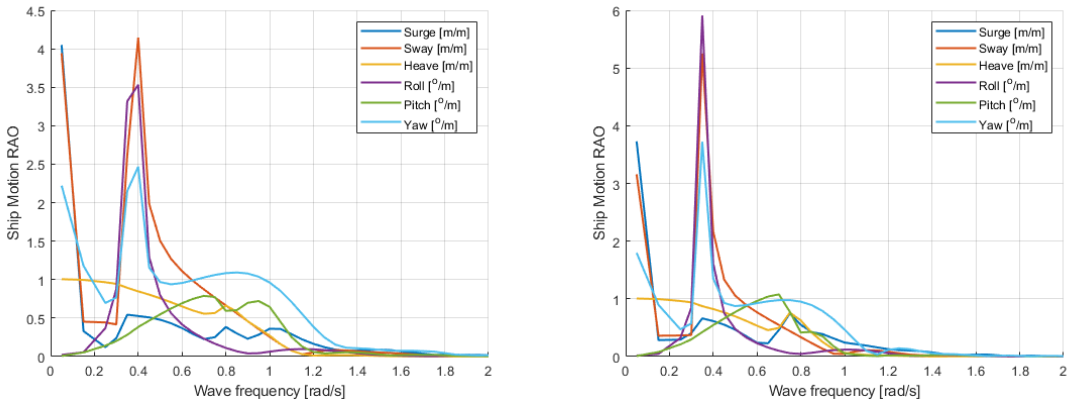

Figure 56: Ship motion RAOs at 120° and 135° waves

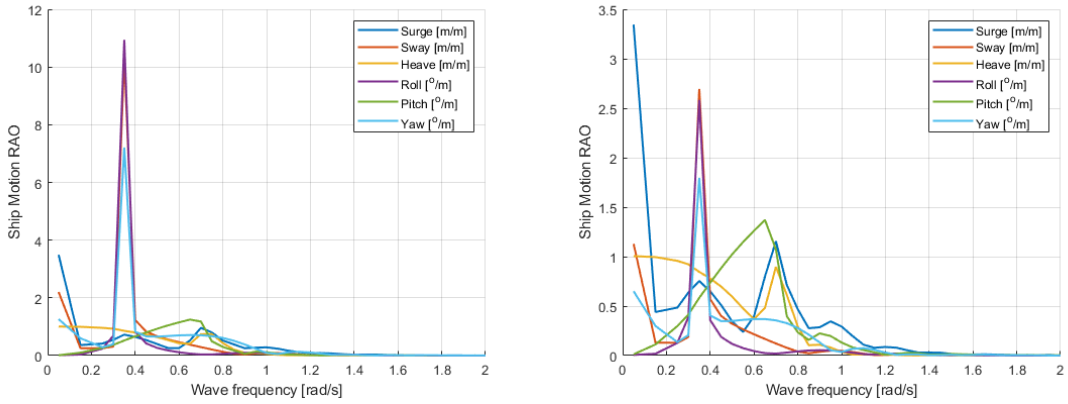

Figure 57: Ship motion RAOs at 150° and 165° waves

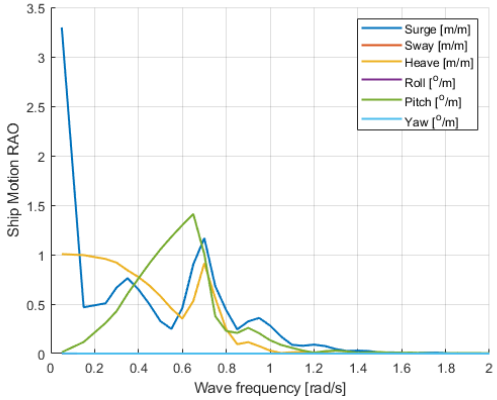

Figure 58: Ship motion RAOs at 180° waves

A.4 Inflow Velocity Fluctuations in All Wave Directions

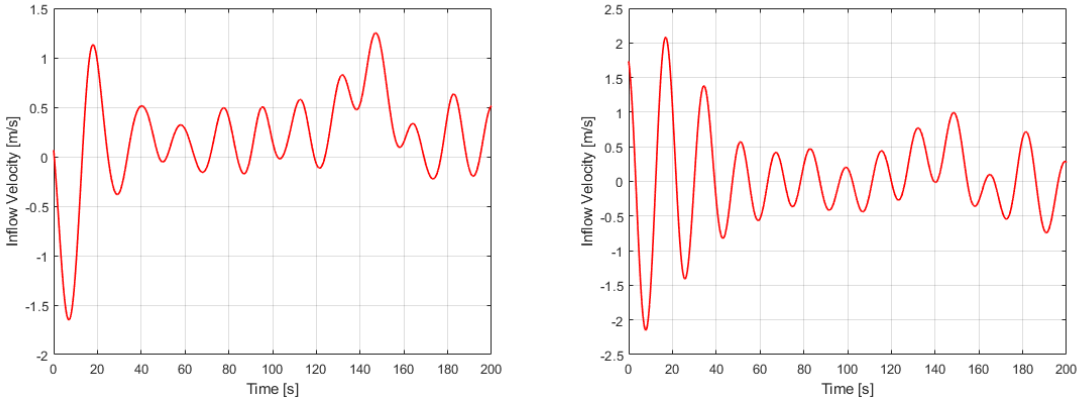

Figure 59: Inflow velocity fluctuation at 0° and 15° waves

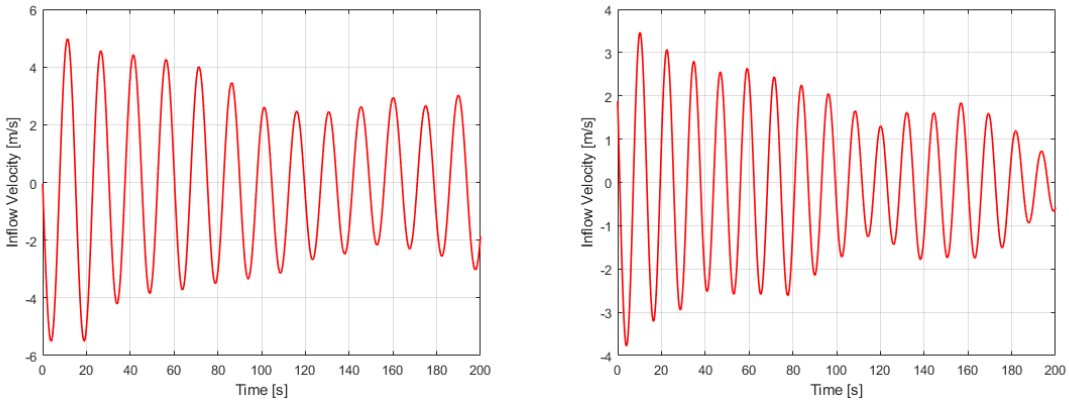

Figure 60: Inflow velocity fluctuation at 30° and 45° waves

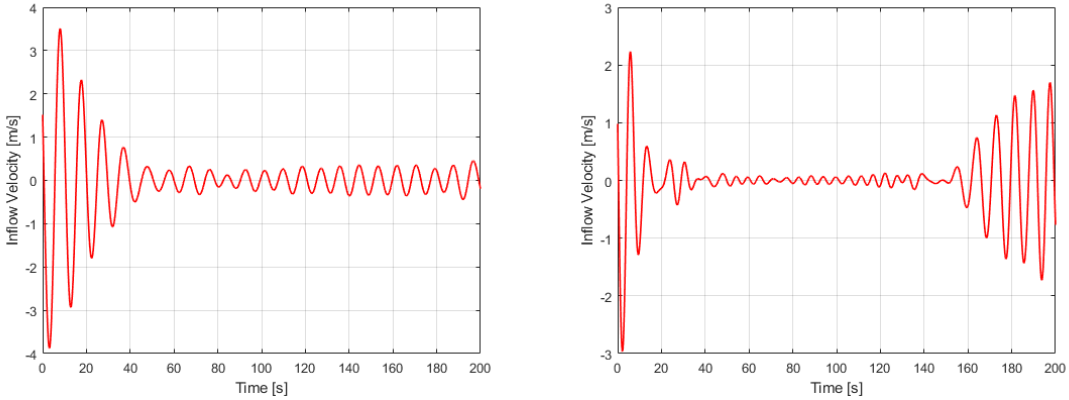

Figure 61: Inflow velocity fluctuation at 60° and 75° waves

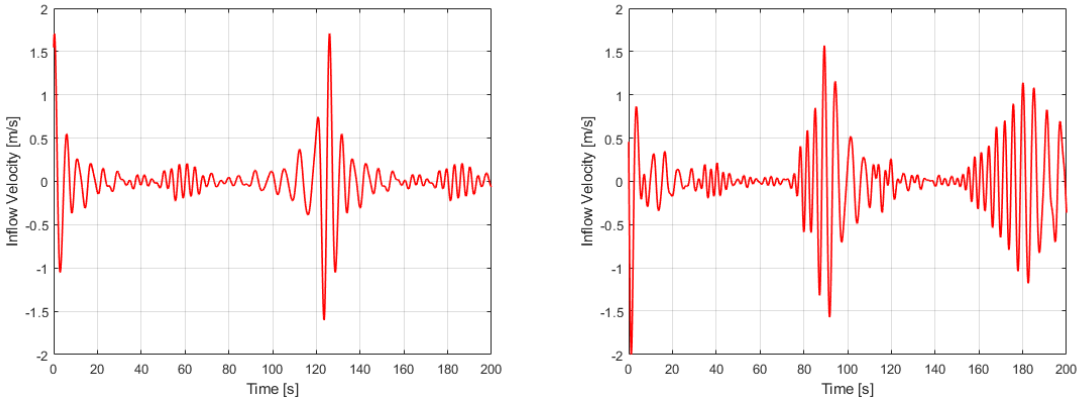

Figure 62: Inflow velocity fluctuation at 90° and 105° waves

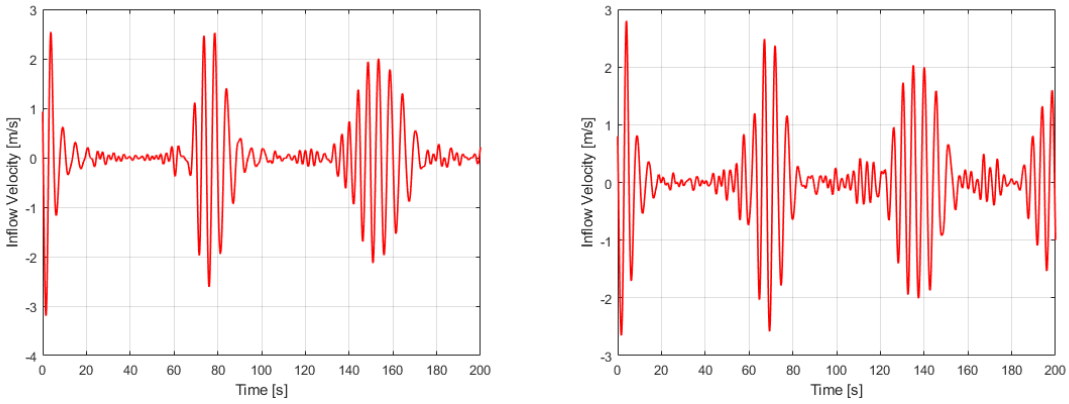

Figure 63: Inflow velocity fluctuation at 120° and 135° waves

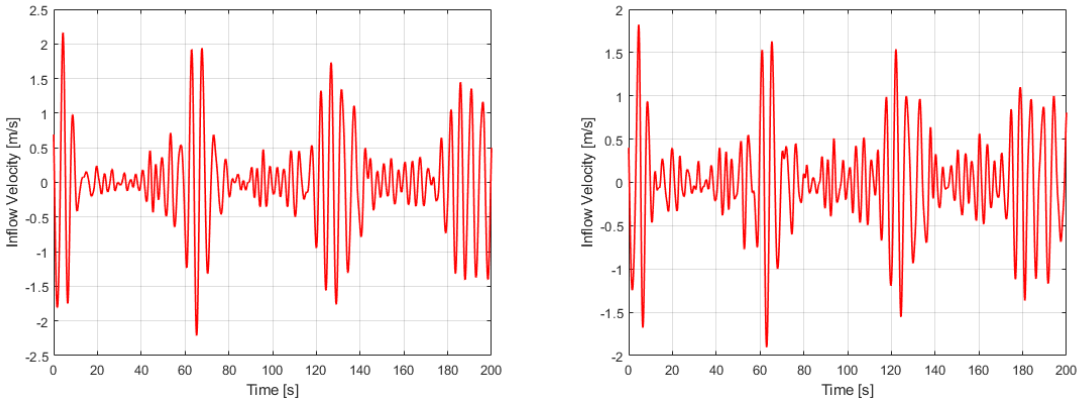

Figure 64: Inflow velocity fluctuation at 150° and 165° waves

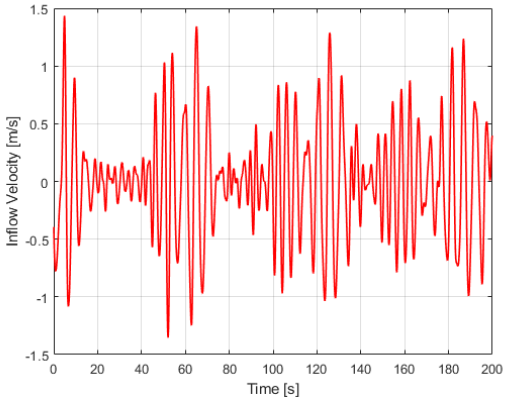

Figure 65: Inflow velocity fluctuation at 180° waves

A.5 Engine Operating Envelopes in All Wave Directions

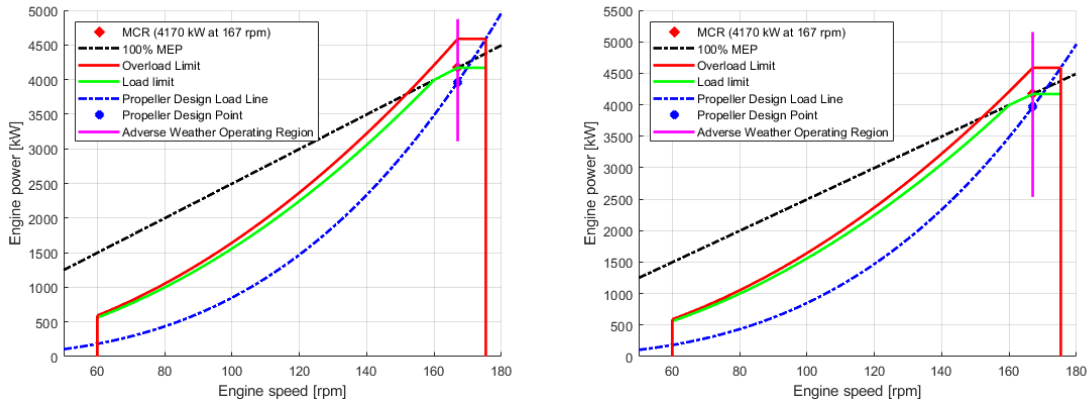

Figure 66: Engine operating envelopes at 0° and 15° waves

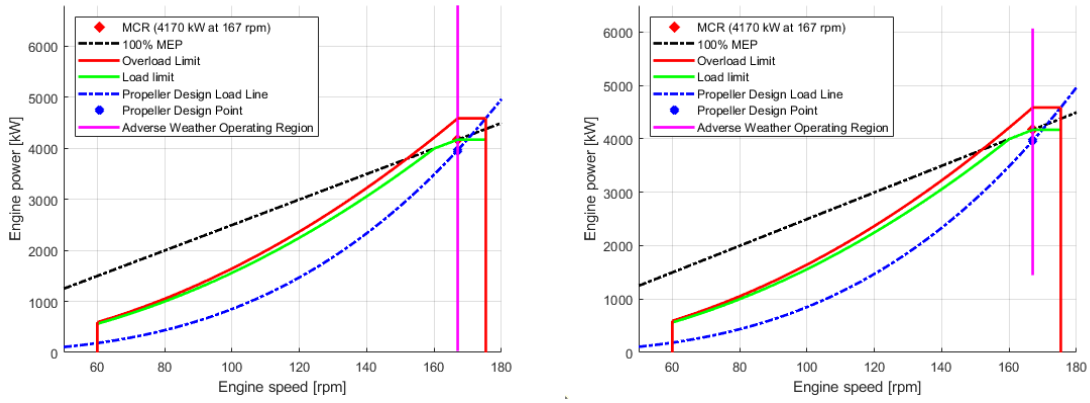

Figure 67: Engine operating envelopes at 30° and 45° waves

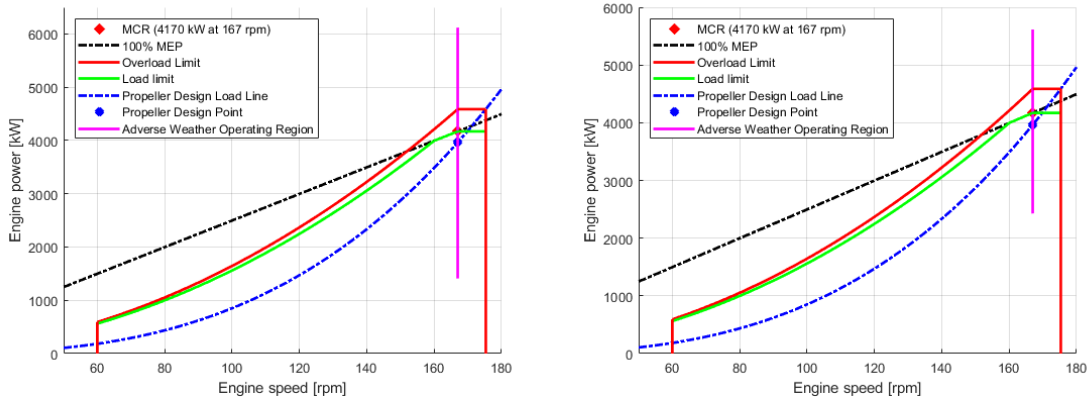

Figure 68: Engine operating envelopes at 60° and 75° waves

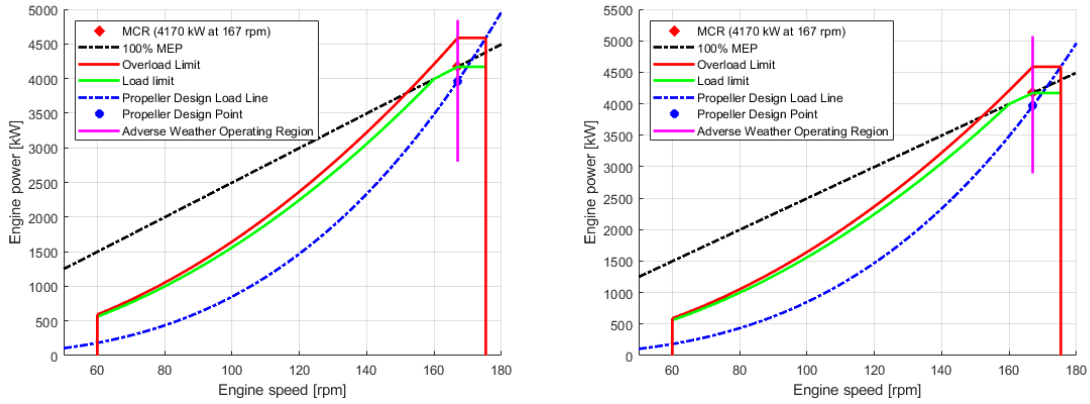

Figure 69: Engine operating envelopes at 00° and 105° waves

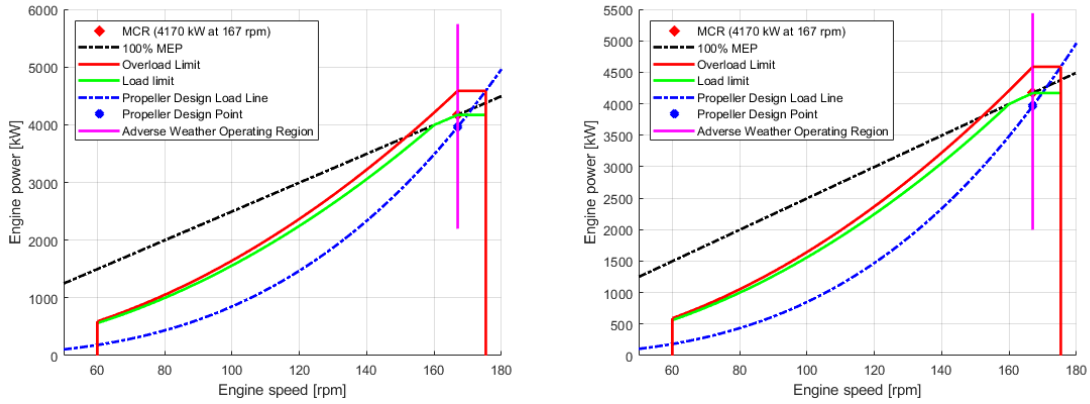

Figure 70: Engine operating envelopes at 120° and 135° waves

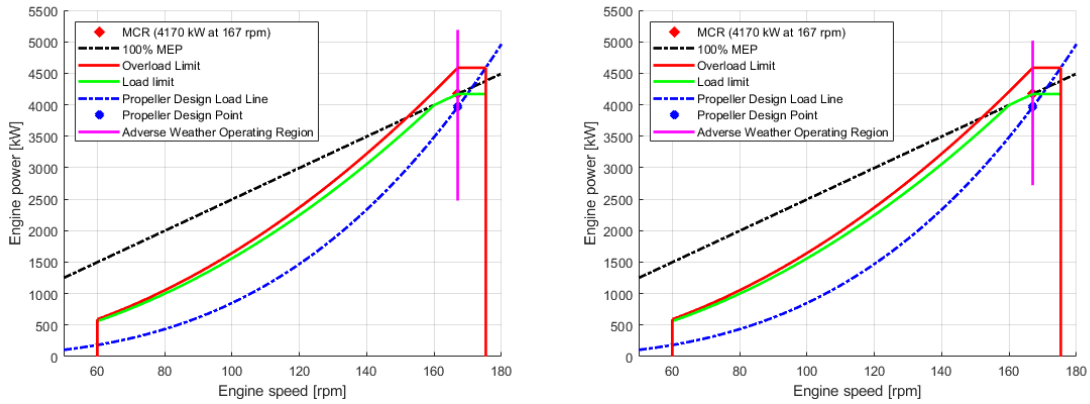

Figure 71: Engine operating envelopes at 150° and 165° waves

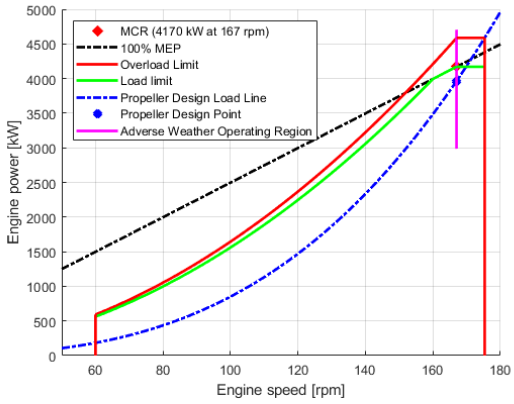

Figure 72: Engine operating envelope at 180° waves

A.6 Ship Thrust Envelopes in All Wave Directions

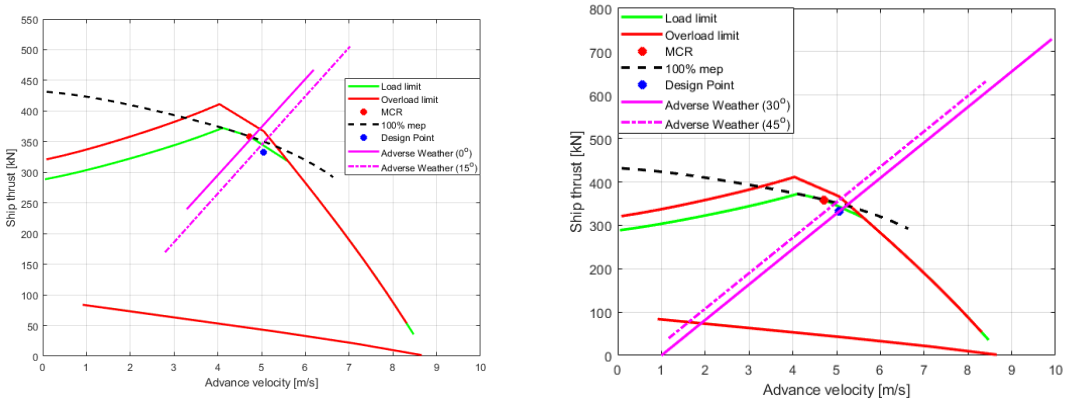

Figure 73: Ship thrust envelopes at 0°, 15°, 30°, and 45° waves

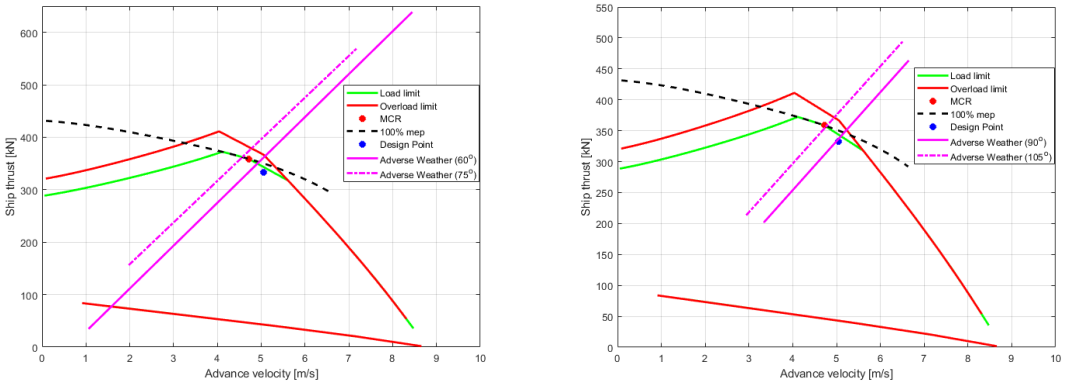

Figure 74: Ship thrust envelopes at 60°, 75°, 90°, and 105° waves

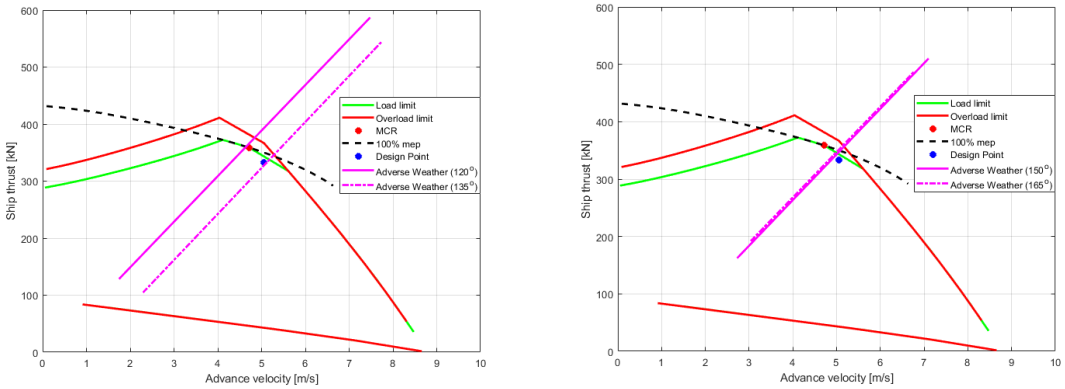

Figure 75: Ship thrust envelopes at 120°, 135°, 150°, and 165° waves

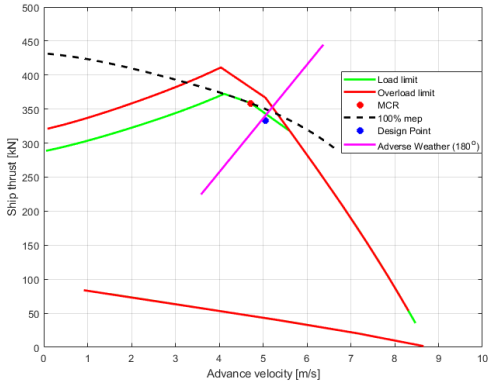

Figure 76: Ship thrust envelope at 180° waves

References

Bertram, V. (1990). A rankine source method for the forward-speed diffraction problem. Technical report.

Bertram, V. (2012). *Practical ship hydrodynamics*. Elsevier.

Bosschers, J. (2009). Procal v2.0 theory manual. *MARIN Report No. 20834-7-RD*.

Bosschers, J., Willemsen, C., Peddle, A., and Rijpkema, D. (2015). Analysis of ducted propellers by combining potential flow and rans methods. In *Fourth International Symposium on Marine Propulsors. June*, pages 639–648.

Bunnik, T., Daalen, V., Kapsenberg, G., Shin, Y., Huijsmans, R., Deng, G., Delhommeau, G., Kashiwagi, M., and Beck, B. (2010). A comparative study on state-of-the-art prediction tools for seakeeping. In *28th ONR Symposium on Naval hydrodynamics*.

Bunnik, T. H. (1999). Seakeeping calculations for ships, taking into account the non-linear steady waves.

Carrica, P. M., Ismail, F., Hyman, M., Bhushan, S., and Stern, F. (2013). Turn and zigzag maneuvers of a surface combatant using a urans approach with dynamic overset grids. *Journal of Marine Science and technology*, 18(2):166–181.

Costabel, M. (1987). Principles of boundary element methods. *Computer Physics Reports*, 6(1-6):243–274.

Crepier, P., Rapuc, S., and Dallinga, R. P. (2019). Cfd investigation into the wave added resistance of two ships. In *Practical Design of Ships and Other Floating Structures*, pages 95–114. Springer.

Dawson, C. (1977). A practical computer method for solving ship-wave problems. In *Proceedings of Second International Conference on Numerical Ship Hydrodynamics*, pages 30–38.

Dubbioso, G., Muscari, R., and Di Mascio, A. (2013). Cfd analysis of propeller performance in oblique flow. In *Third International Symposium on Marine Propulsors, SMP*, volume 13, pages 298–305.

Eça, L. and Hoekstra, M. (2014). A procedure for the estimation of the numerical uncertainty of cfd calculations based on grid refinement studies. *Journal of computational physics*, 262:104–130.

Faltinsen, O. and Loken, A. (1978). Drift forces and slowly varying forces on ships and offshore structures in waves. *Norwegian maritime research*, 6(1).

Faltinsen, O. M. (1980). Prediction of resistance and propulsion of a ship in a seaway. In *Proceedings of the 13th symposium on naval hydrodynamics, Tokyo, 1980*.

Fossen, T. I. (2005). A nonlinear unified state-space model for ship maneuvering and control in a seaway. *International Journal of Bifurcation and Chaos*, 15(09):2717–2746.

Fossen, T. I. (2011). *Handbook of marine craft hydrodynamics and motion control*. John Wiley & Sons.

Guo, B. and Steen, S. (2010). Added resistance of a vlcc in short waves. In *International Conference on Offshore Mechanics and Arctic Engineering*, volume 49118, pages 609–617.

Hirano, M., Takashina, J., Takaishi, Y., and Saruta, T. (1980). Ship turning trajectory in regular waves. *Publication of: West Japan Society of Naval Architects*, (60).

Hon, G. and Wang, H. (2011). The energy efficiency design index (eedi) for new ships. *ICCT Policy Update*, pages 1–9.

IMO (2013). 2013 interim guidelines for determining minimum propulsion power to maintain the manoeuvrability of ships in adverse conditions.

IMO, T. I. (2015). Ghg study 2014–executive summary and final report. *International Ma-ritime Organization, London, UK*.

ITTC (1999). Ittc – recommended procedures and guidelines: Terminology and nomenclature for propeller geometry.

Journée, J. and Massie, W. (2015). Offshore hydromechanics.

Klein Woud, H. J. and Stapersma, D. (2003). Design of propulsion and electric power generations systems. *Published by IMarEST, The Institute of Marine Engineering, Science and Technology. ISBN: 1-902536-47-9*.

Korvin-Kroukovsky, B. V. and Jacobs, W. R. (1957). Pitching and heaving motions of a ship in regular waves. Technical report, Stevens Inst of Tech Hoboken NJ Experimental Towing TANK.

MAN (2014). Man b&w s35me-b9.3-tii project guide - electronically controlled two-stroke engines with camshaft controlled exhaust valves. *MAN Diesel & Turbo, Copenhagen, Denmark*.

MAN (2021). Shaft generators for the mc and me engines. *MAN B&W Diesel A/S, Copenhagen, Denmark*.

MEPC (2011). Resolution mepc. 203 (62); amendments to the annex of the protocol of 1997 to amend the international convention for the prevention of pollution from ships, 1973, as modified by the protocol of 1978 relating thereto.

MEPC (2017). Air pollution and energy efficiency: Results of research project "energy efficient safe ship operation" (shopera). *IMO*.

MEPC (2019). Air pollution and energy efficiency: Updated proposal for an option to limit the shaft / engine power while ensuring a sufficient safety power reserve in adverse weather conditions. *IMO*.

Nakamura, S. and Naito, S. (1979). Propulsive Performance of a Container Ship at Light Condition in Waves. *Journal of the Kansai Society of Naval Architects, Japan*, (173):67–76.

NMRI (2000). Kriso tanker (kvlcc2).

Papanikolaou, A., Zaraphonitis, G., Bitner-Gregersen, E., Shigunov, V., El Moctar, O., Soares, C. G., Reddy, D. N., and Sprenger, F. (2015). Energy efficient safe ship operation (shopera). In *SNAME 5th World Maritime Technology Conference*. OnePetro.

Pinkster, J. A. and Hooft, J. (1976). Low frequency second order wave forces on vessels moored at sea. In *11th Symposium on Naval Hydrodynamics, ONR, London, England, 1976*.

Quadvlieg, F., Rapuc, S., et al. (2019). A pragmatic method to simulate maneuvering in waves. In *SNAME Maritime Convention*. The Society of Naval Architects and Marine Engineers.

Rijpkema, D., Starke, B., and Bosschers, J. (2013). Numerical simulation of propeller-hull interaction and determination of the effective wake field using a hybrid rans-bem approach. In *3rd International Symposium on Marine Propulsors,(May)*, pages 421–429. Citeseer.

Roache, P. J. (2009). *Fundamentals of verification and validation*. hermosa publ.

Saettone, S., Tavakoli, S., Taskar, B., Jensen, M. V., Pedersen, E., Schramm, J., Steen, S., and Andersen, P. (2020). The importance of the engine-propeller model accuracy on the performance prediction of a marine propulsion system in the presence of waves. *Applied Ocean Research*, 103:102320.

Seo, M.-G. and Kim, Y. (2011). Numerical analysis on ship maneuvering coupled with ship motion in waves. *Ocean engineering*, 38(17-18):1934–1945.

Shamoo, A. E. and Resnik, D. B. (2009). *Responsible conduct of research*. Oxford University Press.

Skejic, R. and Faltinsen, O. M. (2008). A unified seakeeping and maneuvering analysis of ships in regular waves. *Journal of marine science and technology*, 13(4):371–394.

Söding, H. and Shigunov, V. (2015). Added resistance of ships in waves. *Ship Technology Research*, 62(1):2–13.

Söding, H., Shigunov, V., Schellin, T. E., and Moctar, O. e. (2014). A rankine panel method for added resistance of ships in waves. *Journal of Offshore Mechanics and Arctic Engineering*, 136(3).

Stapersma, D. and Woud, H. (2005). Matching propulsion engine with propulsor. *Journal of Marine Engineering & Technology*, 4(2):25–32.

Subramanian, R. and Beck, R. F. (2015). A time-domain strip theory approach to maneuvering in a seaway. *Ocean Engineering*, 104:107–118.

Sui, C. (2021). Energy effectiveness and operational safety of low- powered ocean-going cargo ship in various (heavy) operating conditions. *TU Delft Dissertation*.

Sutulo, S. and Soares, C. G. (2006). A unified nonlinear mathematical model for simulating ship manoeuvring and seakeeping in regular waves. In *Proc. Int. Conf. on Marine Simulation and Ship Manoeuvrability MARSIM*.

Taskar, B., Yum, K. K., Pedersen, E., and Steen, S. (2015). Dynamics of a marine propulsion system with a diesel engine and a propeller subject to waves. In *34th International Conference on Ocean, Offshore and Arctic (OMAE2015), St. John's, Newfoundland, Canada*.

Taskar, B., Yum, K. K., Steen, S., and Pedersen, E. (2016). The effect of waves on engine-propeller dynamics and propulsion performance of ships. *Ocean Engineering*, 122:262–277.

Tello Ruiz, M. (2018). *Manoeuvring model of a container vessel in coastal waves*. PhD thesis, Ghent University.

Ueno, M. (2003). Experimental study on manoeuvring motion of a ship in waves. In *International Conference on Marine Simulation and Ship Maneuverability, MARSIM'03, Kanazawa*.

Ueno, M., Tsukada, Y., and Tanizawa, K. (2013). Estimation and prediction of effective inflow velocity to propeller in waves. *Journal of Marine science and Technology*, 18(3):339–348.

Van Daalen, E. and Bunnik, T. (2021). Seacal, version 4.2.0, theory manual. *MARIN Report No. 21447-7-RD*.

Van't Veer, A. P. (1998). Behaviour of catamarans in waves.

Vaz, G. and Bosschers, J. (2006). Modelling three dimensional sheet cavitation on marine propellers using a boundary element method. In *Sixth International Symposium on Cavitation CAV2006, Wageningen, The Netherlands*.

Wang, J. and Wan, D. (2018). Direct simulations of turning circle maneuver in waves using rans-overset method. In *ASME 2018 37th International Conference on Ocean, Offshore and Arctic Engineering*. American Society of Mechanical Engineers Digital Collection.

White, F. M. (2016). Fluid mechanics 7th edition in si units.

Yasukawa, H. and Faizul, A. A. (2006). Experimental study on wave-induced motions and steady drift forces of an obliquely moving ship. *Journal of the Japan Society of Naval Architects and Ocean Engineers*, 3:133–138.

Yum, K. K., Taskar, B., Pedersen, E., and Steen, S. (2017). Simulation of a two-stroke diesel engine for propulsion in waves. *International Journal of Naval Architecture and Ocean Engineering*, 9(4):351–372.

Zhang, W., Zou, Z.-J., and Deng, D.-H. (2017). A study on prediction of ship maneuvering in regular waves. *Ocean engineering*, 137:367–381.